University of Alberta

Advanced Methods for GLAD Thin Films

by

Martin Roman Kupsta

A thesis submitted to the Faculty of Graduate Studies and Research
in partial fulfillment of the requirements for the degree of

Master of Science

in

Micro-Electro-Mechanical Systems (MEMS) and Nanosystems

Electrical and Computer Engineering

©Martin Roman Kupsta
Spring 2010
Edmonton, Alberta

Examining Committee

Jeremy Sit, Electrical and Computer Engineering

Andy Knight, Electrical and Computer Engineering

Anastasia Elias, Chemical and Materials Engineering

Please take time to digest the previous material and prepare for what lies ahead.

To all my fans and admirers. Also to you, the reader, for you too will become a
fan and admirer.

Abstract

Thin films are produced from layers of materials ranging from nanometres to micrometres in height. They are increasingly common and are being used in integrated circuit design, optical coatings, protective coatings, and environmental sensing. Thin films can be fabricated using a variety of methods involving chemical reactions or physical transport of matter. Glancing angle deposition (GLAD) thin films are produced using physical vapour deposition techniques under high vacuum conditions where exploitation of the geometric conditions between the source and the substrate causes enhanced atomic self shadowing to produce structured thin films. This work deals with the modification of these films, *in situ* by altering growing conditions through substrate temperatures control, or post-deposition through reactive ion etching (RIE).

The first part of the thesis deals with the modification of TiO_2 GLAD humidity sensors using RIE with CF_4. The data presented demonstrates improved response times to step changes in humidity. Characterization revealed response times of better then 50 ms (instrument-limited measurement). An etch recipe for complete removal of TiO_2 was also demonstrated with shadow masking to transfer patterns into GLAD films.

The subsequent chapter focuses on modification of thin film growth conditions by increasing adatom mobility. A radiative heating system was designed and im-

plemented with the ability to achieve chuck temperatures of 400°C. Capping layers on top of GLAD films were grown to demonstrate effects of *in situ* heating, and a quantitative analysis of crack reduction with increased temperatures is presented. Lithographic pattern transfer onto a capped GLAD film was demonstrated.

Opposite to the goal of the preceding chapter, the focus of the final experimental chapter was to limit adatom mobility. A LN_2-based cooling system was designed and implemented for the purpose of studying the growth by GLAD of lower melting point materials, which under regular growth conditions do not form well-defined structures. Chuck temperatures of -60°C can be achieved during deposition while still allowing substrate rotation. The growth of helical copper films was used to demonstrate the effects of *in situ* substrate cooling.

Acknowledgements

It has been a long road for me but also for the people that were around me during this time. First and foremost, I would like to thank my parents, Marta and Roman, for all the support and encouragement given to during the tough times and giving me a foundation to always be able to fall back on.

Thank you Dr. Jeremy Sit for rolling the dice and taking on a less than desirable candidate. Thank you for having the confidence and faith in me to be able to go through this journey and come out victorious. Thank you for letting me into the playground and allowing me to play with all the expensive toys. I hope whatever I broke I made better.

I would also like to thank Dr. Michael Taschuk for the ever constant and always motivating whip crack and fist shake. Without his research expertise, vast knowledge, and hawk like control over everything that is research based, this thesis and the lab wouldn't be in shape it is today.

Many thanks go to Jonathan Kwan, Louis Bezuidenhout, and Nicholas Wakefield who took a majority of my abuse but also allowed for good times in and out of the lab. Thanks go out the current members of the GLAD group that I've probably managed to annoy or disturb in one way or another: Michael Fleischauer, Graeme Dice, Jason Sorge, Joshua LaForge, Katie Krause, Matthew Hawkeye, Jaron van Dijken, Sumudu Fernando, Joshua Krabbe, Steve Jim, Dan Smetaniuk and of course

Contents

Please take time to digest the previous material and prepare for what lies ahead.

List of Tables

Please take time to digest the previous material and prepare for what lies ahead.

List of Figures

Chapter 1

Introduction

This thesis presents research which explores new methods for producing thin films through electron beam evaporation and by modifying substrate temperature. Work done in the modification of thin based of humidity sensors for improved response times was developed as well.

As with most research it is easy to set the end goal, but difficult to lay out the path that will get one there. Also common to research, once the journey into the unknown begins, the researcher will encounter many different possibilities to explore avenues and side streets that may not be relevant to the end goal. The work presented in this thesis stems from a goal to incorporate two mature fields in micro- and nanotechnology, microelectrical mechanical systems (MEMS) and glancing angle deposition (GLAD). Through the development of an GLAD compatible etch process and making high resolution pattern transfer into GLAD films possible through development of a vacuum compatible heating system, the bridging the two technologies becomes more realistic. The development of a substrate cooling system afforded the ability to explore more materials and their properties.

Chapter 2 of the thesis provides some theoretical background and an introduction

to some of the processes and concepts that were key in the development of the work found in this thesis.

Chapter 3 investigates methods for modifying GLAD thin film structures to improve humidity sensors and to achieve pattern transfer into a GLAD thin film. First, a dry etch recipe was developed for GLAD thin films. A side effect observed during the recipe development period was applied to GLAD thin films RH sensors grown on interdigitated electrodes (IDE). Since the etch creates larger pores in the GLAD thin film, it was expected that there would be an decrease in the response time of the sensor through higher diffusivity rates into the bulk of the film. To determine the effects and success of the etch on the film, a series of experiments were conducted where etch time was varied on similar base films. A calibration chamber was used where the etched GLAD thin film sensors were calibrated against a commercial sensor. The response time was determined using a second custom humidity chamber where rapid humidity changes, from high to low to high, were observed. By further modifying this etch recipe it was possible to achieve a low resolution pattern transfer into a GLAD thin film by using a shadow mask.

Chapter 4 deals with the heating of GLAD thin films *in situ* and post-deposition patterning. The need for this became apparent when observing capping layers produced using standard unheated methods to have cracks which were long and large. To use standard lithographic methods of pattern transfer to achieve high quality results, a uniform, planar layer was needed. Since thin film growth, especially GLAD, depends on adatom mobility, a simple and effective way to decrease capping layer cracking was needed to increase the temperature of the substrates during deposition. By increasing substrate temperature, adatom mobility is also increased which allows condensed atoms to traverse greater distances on the substrate surface and preferentially orient themselves to produce a higher quality capping layer. In this

2

section, along with my solution to *in situ* heating and its results, a demonstration of pattern transfer is shown by using a mask with features that contains MEMS devices.

Chapter 5 of the thesis deals with the natural complement of the experiments carried out in the previous part: cooling. This has often been discussed and is touted to be the solution allowing the deposition of low melting point materials in GLAD films. The main hurdle with attempting heat removal from a GLAD chuck is the need to preserve substrate tilt and rotation. Temperature measurement of the substrate was achieved using the temperature measurement system from the previous chapter, which is suitable for temperatures down to -185°C. This section presents details of design and implementation of a LN_2-based substrate cooling system along with preliminary results.

The majority of the scanning electron micrographs that are presented in this thesis work were taken by the author himself on a JEOL 6301F, a field emission microscope.

Please take time to digest the previous material and prepare for what lies ahead.

Chapter 2

Theory and Background

2.1 Glancing Angle Deposition

Glancing angle deposition (GLAD) uses physical vapour deposition methods and substrate tilt and rotation to create sculptured thin films (STFs). This process requires an environment capable of reaching and maintaining high vacuum, a method of producing a vapour flux, a method to measure the the rate of emission from the source, and a substrate holder capable of mechanical rotation and spin [1]. GLAD thin films exhibit unique and favourable properties, such as: high surface area, high porosity and columnar nanostructures. With computer-controlled feedback, a high degree of controllability is possible down to 10 nm length scales. Setting a highly oblique angle at which the vapour flux lands on the substrate, a highly porous film will be produced. The resulting films have higher surface area, compared to planar films, which allows for greater exploitation of material surface properties. This high surface area is due to the formation of individual columnar structures. Random nucleation and self-shadowing are inherent to the process, and allow for the production of columnar nanostructures without the need for patterning, although substrate
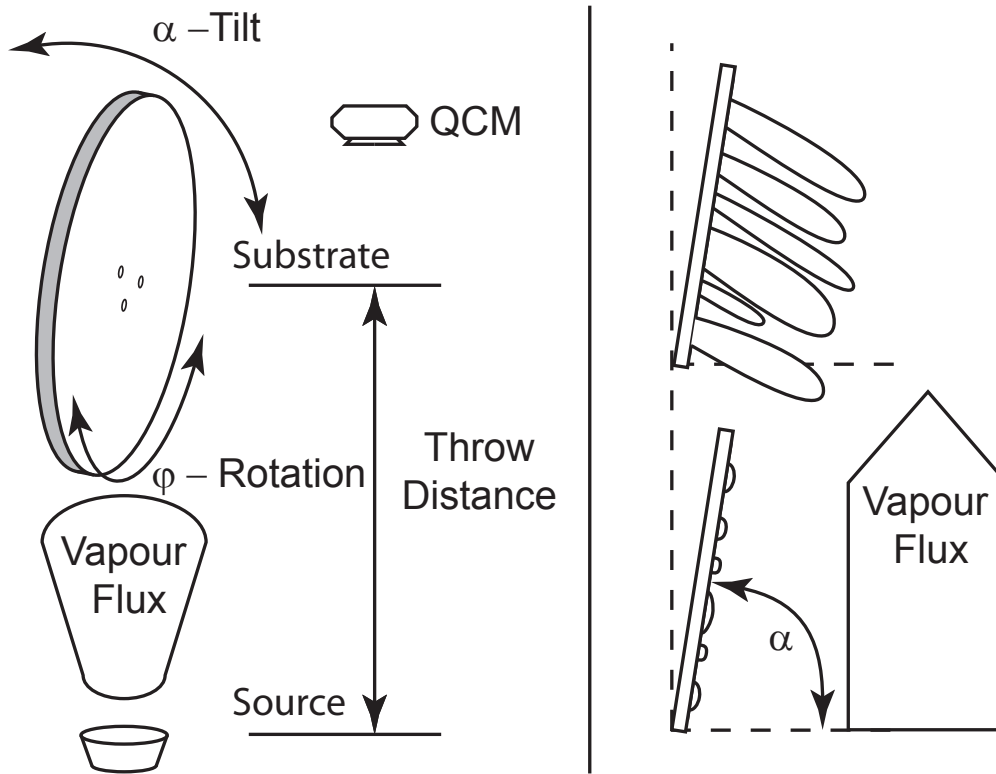
Figure 2.1: Left: A generalized GLAD setup, introducing the GLAD tilt angle α along with substrate rotation φ along with the typical placements of components in a deposition chamber. Right: A grossly exaggerated view of atom nucleation and the continual growth of a film with a highly oblique angle α with a fixed rotation φ, producing slanted posts.

patterning can be employed to further engineer this thin film technology [2].

A generalized GLAD setup is depicted in Fig. 2.1. Alpha, α, enables the glancing angle in GLAD, seen in Fig. 2.1, which mainly affects the porosity/density of the film being grown. When a substrate is held at a fixed α without substrate motion, the resulting film is composed of slanted posts. Vapour flux impinging on the substrate is captured by and condenses on the substrate's topographical high points, resulting in confinement of growth at these points, with the resulting features tending toward the vapour source. By introducing substrate rotation through phi, φ, the

6

azimuthal distribution of the incoming flux can be controlled, allowing the production of different structures. A high vacuum environment is required to ensure film purity and a long mean free path (MFP) to minimize scattering of the collimated vapour flux. Longer throw distance between the source and the substrate ensures a collimated vapour plume, but increases the chance of collision between atoms at higher pressures and also decreases the deposition rate seen on the substrate. The vapour plume can be created through several methods such as physical sputtering of the material from the target or, as is the case in this thesis, thermal evaporation (e-beam evaporation). As the atoms break from the source melt they are released into the vacuum and exhibit a $\cos^n$ distribution [3], where n depends on the ratio between source size and the MFP of atoms, with n increasing with increasing ratio value. By using a quartz crystal microbalance (QCM), it is possible to determine the deposition rate at the substrate and the emission rate of vapour flux from the source. The rate at which the atoms land onto the QCM is related to the rate at which the atoms land on the surface of the substrate through a tooling factor. This tooling factor is used to correct for such geometric effects which in turns enables the fine control of structures being grown on the surface of the substrate.

Knowing the rate of deposition, coupled with substrate motion it is possible to produce a variety of structures such as slanted posts, chevrons, helices and vertical posts which are depicted in the SEM images shown in Fig. 2.1. Periodic, discrete changes of 180° in φ alternate the growth direction to produce chevrons, whereas a low rate of φ rotation will cause a continual change in growing direction which produces helical structures. By increasing the rate of φ spin, the pitch of the helical structures becomes indistinguishable from the column diameter resulting in vertical posts. Other structures are possible, such as square spirals, which are extensions/modifications to the basic four shapes. Broadening of columnar posts will

7
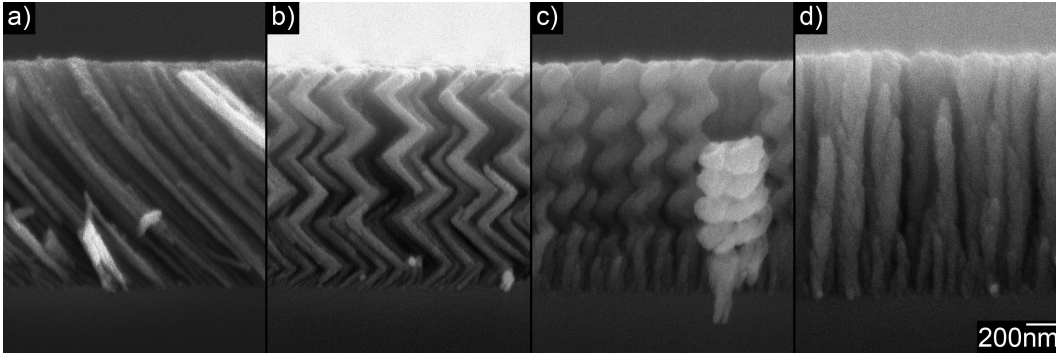
Figure 2.2: Typical films that are possible using different substrate motion algorithms: a) slanted posts, b) zig-zags (chevrons), c) screws (helices), and d) vertical posts.

occur as neighbouring columns become extinct and allow for more vapour flux to land on surviving structures. By using PhiSweep, a method developed by Jensen and Brett to minimize vertical post fanning, it is possible to improve individual column structure [4]. Although it is possible to control the direction in which the flux lands on the surface, there are several other factors that can affect thin film structure: chamber conditions, substrate temperature, surface structure, deposition algorithm, and deposition rate [4–6]. Substrate temperature will be a factor that will be manipulated in order to see the effects of adatom mobility on a planar substrate with more discussion seen in Sec. 2.4. Traditionally in GLAD systems substrate temperatures have not been controlled. Therefore, to create high quality films, high melting point materials are used due to their low surface mobility on unheated substrates.

GLAD is a mature process and has been applied and integrated into existing technologies such as optics, sensors, energy and microfluidics applications to produce enhanced devices. Optical applications include: birefringent indium tin-oxide [7], coatings to increase transmittance of a wide wavelength range [8], and

8

photonic crystals [9]. A GLAD thin film's higher surface area for a given footprint area (compared to that of films deposited with conventional techniques) enables increased interaction with the environment. By tailoring the film to react with an analyte, it is possible to achieve an amplified reaction and coupled with electrical measurements [10] or even optical measurements [11], a powerful sensor is obtained. Mechanical devices such as nanosprings which can be electrostatically deflected for manipulation of peak wavelength transmittance have been demonstrated [12]. By designing a micro-electromechanical system (MEMS) mass-based sensors, which depends on the absorbtion of the analyte to change the resonant frequency, a fast and easily tailored sensor is possible. GLAD is even proving itself to be a valuable addition to the alternative energy arena by providing higher surface area interactions between electrode and electrolyte in microbattery applications [13]. Microfluidics applications are enhanced by the densely packed nanostructures. Capillary effect, due to small distances between neighbour surface, have been successfully demonstrated in production of ultra thin layer chromatography for faster separation and lower solution volumes [14]. A GLAD rendition of relative humidity sensing has already been demonstrated with great success [10, 15–17], and has been subsequently further improved by the techniques presented in this thesis work.

2.2   Humidity Sensing with GLAD Thin Films

Relative humidity (RH) is the measure of the partial pressure of water vapour present in a gaseous mixture of water and air. Variations in RH can have significant and sometimes detrimental effects on processes requiring specific conditions; therefore, rapid and accurate monitoring, analysis, and control of RH are important. Areas that require an elevated quality of RH monitoring include respiration monitors used for neonatal, sleep apnea, or operating room patients [18, 19] and aircraft-mounted

RH sensors for meteorological surveys where a quick and accurate polling of weather systems is required [20]. Other applications requiring monitoring and control of RH include storage of goods including food, and monitoring of structural integrity and chemical processing [21]. Current commercial RH sensors exhibit response times of several seconds (*e.g.*, the Vaisala HMP100 with 8 s response time), which are too slow for some of the above applications.

It has been previously shown that nanostructured thin films produced by glancing angle deposition (GLAD) [5, 22–24] exhibit a measurable and repeatable response to variations in RH while using optical and capacitive methods to observe these changes. Shifts in capacitance of 3 orders of magnitude have been observed for a change of RH from 2% to 92% [16]. In addition, extremely fast response times are observed, typically 90 ms to 300 ms [15–17].

GLAD films are composed of tightly packed columns which form small pores. These pores, typically 10 nm–100 nm in size, affect the diffusion of gas within the film. According to Knudsen diffusion, which describes diffusion through a long, narrow pore [25], at room temperature, water vapour is expected to have a diffusivity of $\approx 4 \times 10^{-6}$ m^2 s^{-1} though a 10 nm diameter pore. When combined with Fickian diffusion [26], the expected diffusion time through a 1.5 μm film would be ≈ 140 ns, much faster than the experimental results reported above. There are no surface interactions in the Fickian diffusion model; the discrepancy between theory and experiment is due to a strong interaction between the analyte and pore wall. To measure humidity, one can measure the film's capacitance, which depends strongly on the interaction between the electric field and the dielectric medium. For a planar interdigitated electrode (IDE) capacitor, the electric field diminishes in strength exponentially with distance from the substrate surface [27]. The electric field is largely confined to within one quarter period (2 μm for our devices) of the IDE [27],

10

a)

Fringe field
height

+   -   +   -   +   -

b)

Period

Electrode

Electrode
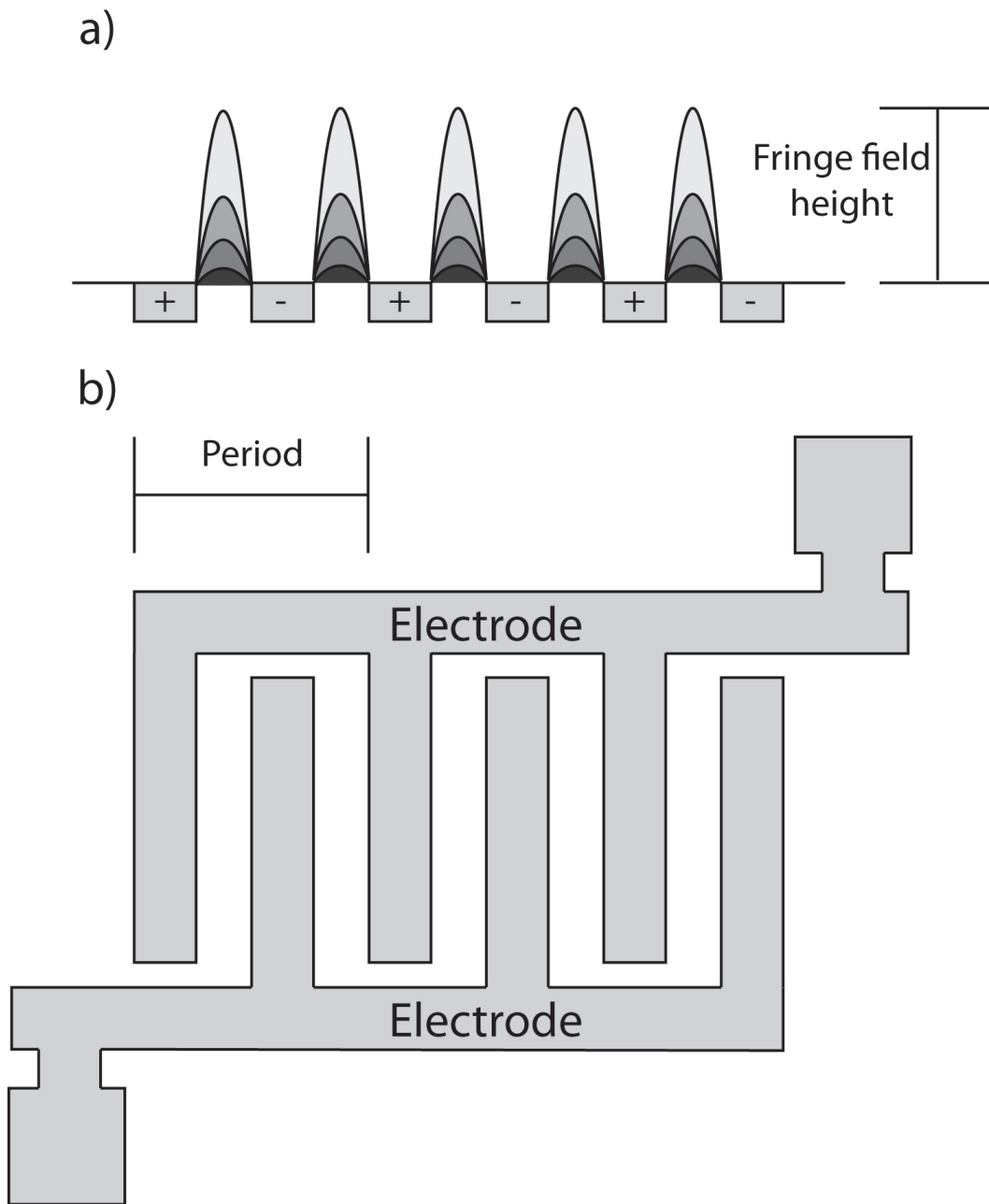
Figure 2.3: A simplified representation of an IDE. The side view is shown in a), which illustrates the an IDEs fringing electric fields. The period nature of the IDE is shown in b).

meaning that the most sensitive region for a device consisting of a GLAD film grown on top of an IDE will be immediately above the IDE, which is also the very last region that the inwardly diffusing water vapour will reach. One method to allow for quick response would be to grow thinner films, but this sacrifices dynamic range. Therefore, to maintain dynamic range, high diffusivity channels are required for rapid delivery of the analyte to the most sensitive region of the sensor. The high affinity of water vapour for TiO_2 combined with the high surface area of GLAD films is responsible for both the high sensitivity and limitation in response speed due to a significant reduction in the effective diffusivity of the water vapour within the film. Chapter 3 demonstrates a method to further increase the effective diffusivity of water vapour (and hence increase the response speed) with minimal effect on device sensitivity.

2.3   Reactive Ion Etching

Two general methods of etching exist: Wet and dry. Wet etching requires having the reactants in aqueous form. As they react with the target material surface the reactants will create aqueous products. These products are carried away by diffusion, allowing for fresh reactant to continue the process. Most etches are calibrated to be used with planar films and provide a relatively constant etch rate. Unfortunately this etch rate cannot be used reliably with GLAD thin films due to the high porosity and the ability for the etchant to infiltrate the voids in film. The wet etchant interaction with the large surface area of the GLAD film creates a difficult situation for controlling and achieving a uniform etch rate. This is because fresh etchant exchange can be impeded further down the film. Typical GLAD thin films have a high feature aspect ratio, tens of nanometre post spacing, with nanometre bases.

A second problem with wet etches is that when liquid is removed from a GLAD

film, clumping of the film columns can occur. The capillary forces between the structures becomes significant, coupled with weak mechanical strength due to the thin bases causes the structures to come together [28–30]. Such an effect, observed in MEMS fabrication, is called stiction. Stiction occurs when structures deform, inhibiting the movement of the feature. It is a primary mode of failure in MEMS devices [31]. By using critical point drying methods it is possible to minimize the effects of clumping, but a more suitable alternative etching GLAD thin films is dry etching.

Reactive ion etching (RIE), consisting of a plasma discharge, is a dry etching technique that can produce anisotropic etches favourable for pattern transfer techniques. Again, due to the porous and columnar nature of GLAD thin films, this etch technique's performance is not typical to that of planar dense films. The basic premise of a dry etch is to produce reactants from an original feed gas by method of plasma discharge. To produce a plasma a voltage is applied between two electrodes creating an electric field. This electric field starts a cascade of collisions between electrons and ions to produce ions, electrons, photons, and neutrals (radicals) [32]. Depending on the products produced, the dry etch can be a physical or chemical process, or a mixture of both. The etching process can be categorized into four types [33]: sputtering, chemical plasma etching, ion-enhanced chemical etching, and inhibitor-controlled chemical etching. Sputtering is a physical event caused by ion bombarding. These ions are accelerated by an electric field and collide with the substrate to dislodge surface atoms. Chemical plasma etching involves the neutral radicals reacting with the material to produce a volatile product. Ion-enhanced chemical etching uses the ions bombarding the surface to remove the volatile product on the sample surface. Finally, inhibitor-controlled chemical etching depends on the ions, which are traveling perpendicular to the electrode, to remove an inhibiting

13

layer on the sample surface thus allowing chemical etching to proceed. Reactive ion etching makes use of ion-enhanced chemical etching and inhibitor-controlled chemical etching. Since plasma etches are done under vacuum, products are removed by the vacuum pump while fresh feed gas is introduced to keep the plasma discharge going. The reactants can still penetrate the GLAD thin film and chemically react with the material's surface. Ion assisted bombardment of the unmasked film will cause material redistribution onto neighbouring walls and to the thin base, but also removal of volatile products from the surfaced caused from the chemical reaction. In some circumstances this can be an advantage when trying to strengthen the columns [34]. Etch recipes can be tailored for etching oxides, polymers or metals, but the final performance will be dictated by the specific material used.

Titanium dioxide (TiO_2) or titania was the the material of choice in the GLAD thin film. As a material it has many general advantages: cheap, abundant, non-toxic, and biocompatible; proven by its usage in health care products as well as in paints, sunscreen, and plastics [35]. More specific properties allow TiO_2 to perform as chemical sensing media (titania nanotubes to sense H_2), photocatalyst (oxidizing organic impurities through UV irradiation), or as a photovoltaic in solar cell applications [35–38]. TiO_2, with its wide band gap and high dielectric value, is becoming a suitable replacement for SiO_2 as the transistor gate dielectric [38, 39]. Thinner gates allow for lower capacitance and faster switching but introduce larger leakage currents, thus higher power dissipation. Therefore by using thus a high-κ dielectric value material, leakage currents can be minimize. Unfortunately, there is no suitable wet etch recipe for TiO_2 [40]; thus a CF_4 dry etch recipe, initially developed for selectively etching SiO_2 against Si, was used [41]. In any dry etch recipe there are several important factors that will determine the success of the etch: feed gas type, gas flow, plasma power, chamber pressure and etch duration [42].

14

In the etching experiments, the use of a polytetrafluoroethylene (PTFE or Teflon) spacer between the substrate was investigated. The PTFE spacer was placed on the RIE electrode on which the samples to be etched are placed. The advantage of using PTFE as the spacer between the electrode and sample was that there was an increase in selectivity between SiO_2 and Si. The PTFE spacer absorbs excess F radicals, which are created by the plasma and etch the Si, whereas CF_3^+ ions are left to chemically etch the intended oxide [41, 43]. Matsutani *et al.* took this recipe and applied it successfully to etch TiO_2 [43]. It was discovered that at pressures around 0.1 Torr, the etch rate of Si was a maximum; with increasing pressure, the etch rate dropped, while for SiO_2 and TiO_2 the etch rate increased. The etch recipe used to etch TiO_2 was by using CF_4 at a pressure of 0.12 Torr with an RF power of 100 W along with the PTFE spacer. Figure 2.3 depicts the reaction inside the RIE chamber during etching.

A more aggressive etch was also researched which allows for quicker removal of TiO_2 from the surface. By using a 3:1 ratio of CF_4:O_2, developed for etching polysiloxane, it was possible to etch TiO_2 and to use aluminum as a masking layer [44]. The addition of oxygen generates more F radicals by reacting with unsaturated fluoride species created by the plasma [33]. Pattern transfer is possible with the complete removal of TiO_2 in a manner that does not form significant clumping, as will be demonstrated in Chapters 3 and 4. Unfortunately residues were observed on the sample surface. These residues are formed through unintended reactions with materials present in on the sample, as well as the inability to remove etch by product. Fortunately, more refined etch recipes and techniques for minimizing the formation of resides in fluorinated plasma exist. The use of H_2 along with fluorine based feed gas assists in gettering aluminum clusters to form AlH_x [33]. This metal contamination is suggested to occur due to exposed electrode surfaces. Other feed gases
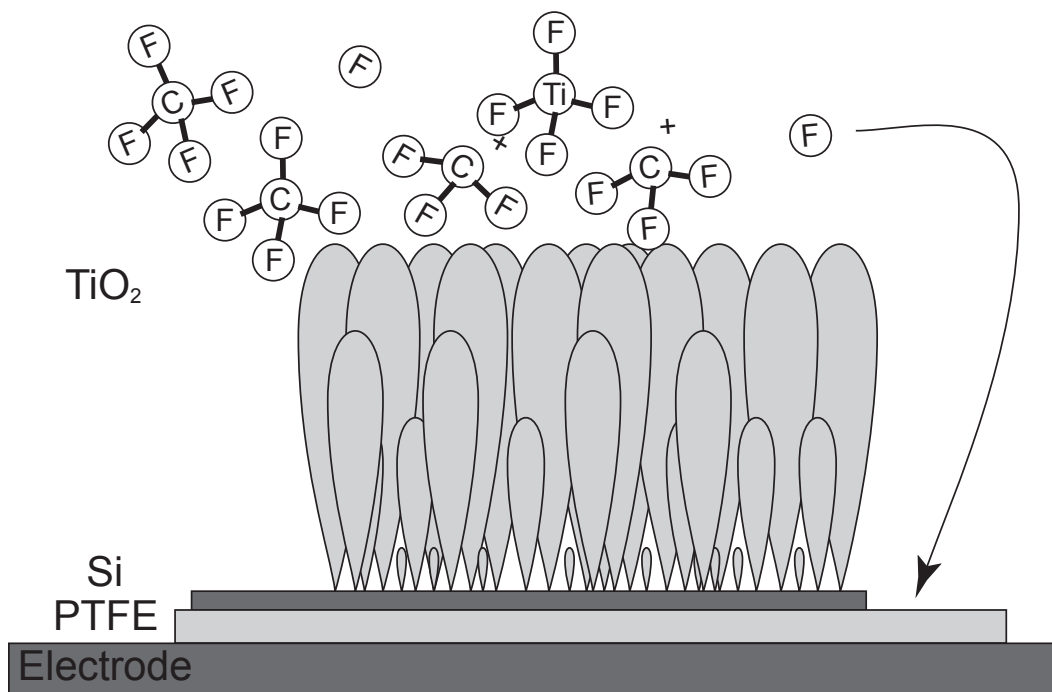
Figure 2.4: A simple visual representation of the RIE setup and its reactions.

that have had promising results with minimal residue formation are: $CBrF_3/O_2$, $SF_6/O_2/H_2$, $CF_4/O_2/H_2/$, $NF_3/O_2/H_2$, CF_4/CHF_3, NF_3/CHF_3 [33, 45].

2.4 Temperature

The properties of thin films can vary as they are dependant on many aspects: deposition parameters (*e.g.*, chamber pressure, deposition rate, geometry), surface properties (*e.g.*, point defects, grain boundaries, voids, temperature), and material properties (*e.g.*, compositional nonhomogeneities, impurities, chemistry) [2, 46, 47]. In this work, surface temperature effects are explored and the effect of adatom mobility on film structure. To maintain desired chuck temperatures it is important to understand methods of heat transfer in vacuum, and improved methods of thermal insulation.

Adatom mobility on a surface is strongly dependent on the amount of energy the atom has, interaction between neighbouring atoms, and the surface temperature. The diffusion length of the adatom increases with the temperature of the substrate [48]. The diffusion length is dependant on the diffusivity constant of the material and is predicted by

$$D = D_0 e^{\frac{-E_a}{kT}},$$

where D_0 is the diffusivity of the material at an theoretical infinite temperature, E_a is the activation energy for the material to break free from its surroundings, k is the Boltzmann constant, and T is temperature in Kelvin. E_a is composed of the energy barrier for surface diffusion, E_d, and the nearest neighbour bond energy, E_n [2]. This energy is the energy that is required to break free from the atoms current site and be free to hop to another site. Therefore with each hop an atom makes from site to site it loses its energy until it cannot break free from its current site.

The GLAD process exploits low diffusivity by depositing materials onto substrates when $T/T_m \leq 0.3$, where T is the temperature of the substrate and T_m is the melting point of the material being deposited. A higher melting point relates to the need for the atoms to have a higher energy content to break free from its current site. Therefore as the high energy atoms condenses on the low temperature surface, which has a low energy content, more significant amounts of energy will be transfered to the surface, to achieve thermal equilibrium. This big difference between T and T_m deprives the adatom of its energy quicker and therefore decreases its ability to achieve long diffusion lengths therefore confining it to a smaller region [47]. The value of 0.3 comes from the structure-zone model (SZM), proposed by Movchan and Demchishin [49], which relates to the first zone where the temperature is low enough to impede any significant diffusion. The traditional SZM models are qualitative and should not be used to define strict boundaries [47]. In a typical GLAD setup the chuck is unheated. The chuck will be at room temperature at the beginning of the deposition and will warm up from the energy radiated from the source and the condensation of high energy evaporant adatoms. Our systems have an aluminum chuck mounted on an aluminum rotating head piece with good thermal contact. Since aluminum is a good conductor of heat, the absorbed energy is conducted to the rest of the deposition system, thus minimizing temperature rise of the chuck and the substrate, during deposition. For typical deposition of TiO_2, which lasts about an hour, substrate temperatures towards the end of the deposition are seen to approach 60-70°C, measured through a thermocouple. Although hot to the touch, the temperature is still low enough to allow for handling of the chuck and substrates shortly after deposition. Therefore to achieve substrate temperature control an understanding of heat transfer mechanisms in vacuum needs to be established.

Three methods of heat transfer exist: conduction, convection and radiation. Conduction occurs when when thermal energy is transferred to neighbouring atoms to minimize the heat gradient in the material. As a simplified explanation, heat transfer by conduction along an object is proportional to the product of the temperature gradient and the thermal conductivity of the material. Convection occurs in fluids, such as liquids and gases, where individual molecules in the fluid carry heat away from a heated surface. Circulation of the fluid's molecules allows the surface to impart its energy to more molecules thus putting the surface surroundings at thermal equilibrium with itself. At vacuum pressures, however, due to the greatly reduced density of gas molecules in the chamber, energy transfer due to convection will be negligible. Radiative heat transfer occurs when an object's heat energy is converted into electromagnetic radiation and is emitted from the surface to minimize the heat gradient present between the object and its surroundings. The rate of heat conversion is governed by the Stefan-Boltzmann law, which yields a relation between temperature and power

$$W = \varepsilon \sigma A T^4,$$

where ε is the emissivity of the surface, σ is the Stefan-Boltzmann constant, A is the area of the radiating surface, and T is surface temperature. Therefore higher surface temperatures will produce a situation where the main mode of heat transfer can potentially be through radiation. To minimize heat transfer caused by convective losses, experiments can be done in a vacuum while insulating materials can be used to minimize unnecessary conductive losses. With this knowledge, substrate conditions can be manipulated to a desired temperature to conduct experiments pertaining to adatom mobility.

Column broadening, typical to GLAD thin films, could be explained using dif-

19

fusivity and heat transfer. As the atoms land on a surface they diffusive until they settle, with sufficient time. As more atoms land on the existing island, formed by previous atoms settling on the surface, their interactions are no longer the same as for the original atoms. Therefore island size that was originally determined by the original surface-adatom interaction is no longer dominant. Due to radiative heating and conduction of heat from the adatoms, coupled with the thermal conductivity of the deposited material and lack of substrate temperature control, it should be expected to see column broadening due to the higher adatom mobility. As the columns start to broaden and dominate neighbouring columns, flux that was intended for the neighbouring columns start to accumulate on the surviving column. This redistributes flux compounds, and is compounded by, the effect of broadening. Although, if atoms are not given sufficient time to settle, by increasing the deposition rate from the source, it can be speculated that adatom can be buried by incoming atoms and forced to settle.

Heated substrates combined with the GLAD process has been explored by a few other groups [50–53]. In general, the use of heated substrates in GLAD process results in degeneration of the intended structure [52]. Commercial systems for suitable heating exist, one example being from Kurt J. Lesker (part number QLH-ARRAY2), a dual quartz lamp heater which is capable of 1000 W output. Another solution is the use of a tantalum resistive heater on the backside of the substrate holder [51, 52]. Heating of substrate is relatively easy and fairly forgiving when compared to substrate cooling, especially when trying to preserve substrate rotation.

Although radiative heat transfer works well for achieving elevated temperatures, thermal contact is need to achieve adequate heat transfer when attempting to cool a substrate. Several groups have achieved cryogenic temperatures and deposited

20

films at oblique angles [50, 54, 55]. All reported methods of substrate cooling with oblique angle substrate capabilities do not allow for φ rotation, a key requirement for the GLAD technique. This limitation is probably due to the inflexibility of the cold finger that is used to extract heat from the substrate via conductive heat transfer. Several points need to be understood when working at sub-ambient temperatures [56]: contact resistance is different between static and dynamic situations, conductance is enhanced by higher contact pressure and smoother surfaces, thermal resistance decreases with smoother surfaces, thermal resistance increases with thickness of intermediate layers (such as oxides). With a substrate cooled to 113 K, cobalt was grown at an α of 60° producing densely packed films with columnar grain structure [55]. Cooling of the substrate down to 22 K and depositing palladium (which has a relatively high melting point) and an α of 85° produced slanted posts with higher surface areas compared to room temperature films [54]. Unfortunately, lower melting point materials have not been explored at these lower temperatures let alone with the ability to rotate the substrate to achieve similar film structure tailoring as seen in Figure 2.1.

2.4.1   Temperature Measurement

There are several ways to obtain an estimate of the surface temperature during a process such as: thermistors, thermocouples, IR heat guns, thermometers, *etc.* Common practice, as seen in literature, for *in situ* temperature measurements is to use a K-type thermocouple which has been spot welded to the substrate holder. Although K-type thermocouples have a wide range of temperature measurement, are relatively cheap, and exhibit high sensitivity across their whole range, they are not favoured for use in vacuum as per American Society of Temperature Measurements (ASTM) due to the preferential vapourization of chromium in the thermocouple,

which may alter calibration [57]. K-types are made from thermal electric elements from the following materials: Chromel for the positive thermoelectric element, KP, (90% nickel and 10% chromium) and Alumel for the negative thermoelectric element, KN, (95% nickel, 2% manganese, 2% aluminium and 1% silicon) [57]. A good substitute for the K-type thermocouple with comparable attributes is the T-type thermocouple, which is meant for use in vacuum along with cryogenic temperatures. The T-type thermocouple is made from thermoelectric elements which do not contain chromium, and therefore suitable for vacuum environments: Copper for the positive thermoelectric element, TP, and Constantan for the negative thermoelectric element, TN, (55% Copper and 45% Nickel) [57].

It is advantageous to use a thermocouple for temperature measurement due to their wide temperature range and ability to produce their own signal withouth external excitation. Thermocouples, through the Seebeck effect, produce a voltage with a change in temperature at a junction between two differing metals. Materials combinations that produce a relatively linear temperature to voltage output are give a letter designation by ASTM and NIST [58]. Materials that produce a non linear output or that have not been calibrated pose a more serious problem. By connecting a thermocouple to test leads and feedthroughs without precise knowledge of interconnections' material composition, two more thermocouple junctions are created. They produce voltages V_2 and V_3 which produce a temperature-dependent offset in the measured voltage. Therefore without the knowledge of the sensitivity of these two new junctions, the known thermocouple voltage, V_1 cannot be accurately converted to a temperature value. This scenario is depicted in Figure 2.5a. One method of nullifying this effect is to use two thermocouples in the circuit [59]. By using a second identical thermocouple, seen in Figure 2.5b, and connecting the two like thermocouple elements, it is possible to negate voltages V_3 and V_4 created at

22
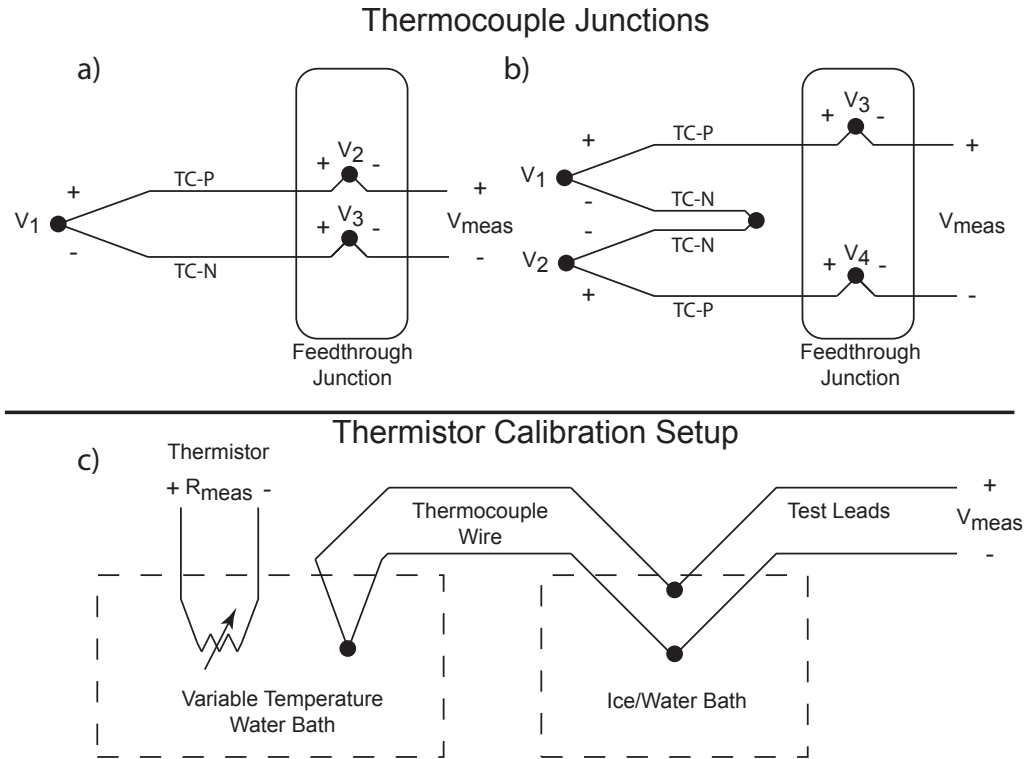
Figure 2.5: Top: Thermocouple junctions created when connecting to feedthrough using one (a)) and two (b)) thermocouple setup. Calibration of thermistor setup, shown in c), using a ice bath setup for the junction created between the multimeter and the thermocouple.

the feedthrough/test lead connections, albeit with a trade-off in complexity. Introducing another thermocouple, a second standardized voltage producing junction, V_2 is coupled with the voltage V_1 produced by measuring the unknown surface. By fixing this second junction at a known (cold) temperature, it is possible to obtain the voltage produced by this junction and ultimately obtain the temperature of the unknown surface. This method is known as cold junction compensation (CJC) [60]. Since the temperature of the CJC is low and relatively constant a simple thermistor can be used to probe the temperature of the junction, but of course in order to rely on the output of the thermistor it must be calibrated.

23

The experimental setup for the calibration of the thermistor is depicted in Figure 2.5c. By placing the connections to the thermocouple in an ice bath, which is at the triple point of water [61], allows the use of NIST thermocouple coefficients [58] with a high degree of accuracy. A thermocouple and a thermistor are placed, in close proximity, onto or into a medium of which the temperature varies. The connection to the test leads is put into an ice bath where water and ice are present, thus providing a constant temperature of approximately 0°C. As the medium which the two probes are sensing changes a relationship is formed between thermistor resistance and thermocouple voltage, which is the converted in the temperature, to ultimately produce a thermistor resistance to temperature relationship. If it were possible to keep the walls of the vacuum chamber at a constant temperature then there would be no need for the thermistor.

Chapter 3

Etching[*]

3.1 Introduction

Etching, the process of removing a film, is one of three crucial techniques in thin film technologies. Selective etching, via patterning through photoresists, enables the fabrication of engineered micro- and nanostructures. While GLAD thin films already exhibit columnar nanometre sizes, by developing an etching procedure it would be further possible to create microstructures composed of nanostructure. Since resonant frequencies of comb drive structures depend on mass of the structure, the integration of GLAD thin films into these devices would allow for wider frequency shifts as more analyte can be absorbed to produce a large mass shift.

Typical etching methods are calibrated for the removal of planar, low porosity films. New etching techniques and recipes need to be developed for GLAD thin films which exhibit a highly porous, columnar structure. Applying wet etches to GLAD thin films will cause clumping, known as the nanocarpet effect, due to capillary force between structures, and quick removal of film with limited control, due to the high

---

[*]Portions of this chapter have been published in "Reactive Ion Etching of Columnar Nanostructured TiO$_2$ Thin Films for Modified Relative Humidity Sensor Response Time" by M.R. Kupsta, M.T. Taschuk, M.J. Brett, J.C. Sit in IEEE Sensors

surface area in contact with the etchant [28–30].

3.2 Experimental Setup

The experiments detailed in this chapter were performed using commercial equipment, standard processes, and calibrated custom equipment.

3.2.1 GLAD Thin Films and IDEs

Films with vertical columnar morphology were grown by electron-beam evaporation of TiO_2 source material (3-6 mm pieces, rutile, 99.9% from Cerac, Inc.) using the GLAD technique, as detailed in Chapter 2. The substrate was held at $\alpha = 81°$ with a φ rotation speed of 6-8 rpm. The deposition rate was maintained at 1.1 nm s^{-1} measured at the QCM, which corresponds to 0.7 nm s^{-1} at the substrate. Films were grown to thicknesses of 880 nm, 2.7 μm and 4.7 μm. Oxygen gas was added during deposition to promote the growth of a more stoichiometric film. Chamber pressure was maintained at 6.0×10^{-5} Torr (8.0×10^{-3} Pa) by varying oxygen flow rate and the position of the high vacuum gate valve.

Aluminum films were also grown on top of the 880 nm TiO_2 films via electron-beam evaporation at a rate of 0.4 nm/s at the QCM for a thickness of 400 nm with $\alpha = 60°$. Shadow masks, fabricated by Stencils Unlimited and made out of stainless steel, were placed over the base films during evaporation. These samples also had a 200 nm aluminum layer grown on top of the Si wafer, prior to the 880 nm TiO_2 film deposition. By using a shadow masking technique it is possible transfer patterns onto the GLAD thin films using e-beam evaporation without extra process steps which involve solvents and solutions, which cause GLAD thin film clumping, typically used in photolithography.

Testable RH sensor devices consisted of 2.7 μm TiO_2 films of TiO_2 deposited

26

on countersunk IDEs, fabricated by Micralyne, Inc. The gold electrodes were countersunk into a SiO_2 insulating layer to produce a planar top surface, allowing the deposition of GLAD films with minimal shadowing defects. Traditional IDE structures have significant steps in height, which interferes with the shadowing during the GLAD process [62]. The electrodes used here were 3 μm wide with a 5 μm gap between adjacent electrodes. Typically, total IDE areas were 1 cm^2, though IDE areas of 0.64 cm^2 were sometimes used. However, sensor output is reported in terms of areal capacitance [F cm^{-2}], so the variation in area does not impact the results reported here.

3.2.2 Wet Etching

Wet etching does not require an elaborate setup, but caution must be applied as chemical are potentially hazardous if handled inappropriately.

The suitability of applying a wet etch to GLAD thin films was explored before continuing on with a dry etch recipe. The advantages offered by wet etch processes are that they are cheap to execute and would not require sophisticated equipment to perform. The etchant of choice is a buffered oxide etch (BOE or BHF) intended for SiO_2 [63], as no specific etchant exists for TiO_2 [40]. The etch was performed inside the Nanofab cleanroom at a temperature of 20°C. Samples were placed into the BOE and etched for up to 30 s. After etching the samples were rinsed with de-ionized water and placed into a beaker for transport to a critical point dryer.

3.2.3 Dry Etching

Initial testing of various dry etch recipes was performed with 880 nm films of TiO_2 deposited on Si wafer substrates (3 in. diameter, p-doped <100> from University Wafer).

Reactive ion etching of samples was performed in a PlasmaLab μEtch. CF_4 etch gas was added for a total flow rate of ≈ 100 sccm while chamber pressure was maintained at 1.2×10^{-1} Torr (16 Pa). Plasma power was provided by an RF source set to 100 W. Target voltages of −240 V to −280 V were observed. For some of the etches, a PTFE spacer was placed between the target and the sample. The circular spacer has a thickness of 0.4 cm and a diameter of 14 cm, fully covering the target.

3.2.4 Relative Humidity Chambers and Testing

The impedance response (magnitude and phase) of the sensors was characterized as a function of relative humidity. Sensor response changes as it is cycled through high and low humidities, previously observed [64]. To accelerate this effect to reach steady state sooner, each sensor was cycled through five complete cycles, from 0% to >90% RH and back. The last complete cycle was considered a stable characterization for the device, after the loading effect is complete, and before any significant sensor ageing can occur [64]. The device calibration is used to convert from impedance to %RH in the subsequent response time experiments. The devices were grown in a single deposition, and were tested sequentially. The RH characterization routine was a 96 h, continuous procedure. Each device was tested for 24 h in the calibration chamber setup, and then was tested in the response time chamber setup. Immediately after, each device was subjected to the 48 h UV treatment, followed by another 24 h in the calibration chamber setup and then an additional testing cycle in the response time chamber setup. The performance of the devices was very similar, despite the delay in testing subsequent devices.

The UV irradiation treatment of the IDE sensors, similar to previous work [64], consisted of an 8 W lamp (UVP MRL-58), placed 4.5 cm above the sample in air. This treatment has been shown to counteract film aging and increase the electrical
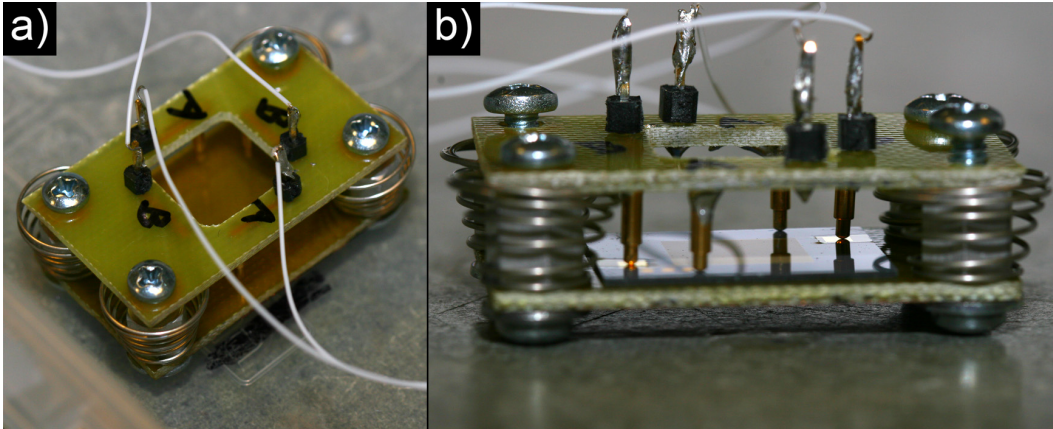
Figure 3.1: Nondestructive IDE sample holder used in testing and characterization of GLAD RH sensors. It replaced the method of applying conducive epoxy to the electrodes and embedding a wire into the epoxy mound. An oblique image of the holder is provided in a), and the holder with an IDE ready for probing is shown in b).

dynamic range.

A nondestructive method of interfacing the sample with the testing equipment needed to be designed as it was crucial to characterize the effects of each process step to the sensors response. The implementation of this design is depected in Figure 3.1; it consists of few parts: two copper printed circuit boards (PCBs), several screws, nuts and springs, spring contact pins, and header pins. The PCB were drilled to accommodate the screws, spring contact pins and header pins. A track was cut out in the PCB to route the contact pins to the header pins. The spring contact pins were aligned to contact pads on the IDEs. Figure 3.1b shows an IDE in the sample holder.

3.3   Experimental Results

Visual characterization of etch development was done by using an SEM to aquire an image of the sample. When the etches were applied to the sensors a more detailed analysis was done; effects on humidity response were studied via impedance and response time measurements.

3.3.1   Wet Etching

As different etch times were tested, it became quickly apparent that wet etching of GLAD TiO_2 is not a suitable method for controlled removal or alteration. Etch times of plain 880 nm films were on the order of 10 s. It was also observed that with the removal of the film, a white cloud was suspended on top of the solution, which indicated that the film was lifted off. Figure 3.2a and 3.2b show the removal of the film through wet etching, but it is clear that it is an abrupt transition. Since a BOE is specifically tailored to remove SiO_2, it is likely that the native oxide on which the GLAD thin film was deposited was being removed and thus removing the foundation for the film. It is evident that clumping of the film does occur when the film was just rinsed and dried in air, as seen in Figure 3.2a. By using critical point drying it is possible to minimize, but not eliminate, the effects of clumping, as seen in Figure 3.2b. Another factor to consider while using wet etching methods would be that the columns of a GLAD thin film exhibit narrow bases and broaden as they grow; therefore, if a wet etchant were used, it would attack the narrow bases more rapidly then the top of the film.

Although limited success was achieved using the BOE wet etch on the TiO_2 film, the pattern transfer experiment was nonetheless carried through. Using the patterned TiO_2/Al substrates, the etching experiment was performed again. Figures 3.2c, d and e demonstrate the result of this experiment. The etch did not

30
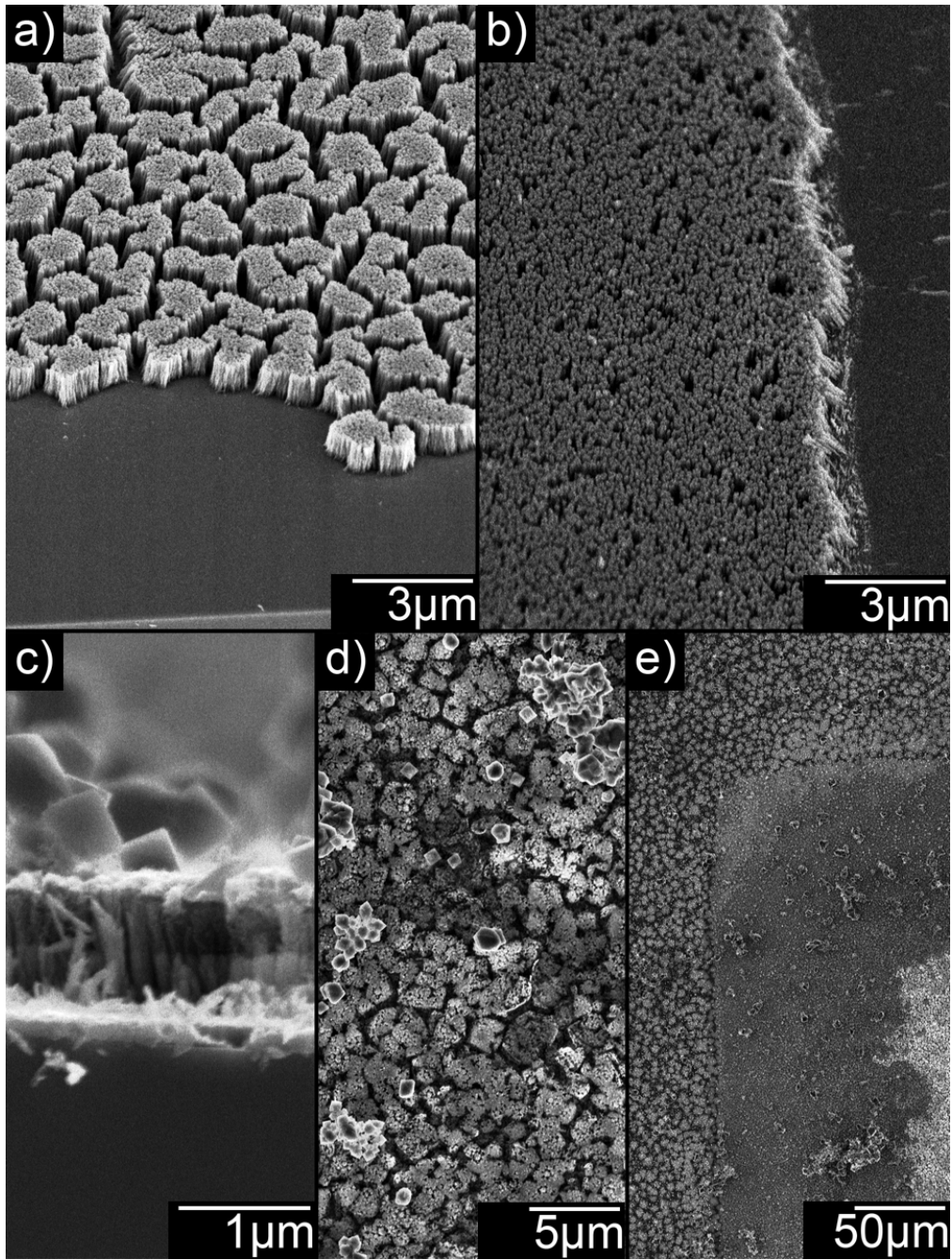
Figure 3.2: Wet etch effects on TiO$_2$ GLAD thin films a) severe clumping and b) reduced clumping with critical point drying. Etching of aluminum capped films: c) side view of TiO$_2$ GLAD film with AlF$_3$ crystals on top, d) top down view of crystals and, e) zoomed out image of unmasked and masked region after etching and critical point drying.

perform as expected even though the same underlaying base layer was used under the same etching conditions. The two aluminum layers are visible in the Figure 3.2c along with large crystals on top of the surface. A closer image of the crystals is shown in Figure 3.2d while a zoomed-out view showing minimal removal, but some clumping of the GLAD thin film, is shown in Figure 3.2e. Unfortunately, it became apparent that the hydrofluoric acid (HF) in the BOE solution reacts with the aluminum to form AlF_3 crystals [65].

It was clear that from these experiments done here that a different method of removal was needed, therefore a wet etch was not used.

3.3.2 Dry Etching

Base films

A series of 880 nm thick TiO_2 vertical post films were grown and later treated with CF_4 plasma etch (100 sccm, 120 mTorr, 100 W). The unetched film (Fig. 3.3a) is comprised of vertically aligned columns of approximate equal size and evenly distributed in the plane of the substrate. As grown, GLAD thin films exhibit a rough and textured surface. Towards the bottom of the film, columns whose growth has been extinguished due to the competitive growth process are observed. Both of these features add to the high surface area of GLAD thin films. All of our etches presented here began with samples from this batch.

Following Matsutani *et al.* [43], we used a PTFE spacer placed between the RIE electrode and sample to absorb free fluorine radicals generated in the plasma. Normally, samples to be etched would be placed directly on the metal RIE electrode. Fig. 3.3b shows the result of this 60 s CF_4 plasma etch with a PTFE spacer. Applying this recipe created channels 2–3 times the width of a single columnar structure, while the remaining columns retain a majority of their height and thickness. Many

extinct nucleation sites are removed and the column surfaces are smoother. A majority of the columns are not fused with neighbouring columns, but the initial stages of island formation are present. The results of longer etches are shown in Figs. 3.3c and 3.3d. As the etch times increases, the islands become more distinct and larger diffusion channels form. Although the columnar vertical striations are still visible in all the etches, the columns appear to be fusing to neighbouring columns. Film thickness is not strongly affected by the etch, decreasing by 10% for a 180 s etch.

Results of etching without the PTFE spacer are seen in Fig. 3.4. Obvious severe clumping of the columns occurs even for short etch durations. Increasing etch times result in removal of more material. As before, film thickness does not seem to be strongly affected by the etch duration. Mechanical failures and delamination in the etched films were not seen.

Patterned Films

Also explored were the effects of using an etch recipe consisting of 3:1 mixture of CF_4:O_2 [44] for a total flow of 100 sccm at 200 W of RF power. This proved to be the most potent recipe for etching the TiO_2, but was not suitable for the sensors. However it is suitable for pattern transfer as it can remove the film material completely.

An experiment was first done to see if a simple CF_4 etch recipe, used previously, would remove the film completely. The base film used was the 4.7 μm TiO_2 seen in Figure 3.5a. It is clear that even after 8 minutes of etching, the film has an insignificant change height and thus eches slowly. By using an etch recipe with O_2 and higher power, it was possible to achieve complete removal of the film. It is clear from Figures 3.5c, d and e that the etch has the ability to work downwards like seen in a typical etch of a planar film.
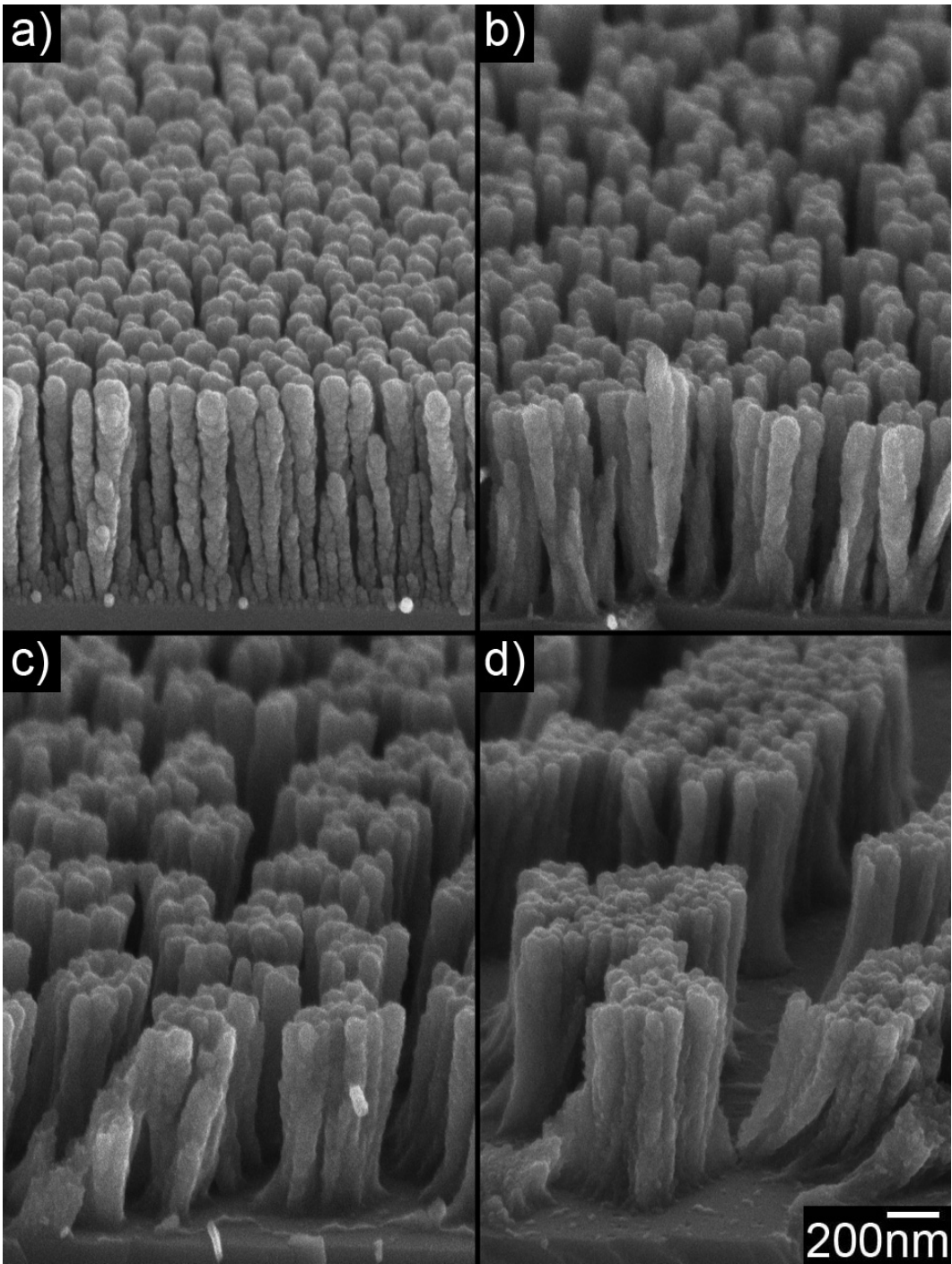
Figure 3.3: Effects of using a CF_4 plasma etch recipe (100 sccm, 0.12 Torr, 100 W with a PTFE spacer) on a 880 nm TiO_2 GLAD film: a) unetched, b) 60 s, c) 120 s, d) 180 s. [© 2009 IEEE]
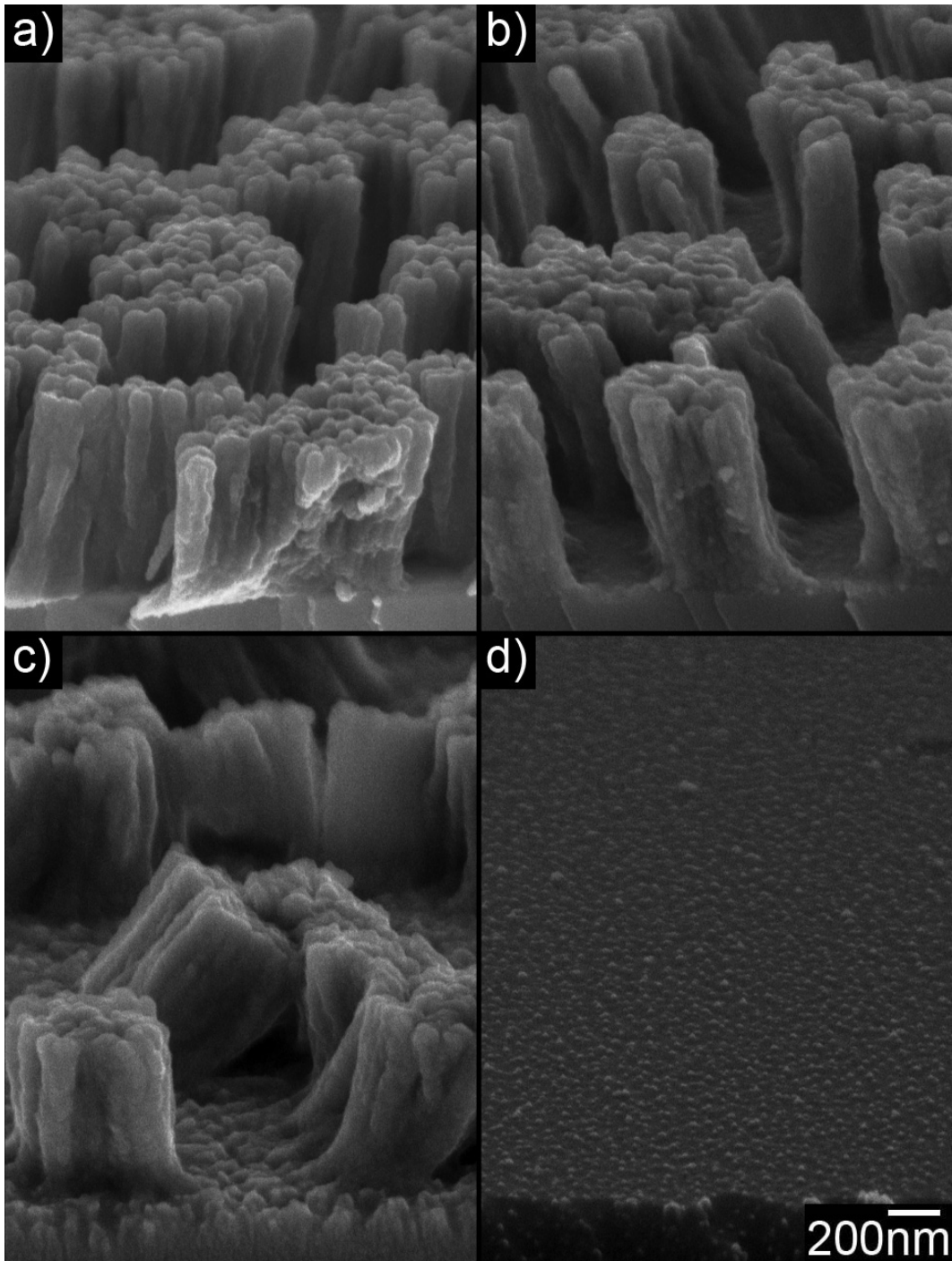
Figure 3.4: Effects of using a CF_4 plasma etch recipe (100 sccm, 0.12 Torr, 100 W without a PTFE spacer) on a 880 nm TiO_2 GLAD film: a) 30 s, b) 60 s, c) 180 s, d) 300 s. [© 2009 IEEE]
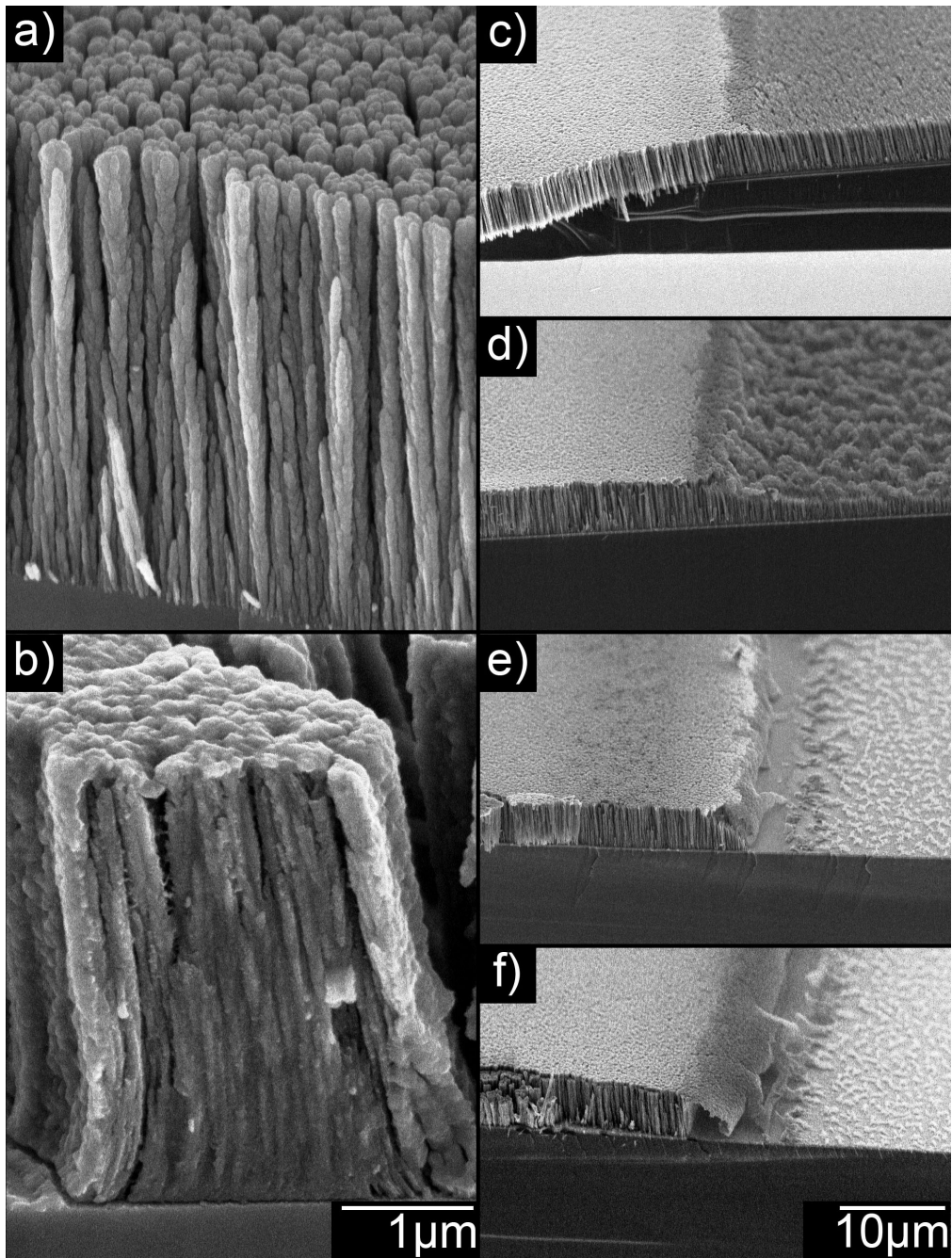
Figure 3.5: Shown in a) 4.7 μm TiO_2 base film, b) is film after 8 min with CF_4 etch. The series on the right is the same film with a with 200 nm of Al, patterned through a shadow mask. Etch recipe changed to include oxygen and increased power of 200 W: c) 1 min, d) 5 min, e) 10 min, and f) 20 min.

Although the etch recipe proved to be successful, using shadow masking techniques to transfer patterns has poor resolution and leaves very rough edges visible even at low magnifications.

Sensors

After exploring these different recipes, it was concluded that the CF_4 etch including the PTFE spacer was most appropriate for our sensors. To test device performance after these applying our etch, a set of 2.7 μm thick TiO_2 sensors (grown on IDEs) were produced. SEM images of the sensors before and after the etch process are given in Figs. 3.6 and 3.7. Cross-sectional views show the presence of larger columns growing at the edge of the electrodes [66]. These nodular columns illustrate how even small differences in height can result in large defects in a GLAD film due to the highly oblique deposition angles and sensitivity of the shadowing to the underlying topography. The top-down views in Figure 3.7 show how the defects at the edges are producing larger gaps in the film.

3.3.3 Sensor Characterization

Sensors were analyzed using several methods. Film structure was imaged by using an SEM (JEOL 6301F). Sensor response was investigated using two custom environmental chambers described in detail elsewhere [17]. In brief, sensor response time was obtained by monitoring step response to low and high humidity with a period of 60 s and calibrated against a commercial sensor after each process step.

Calibration

The environmental chamber setup was used to compare sensors against a commercial RH probe (Vaisala HMP100). Accuracy of the commercial RH probe has been
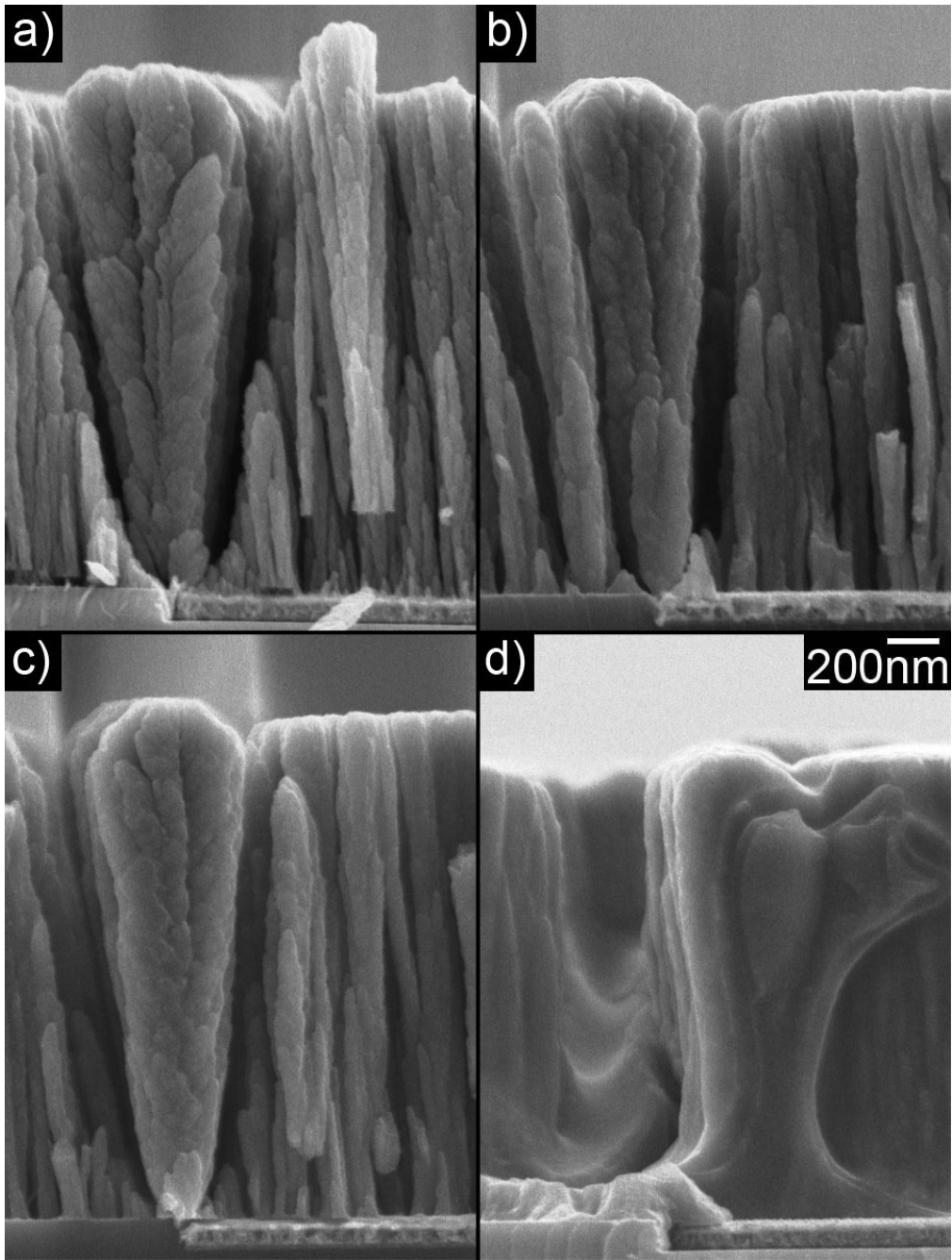
Figure 3.6: A side view of the unetched sensor is shown in a). All sensors shown begin with a 2.7 μm base film of TiO_2 with the large columns attributed to the defects on the SiO_2/Au interface. The sensors are then modified via a CF_4 RIE etch recipe tailored for GLAD thin films. Corresponding etch duration are: a) 0 s, b) 15 s, c) 30 s and d) 60 s. [© 2009 IEEE]
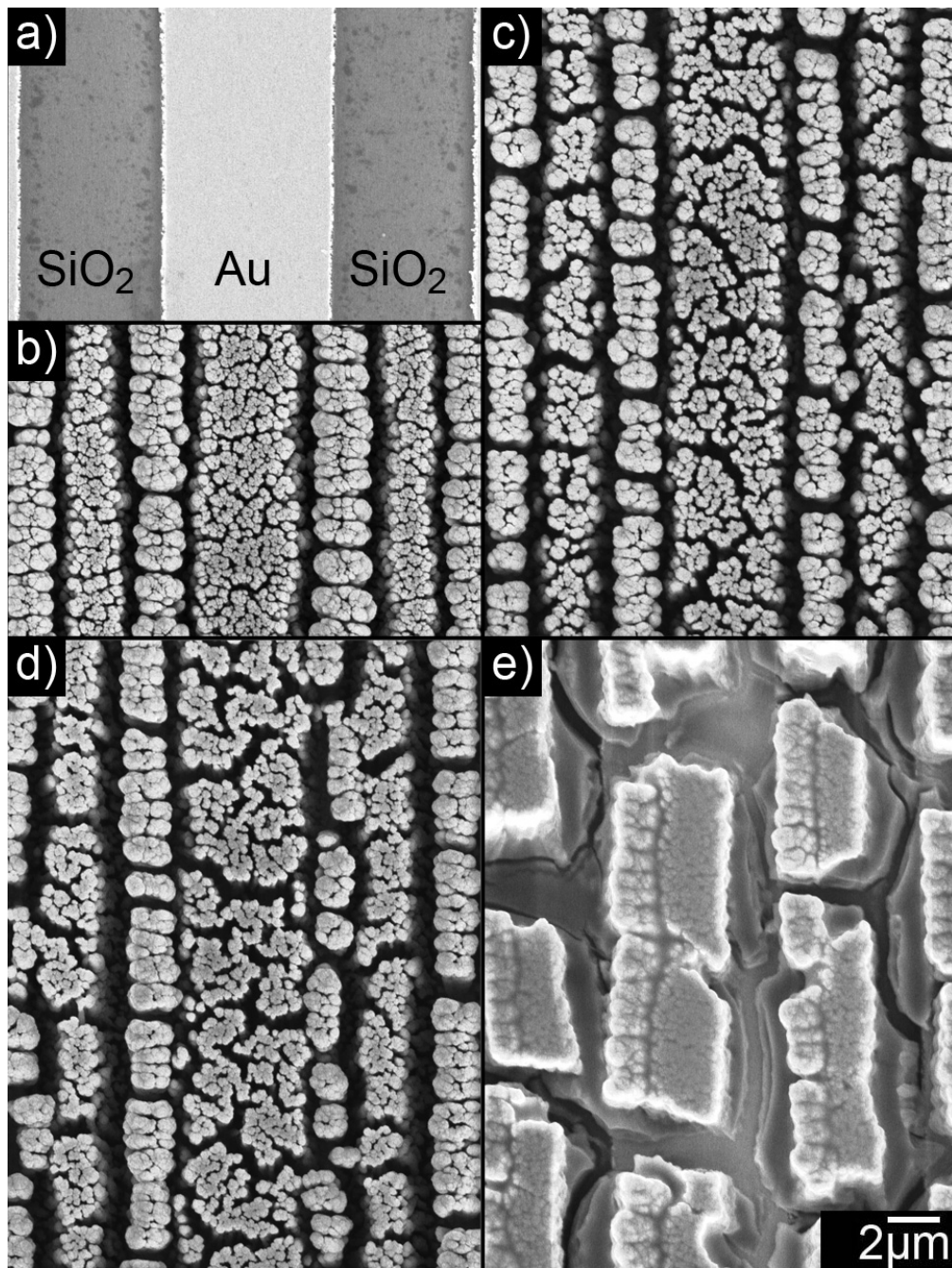
Figure 3.7: A top down view of the un-coated IDE is shown in a) whereas the as unetched sensor is shown in b). The resulting wide pores visible in b), c) and d) are responsible for the faster speeds observed here compared to unetched sensors. Corresponding etch durations are: b) 0 s, c) 15 s, d) 30 s and e) 60 s. [© 2009 IEEE]
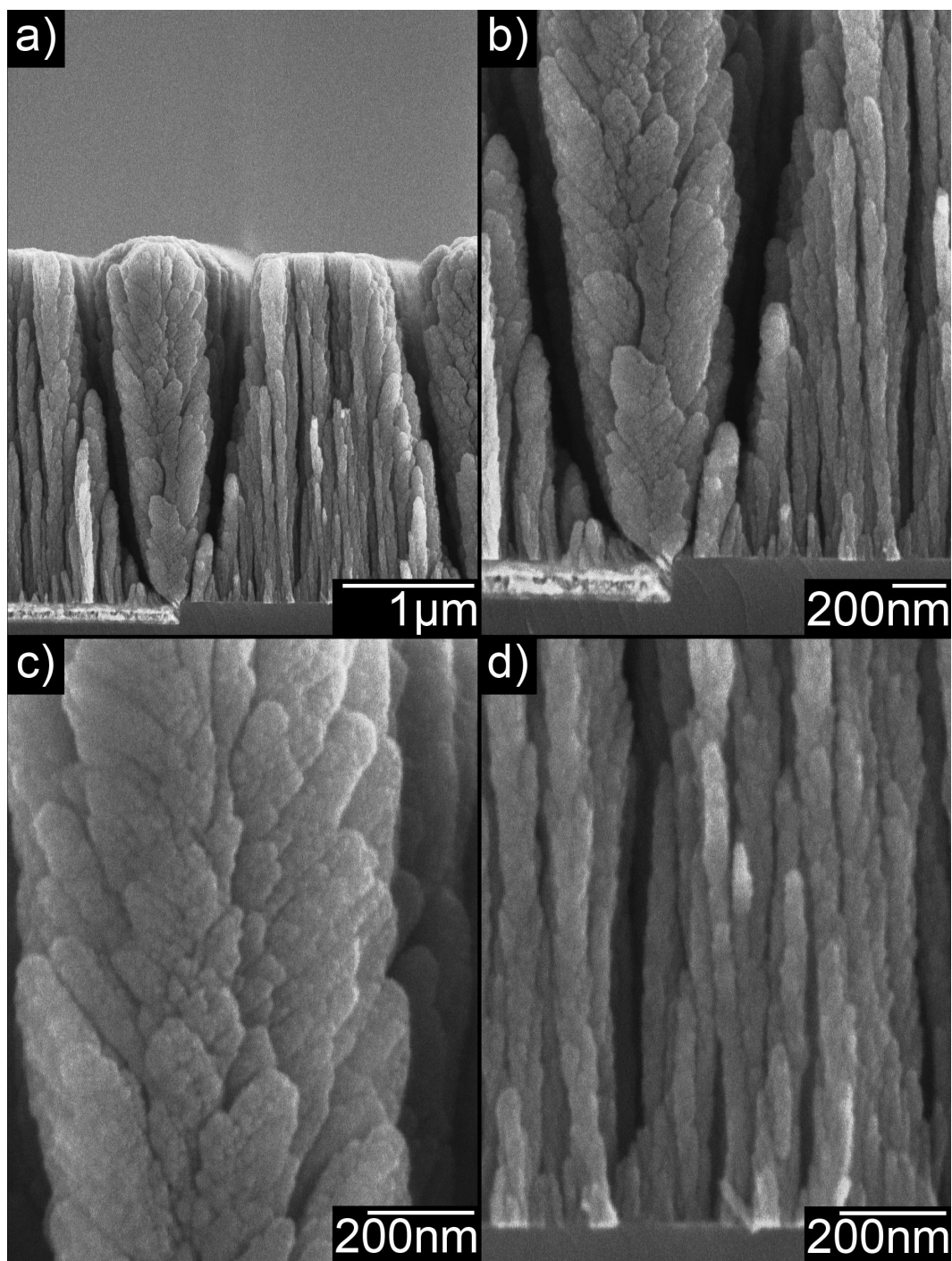
Figure 3.8: SEM images depicting defect post growth from a nodule formed on the interface between the SiO_2 and Au electrode of as deposited sensor. In b), defect post growth is shown to be starting from an Au nodule. A comparison between column structures features is shown in c) and d), where c) is the defect nodule column with numerous features/scales and d) shows regular GLAD film structure.

previously characterized and reported [17]. The electrical response of the sensor was measured using a LCR meter (1 kHz, 1 V_{rms}, Quadtech 1920). Two mass flow controllers (MKS M100B), controlled via PC software, were used to set the ratio of dry and moist nitrogen gas flowing into the small sample chamber. There was a 5 min settling time before the measurements were taken. Measurements were taken at room temperature; typical values were between 20°C to 22°C.

Typical data collected from this setup is shown in Figure 3.9 over a 24 hour period. In Figure 3.9a, the output from the commercial sensor is shown which indicates that indeed the chamber does cycle from high to lower humidities and that a 5 minute settling time is appropriate to achieve consistent values. The output from out sensor is shown in Figure 3.9b. By knowing the humidity of the chamber and the impedance of the sensor at that humidity we were able to construct a cross reference, Figure 3.9c, so that we could related the impedance characteristics to humidity values.

The electrical response of the unetched sample seen in Fig. 3.10a is typical of these devices: ≈ 2 nF cm^{-2} at 0% RH, increasing to ≈ 1 µF cm^{-2} at 92% RH. The device is capacitive at low humidities, but rapidly becomes more resistive as the RH increases. Limited hysteresis is observed above 50% RH. The operating range of the device is not strongly affected by the etch duration. However, the etch does introduce large changes to the shape of the capacitive response. As the etch time increases, a hysteresis is observed, which increases to nearly an order of magnitude for a 60 s etch. Device phase response is especially sensitive to the etch time.

The effect of the UV treatment reported previously on the etched devices was also investigated. The response of the unetched device with a UV treatment is given in Fig. 3.11. The capacitive response shape, the increase in operating range, and the introduction of a slight hysteresis around 60% RH are all consistent with our

41
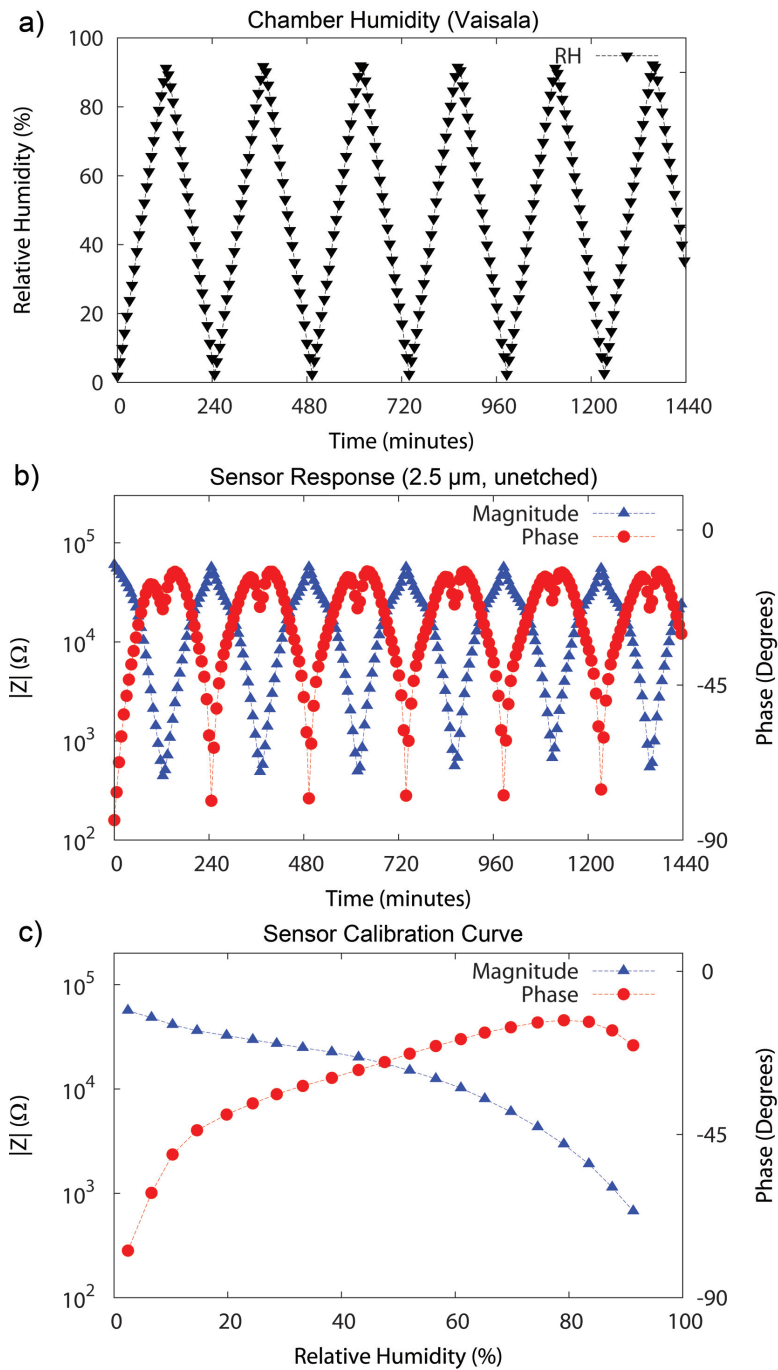
Figure 3.9: Typical calibration procedure for an IDC before step response measurement: chamber humidity, in a), is obtained using the Vaisala sensor. The senor response, in b,)is obtained through the LCR meter. Calibration of sensor, in c), is done through cross referencing the 5th complete cycle from a) and b).
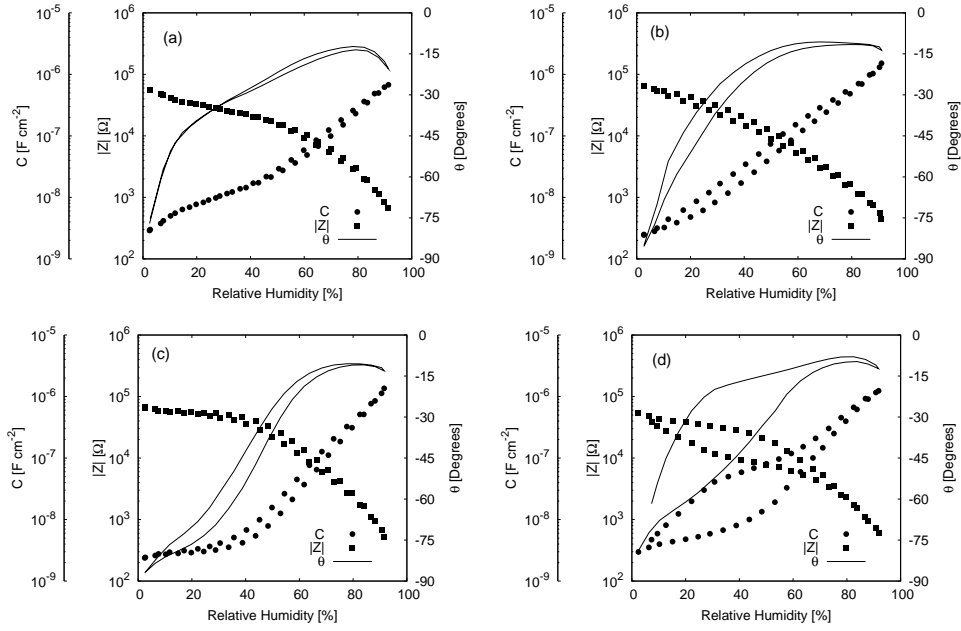
Figure 3.10: Capacitive, impedance and phase response of GLAD RH sensors etched for (a) 0 s, (b) 15 s, (c) 30 s, and (d) 60 s. [© 2009 IEEE]
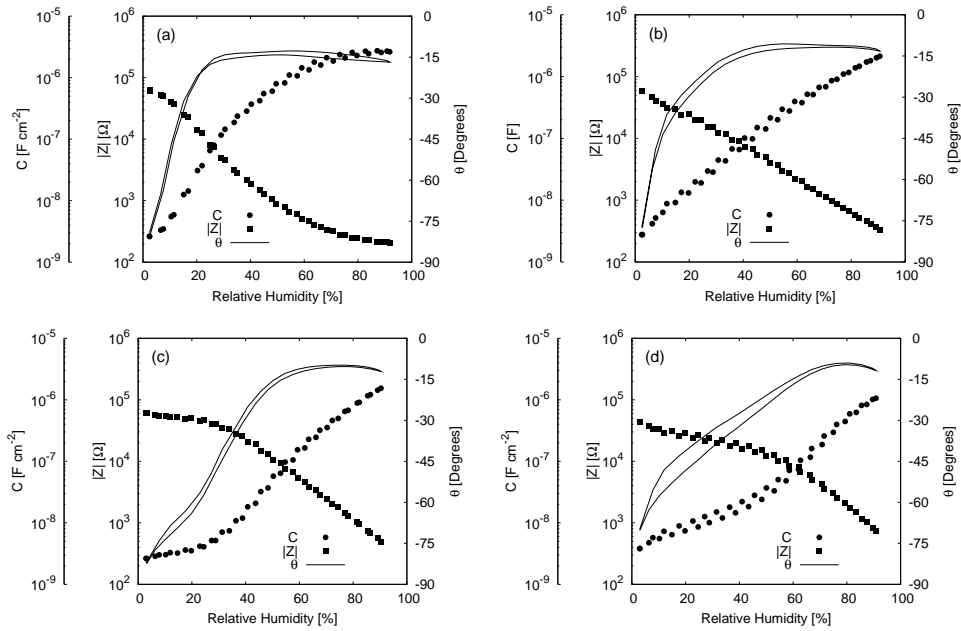
Figure 3.11: Capacitive, impedance and phase response of GLAD RH sensors etched for (a) 0 s, (b) 15 s, (c) 30 s, and (d) 60 s and then given the 48 hour UV treatment. [© 2009 IEEE]

earlier report [64]. The UV treatment has affected the phase response of the device. As in the as-deposited case, the device is capacitive at low RH, but the phase angle increases more rapidly to a limiting value of $-15°$. The operating range of the etched devices is increased slightly as a result of the UV treatment. In addition, the UV treatment has significantly reduced the hysteresis induced by the etching. The range over which the devices are at the limiting phase of $-15°$ decreases as the etch time increases.

Step Response

Two solenoids (Evolutionary Concepts Inc. 620-412N) controlled the flow between dry nitrogen and moist nitrogen. Flow rates were maintained at 2 L min^{-1} using flowmeters (Cole Parmer FF-32004-10). The capacitive response of the sensor was polled at a rate of 25 Hz using a LCR meter (probe signal: 1 kHz, 1 V$_{rms}$, Quadtech 1715). On occasion, our meter would log a new data point with identical values to the proceeding point. To maintain data integrity and ensure accurate fitting, such data points were removed.

Typical time-resolved sensor response for as-deposited, etched, and etched plus UV treatment are given in Fig. 3.12. The adsorption curves were fit with a single exponential rise, defined by

$$RH(t) = \begin{cases} y_0 & \text{for } t \leq t_0 \\ y_0 + y_1 \left(1 - \exp\left(-\frac{t-t_0}{\tau}\right)\right) & \text{for } t > t_0 \end{cases} \qquad (3.1)$$

where y_0 and y_1 are limiting values before and after the switch in RH, t_0 is the switch time and τ is the response time constant. The desorption curve was fit with a two component exponential decay, to capture the fast decrease after the switch as well as the long slow decay afterwards. The desorption curve model is defined by

44

Table 3.1: Adsorption and desorption response times (τ_1) as a function of etch duration. For etched sensors, measurements are limited by the LCR meter measurement rate.

Etch Time (s)	Adsorption (ms)	Desorption (ms)	UV treated Adsorption (ms)	Desorption (ms)
0	151 ± 4	129 ± 15	153 ± 12	135 ± 4
15	53 ± 5	67 ± 14	43 ± 14	56 ± 5
30	42 ± 3	50 ± 3	52 ± 17	52 ± 4
60	49 ± 8	52 ± 5	66 ± 16	46 ± 7

$$RH(t) = \begin{cases} y_0 & \text{for } t \leq t_0 \\ y_0 \quad -y_1 \left(1 - \exp\left(-\frac{t-t_0}{\tau_1}\right)\right) & \\ \quad\quad -y_2 \left(1 - \exp\left(-\frac{t-t_0}{\tau_2}\right)\right) & \text{for } t > t_0 \end{cases} \tag{3.2}$$

where y_0 and t_0 are as defined for Eqn. 3.1, y_1 and τ_1 describe the initial rapid decrease in signal, and y_2 and τ_2 describe the long, slow decay occurring afterwards. As seen in Fig. 3.12, the etched sensors respond on the same time scale as the 40 ms measurement interval of our meter. As a result, it was necessary to treat t_0 as a fit parameter to produce good fits.

The time constants for the as-deposited case are $\tau_1 = 151 \pm 4$ ms for adsorption, and $\tau_1 = 129 \pm 15$ ms for desorption, not including the desorption tail. Our measurements of response time after the etching and UV process are limited by the 25 Hz acquisition rate of the LCR meter. For adsorption and the fast component of desorption, the observed value is very close to the 40 ms limit of the LCR meter for all etch times. As a result, these numbers are not considered to be a reliable measurement of the sensor response time, but rather an indication that we are limited by the setup for all etch times. The numerical results are summarized in Table 3.1.
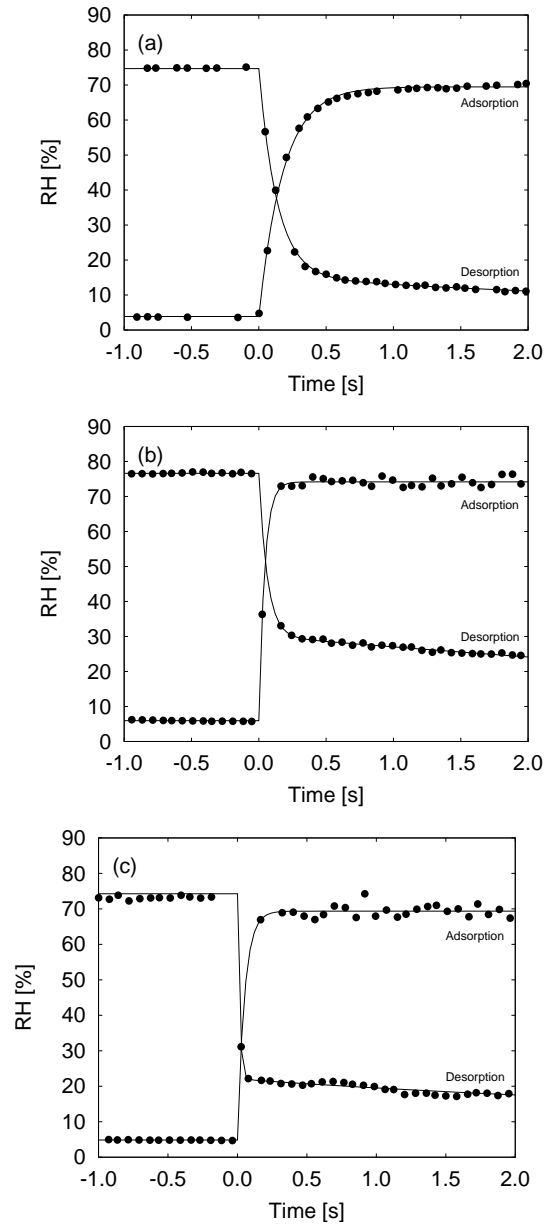
Figure 3.12: Time-resolved response of (a) as-deposited sensor, (b) sensor with 30 s etch, and (c) sensor with 30 s after etch and 48 h UV treatment. The solid lines in the figures are best fit to the functions described in the text: single exponential rise for the adsorption, and a two component exponential decay for the desorption. [© 2009 IEEE]

46

3.4 Discussion

The etch process presented has improved the adsorption times of our sensors studied here by at least a factor of 3. Furthermore, the fastest sensor produced here exhibits adsorption times that are approximately six times faster than previous, more uniform sensors [17]. However, the desorption times for our etched and unetched cases do not recover as well as previous sensors. We suspect that the longer desorption times are due to the nodular defects observed in our films. Previous sensors without long desorption times did not exhibit these defects. We note that this factor of 3–6 is a lower limit due to our equipment. Our conventional lab equipment only offered us reliable readings down to ≈ 50 ms. At the time of writing, no off-the-shelf device satisfies our requirements. We are confident that with the construction of a custom, high speed, impedance polling circuit, we will be able to better characterize the response of our sensors. While the results of the etch process are encouraging, several issues concerning sensor performance remain open for further investigation: etch damage to the films, the more pronounced desorption response tail, hysteresis, nonlinearity in response, equipment issues for accurate response time measurements, and the underlying physical limits of sensor readout time.

The CF_4 plasma etch is a suitable etchant for TiO_2 columnar thin films. Introducing a PTFE spacer between the substrate and electrode minimized post clumping and allowed smaller, more evenly distributed, channels to form. Possible explanations for this effect may be the reduction of electric field present at the substrate surface which in turn reduces the ion flux on the film (reducing the chemical reactions), or preferential adsorption of fluorine radicals by the PTFE [43] (reducing the physical etching). The CF_4 etch also reduces column roughness, with increased etch times leading to very smooth features. Smoothing of the columns could be reducing the effective surface area as well as decreasing the amount of analyte absorption

sites. Another possible effect that could lower the effective surface area is an etch byproduct coating the columns.

From the SEM images of the etching process presented in Figs. 3.3 and 3.4 one can see that our process is causing some of the columns to fuse together. The island formation may in part account for the somewhat reduced impact of the UV treatment by reducing the surface area optically accessible to the UV for devices with longer etch times, observed in Fig. 3.11. It is clear that the characteristic UV-induced capacitive response curve observed in previous work [64] and Fig. 3.11a is not visible in Fig. 3.11b. The clumping of GLAD columns may reduce the area accessible to the UV treatment for longer etch times.

We observed long desorption tails for both etched and unetched films. While the origin of this behaviour is not fully understood, we note that previous work indicates that adsorption times and desorption times can exhibit similar response curves, with a single exponential dependence for both [16, 17]. The growing conditions for our films were similar to the devices produced earlier except for increased deposition rate, which is expected to have minimal impact on in desorption/adsorption behaviours. Another, more plausible, difference is the planar quality of our IDEs which produce a significant difference in the film structure and thus the adsorption/desorption behaviour. These defects can be observed in Figures 3.6 and 3.7. The fact that we have previously produced sensors without the long desorption time noted here suggests that we should be able to combine the beneficial effects of both sensors with future work. It could be possible that the mechanism causing the longer desorption tails, is also present during adsorption. The difference between the two scenarios is that high RH is reported through higher values of capacitance, whereas low values of RH result in capacitance an order of magnitude smaller. Therefore if the mechanism accounts for a fixed magnitude shift in capacitance, it will be more

48

visible at lower values of capacitance (or low RH) and insignificant during higher values of capacitance (or high RH).

The presence of two time constants in the desorption curve may be due to the manufacturing defects shown in Figs. 3.6 and 3.7. These large columns (defect posts) formed on the interface between the electrode and SiO_2 insulating layer have a volume larger than surrounding columns with different surface properties. Our devices are therefore composed of a nonhomogeneous film with two distinct column populations, each responding differently to the change in surrounding humidity. Water that adsorbs to the internal surface area of the defect posts may exhibit an "ink bottle" effect, where desorption is limited by narrow constrictions in which water vapour may remain condensed below the equilibrium dictated by the Kelvin equation. In such cases, a hysteresis is also expected, which we observe in our current results.

Another interesting point related to the defects seen in Figs. 3.6 and 3.7 is the fact that the as-deposited sensors presented here are faster than thinner sensors produced earlier: adsorption times of 151 ms for a 2.7 μm film for the present study compared to 365 ms for a 1.5 μm film produced for an earlier study (previous report also corrected for chamber mixing time; 365 ms value includes 90 ms chamber mixing time) [17]. By applying our etching procedure we can purposefully create larger diffusivity channels with the ability to optimize the process for optimum performance. In general as sensor film thickness increases the response time decreases, so this factor of 2 difference is quite significant. The films produced for the earlier study do not exhibit the defects noted here, likely due to the use of a different batch of IDE substrates. We expect that the presence of these defects act as high diffusivity channels to the bottom of the sensors, essentially duplicating the effect of the etch process studied here. The etch process would be expected to show an

49

even greater improvement to a more homogenous film than that reported here, since the starting point of such a sensor would be much slower. While the films produced on defect-free substrates are more homogenous, the response time of a sensor on a substrate with defects is much improved, and without any noticeable reduction in the device's dynamic range. Closer observation reveals that an unetched device with a defect-filled film responds faster than the homogenous film. These features are not always present, as seen in previous reports [16, 17]. These nodular artifacts offer insight to the manufacturability of the RH sensors by showing that the process has a high defect tolerance. Introducing defects to, or seeding, the substrate has been used previously to produce extremely porous films [67].

The large improvement on sensor response presented here has caused us to refocus our attention on the testing apparatus. The results here are limited due to the use of commercial LCR meters, which require a measurement period longer than the response time our sensors now exhibit. The use of custom electronic readouts is an obvious path forward, but we may in fact be facing a more serious physical limitation in the near future. The results presented here are for a 1 kHz probe signal, which imposes a fundamental limit on the measurement speed which will be possible. While the use of higher frequencies is possible, the dielectric constant of water decreases with frequency [68].

A possible mode of operation which may avoid this limitation would be the use of phase as the sensor readout. This approach would be relevant for climatological applications, which require high speed measurements at low concentrations [20]. However, in general, there will be a tradeoff between sensor electrical dynamic range and sensor response time. To optimize the performance of our sensors for a broad range of applications, it will not only be necessary to implement a more sophisticated electronic readout scheme, but also to characterize fully the frequency-dependent

50

response of our sensors.

3.5 Conclusions and Improvements

A CF_4-based dry etch recipe, suitable for TiO_2, was tailored for modifying GLAD RH sensors and pattern transfer. Using a PTFE spacer in the RIE chamber, etching characteristics can be modified to create high-diffusivity channels for sensors while reducing the physical etching performed by the ions. Along with the improvement in sensor response characteristics, post-deposition 48 h ultraviolet irradiation of TiO_2 nanostructured RH sensors was shown to reduce hysteresis introduced by the etch. Finally, by introducing O_2 into the etch recipe, it was possible to achieve efficient removal of TiO_2 GLAD thin films, making this etch recipe a suitable candidate for pattern transfer, with the use of an aluminum masking layer. Pattern transfer was achieved by using a shadow masking on top of the GLAD film, which was able to produce low resolution features. Under low magnification SEM the edges were jagged. Etching caused the edges to curl and collapse indicating poor structural stability which is possibly due to the thickness gradient inherent to shadowing masking.

By applying a CF_4 etch recipe to GLAD based RH sensors it was possible to modify the response time from ≈150 ms to an instrument limited ≈50 ms. Although desorption tails seemed to become more significant with the application of the etch, a possible solution would be to use higher quality, more planar, IDEs therefore minimizing the creation of the defect posts seen on the interface between the Au electrode and SiO_2 insulating layer. To be able to fully characterize the sensors response, a custom impedance measuring circuit should be designed and implemented. A possible solution is to use high speed analog-to-digital converters that have adequate resolution along with pulse generating circuit to stimulate the sensor. Another potential solution would be to use capacitance to digital converters. This improvement

51

could also be integrated into a microcontroller based data acquisition circuit which also has control over the gas flow solenoid switching.

The sample holder that was designed could be modified and incorporated into a custom humidity chamber for a more streamlined system. Since sensor response is modified by the application of UV radiation, the holder could be fitted with an ultra violet LED illuminating the sensor. This UV LED would controlled for duty cycle and exposure duration. Since current humidity chambers are larger then what is need, a smaller container should be designed. This would also assist in sensor placement consistency, thus eliminating a source of error in response time by misalignment between the sensor and the gas port.

By further tailoring the etch recipe it may be possible to achieve better results with GLAD thin films. Experimenting with RF power, chamber pressure, etch duration and feed gas ratios may ultimately lead to better column thinning as opposed to clumping, needed for RH sensor modification, and anisotropic etching, needed for pattern transfer.

Pattern transfer via shadowing masking could be improved by developing a better method of minimizing the distance between the mask and the substrate. A potential solution would be to embed magnets into the substrate, while producing a mask out of a ferromagnetic material such as stainless steel.

Chapter 4

Depositing onto Heated Substrates

4.1 Introduction

In a physical vapour deposition (PVD) e-beam system, atoms evaporated have a high energy content compared to their solid state counterparts. Heat of vapourization is the major component in an energy calculation of the evaporated atom: Titanium's heat of vapourization is 425 kJ/mol compared to the specific heat at its melting point (1941 K) of 49 kJ/mol. In the literature, thin films by GLAD or related techniques have been predominately grown on substrates at the "room temperature" range, and with no active temperature monitoring or control even though significant amounts of energy are being transferred into or out from the substrate through condensation of matter, conduction, and radiation. This chapter details the design and implementation of a system for *in situ* substrate temperature monitor and heating that can maintain elevated temperatures between 150°C and 400°C. With this increase in substrate temperature adatoms are more mobile before settling,

changing film properties, such as broadening and film stress. Growing glancing angle deposited (GLAD) thin films at elevated temperatures onto seeded substrates could be used to match column diameter with seed diameter. Another consequence of higher adatom mobility, while depositing thin films at lesser oblique angles, would be to have the ability to obtain a higher quality planar film with less stress. This lower stress film would lend itself to be used a capping layer for GLAD thin films. A high quality capping layer would allow the underlaying layer be hermetically sealed from atmosphere, making GLAD more suitable in microfluidic applications, it would also allow for more ideal conditions for standard lithographic pattern transfer. By using lithography with a GLAD film device layer would allow the development of highly sensitive gas/mass based sensors due to GLAD thin film's high surface area and MEMS sensitivity to mass shifts.

4.2   Experimental Setup

4.2.1   Design and Installation

Many revisions have taken place to reach the final setup detailed below. The first revision used a 250 W infrared heating bulb from Phillips, typical for heating food or in bathrooms, which was installed inside an unused 6-inch port in our AXXIS deposition system. The chuck needed to be angled at $\alpha = 45°$ in order to face the heat source. The second iteration added insulation of the chuck using glass spacers while coating the front face of the chuck with black ceramic paint. The purpose of the glass was to insulate the substrate holder from the rest of the system so as to maximally retain the heat energy in the chuck. The purpose of the paint was to increase the emissivity of the surface as to absorb more infrared energy. Although temperatures of 250°C were possible, the heating time was 2 hours and caused

unwanted heating of the entire system. The main shortcoming of this setup was that the heat source was too far away from the intended target, 30 cm, which did not allow for adequate focus onto the substrate.

The next iteration of this system was to locate the heating source closer to the chuck. A 500 W quartz halogen bulb was placed behind the chuck using porcelain/ceramic mountings typical for 119 mm bulbs. This setup allowed for the use of a reflector which not only allows focusing but also allows the radiation from the source to heat the chuck directly. A ceramic holder for the bulb was taken from a flood lamp, typically used at construction sites to provide light.

Further improvement to the design was made by replacing the single 500 W bulb with two 250 W bulbs. These bulbs are 78 mm long and allow for a tighter, more compact design which will be needed for the installation of an LN_2 cooling system detailed in Chapter 5. This modification also allowed for heating to be distributed more evenly across the chuck and possibly reduced temperature gradient formation. Custom reflectors and brackets were manufactured to accommodate the shorter bulbs. The material of choice is stainless steel as it has a much higher melting point then aluminum, which was used as the original reflector. The original aluminum reflectors failed catastrophically by deforming and melting. Once the reflector was lost, chuck temperature would fall rapidly regardless of the power output of the lamps.

A variable power source was used in order to allow the substrate holder to be heated to specific temperatures coupled with real time temperature monitoring using a T-type thermocouple. A variable transformer with an input rated for 120 VAC at 5 A, was suited to provide voltages between 0 - 130 VAC at 5 A. Connection to the lamps was made through a 6–pin feedthrough where 2 pins were for the lamp power, 2 pins for the thermistor and remaining pins were for the thermocouple. Figure 4.2
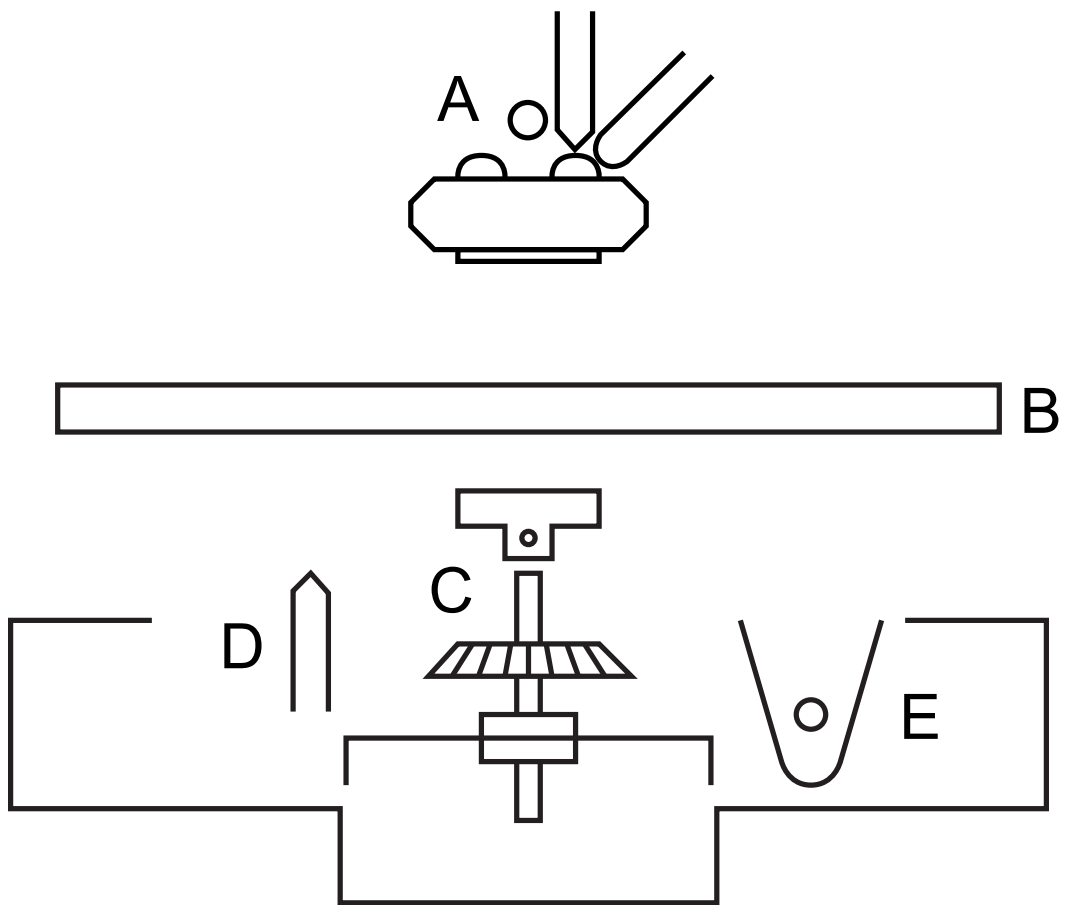
Figure 4.1: Mechanical schematic of substrate heating system: A- Thermistor and thermistor in contact with cold water cooling line for QCM, B- OFC chuck, C-interchangeable head piece, D- T-type thermocouple for probing chuck temperature, E- lamp heat source.
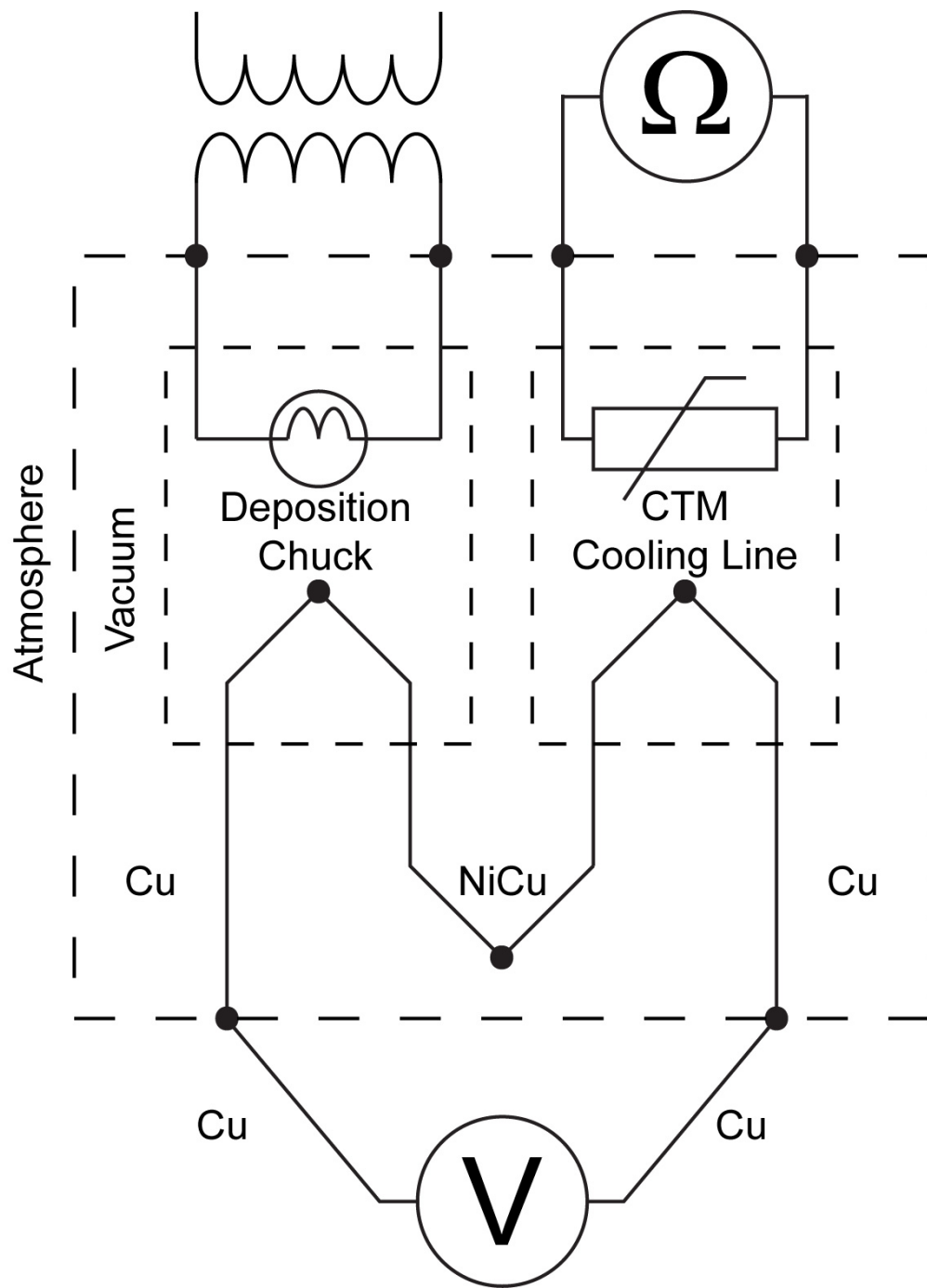
Figure 4.2: Electrical schematic of substrate heating system depicting external feedthrough connections and internal connections. Two DMMs are outside the vacuum to measure voltage output from the T-type dual thermocouple circuit and thermistor resistance. The variable transformer supplies power to the bulbs inside the vacuum.

gives a schematic of the electrical connections inside and outside the vacuum. The dual thermocouple setup, described in Chapter 2, was used.

Power transfer inside the vacuum was done by using 16 AWG copper motor lead wire. When running the wire near the bulb, which emits enough heat to char the enamel on the wire, alumina tubes were used to protect the wire from shorting to the metal arm and also assisted in fastening down the wires. Sufficient slack in the wire was left to allow α rotation from 180° to 0°. With the heat source now inside the deposition arm, there was no restriction at which angle heating of the chuck could occur.

Temperature measurement of the chuck was initially achieved by placing a stationary thermocouple in the vacuum which would physically contact the backside of the rotating chuck. Initial design of the temperature measurement circuit was simple and consisted only of a single thermocouple, through the feedthrough, being read with an assumed 20°C offset due to feedthrough junction being room temperature. Unfortunately this was a flawed approach: as the chamber would warm up, the junction created at the feedthrough would warm up and cause the measurement to drift. A refinement of the thermocouple circuit included the use of a second thermocouple and a thermistor, both attached to the water cooling line of the QCM. This setup is called cold junction compensation, explained in Chapter 2. For minimal temperature drift, the second thermocouple and thermistor were placed on cooling water line for the QCM. With the two in close proximity, on the QCM, it was possible the determine the temperature of the thermocouple from the calibrated thermistor. The third iteration of the measuring setup rose from information that K-type thermocouples are of limited suitability to vacuum environments, which prompted a switch to T-type thermocouples. Contact between the thermocouple and the chuck was maintained through an apparatus that sandwiched the thermocouple wire between

58

Table 4.1: Material Property Comparison for Fabricating System Parts

Material	Melting Temperature (°C)	Thermal Conductivity (Wm^{-1}°C^{-1})	Thermal Expansion (°C^{-1})	Electrical Conductivity (ohm-cm)	Emissivity (unitless)
Aluminum	658	220	24×10^{-6}	3×10^6	0.09
Copper	1080	388	17×10^{-6}	1.7×10^6	0.07
Macor	1100	1.46	9.3×10^{-6}	10^{16}	0.90
Fused Silica	1140	0.55	7.9×10^{-6}	10^{16}	0.88
Stainless Steel	1370	16	16×10^{-6}	7×10^7	0.30

two pieces of glass, which ensured thermal isolation and pressure needed to keep the surfaces in contact.

4.2.2 Isolation and Energy Transfer

A typical AXXIS system is made of stainless steel with certain parts made of aluminum, like the rotating shaft/head pieces used for substrate motion. Metals are typically known for their good heat conduction and low emissivity. Temperatures of 400°C, which is uncomfortably close to the melting point of aluminum, are easily obtainable using this design. Experiments that were conducted at 400°C while using an aluminum chuck caused the chuck to deform. Therefore, a new design was needed to isolate the substrate holder from the rest of the system to minimize heat damage and to select materials with suitable melting points to preformed under these conditions. Table 4.1 provides a comparison of different material properties [69, 70].

Absorption

Our deposition chucks are typically made of aluminum. Polished aluminum, or any metal in general, has a very low emissivity as it is highly reflective. Paints are cheap, easy to apply, are very good absorbers of IR and enhance emissivity

59
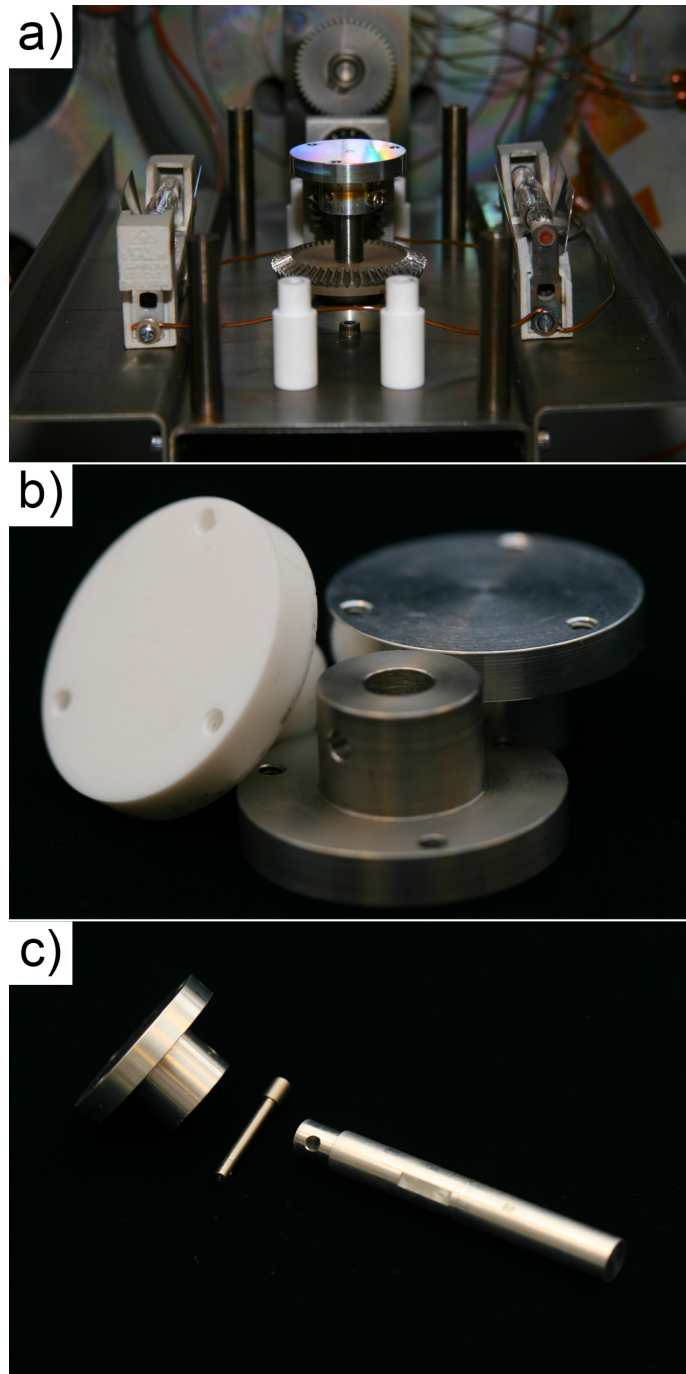
Figure 4.3: The depiction of the heating installation: a) the dual lamp setup, b) the interchangeable head pieces (left Macor, bottom stainless steel, right aluminum), c) new shaft assembly consisting of head piece, pin and stainless steel shaft.

and absorbtion of reflective surfaces [71]. Since the chuck will be exposed to harsh environments such as high vacuum and high temperature, a suitable paint had to be selected. NASA has done extensive work with regards to absorption of infrared (IR) in ultra-high vacuum (UHV) conditions [72]. It is possible to purchase high heat ceramic paint from a local hardware store. The main difference is that we are not as concerned about outgassing due to our deposition design, as the AXXIS systems are equipped with a Model 10 On-board Cryo-pump from CTI-Cryogenics, capable of high pump speeds (9000 L/s for water). Therefore any outgassing, albeit small, will not compromise the quality of the vacuum. The main limitation of these systems is that they are lined with viton seals (*e.g.*, on the chamber door), limit the AXISS system base pressures to $\approx 5 \times 10^{-8}$ Torr. The black ceramic paint used is made by DuPont. Three coats were applied after which the chuck was allowed to dry for 15 min. The painted chuck was then placed into an oven to cure at 150°C for 48 hours. This ensures a majority of the solvents used to aerosolize the paint have evaporated but also cures the ceramic for optimal performance when heated. The final finish on the chuck is a matte black.

Conduction

To allow for substrate tilt and rotation (α/φ), the chuck has to be mounted to the deposition arm. This is accomplished by connecting the chuck to the rotating shaft. For an unmodified system, this shaft is made out of aluminum which when coupled to the aluminum chuck by using stainless steel screws will make good thermal contact. Macor was the ideal candidate for insulating head piece. Macor, which is vacuum compatible, is machineable ceramic made by Corning. It has a sufficiently high working temperature (1100°C), and low thermal conductivity. A key design consideration was to maintain the ability to return the system to its original con-

61

figuration for other users of the system. Therefore a new shaft was designed and fabricated out of stainless steel and is depicted in Fig. 4.3. The shaft was split into two pieces, the head piece and the main shaft which remains semipermanently installed in the system. Multiple head pieces were fabricated: aluminum, stainless steel, and Macor. All head pieces have a through hole, which accommodates a pin to ensure the head piece stays connected to the shaft. The head pin also has a hole which fits a cotter pin so the head pin cannot slide out. This ensures a tight fit with minimal backlash and play, a set screw is used through a tapped hole in the head which aligns with a dimple drilled into the shaft.

Emission

Since one of side of the chuck (front, which is where samples are mounted) remains polished, emissivity remains low, but with the painting of the backside of the chuck emissivity was increased. This modification works for better and for worse: increased absorption of energy through IR radiation from the lamps, but also increased emission of energy through IR. Therefore, areas that are being illuminated by the quartz halogen bulbs have a net energy transfer to the chuck. Areas not illuminated are emitting net IR energy into the deposition arm and the surroundings. To minimize the loss of energy from the chuck through emission, the inside of the deposition arm was lined with aluminum foil, shiny side facing the chuck such that energy radiated from the chuck can be reflected back.

4.2.3   Measurement

To measure the temperature of the chuck, the thermocouple junction is placed in contact with the back side of the chuck. There are many different metal junction combinations that can be made, all of which have properties suitable for different

environments. For these thermocouples to be assigned a letter designation they must meet specifications as set out by the National Institute of Standards and Technology (NIST) [58].

The final selection for the thermocouple was chosen on its minimum and maximum temperature range, its vacuum compatibility, and lack of Curie point. A thicker gauge of wire was selected for its ability to handle higher temperatures. The insulation was also stripped back in order to reduce the possibly of melting the Kapton insulator.A tension needs to be induced when forming a contact between the chuck and the thermocouple; therefore, the thermocouple was bent so that it would act like a spring to ensure continuous contact with the chuck. A holder was made to provide a foundation for the thermocouple, it was placed between two pieces of glass which act as a thermal insulator and which are pressed between two brackets which hold onto a stainless steel standoff mounted to the deposition arm. A further enhancement that was made to the chuck was to cut a shallow groove into the chuck so the thermocouple can be confined into the groove as the chuck rotates.

Before placing the thermistor into vacuum, it was calibrated against the two thermocouples by using an ice bath experimental setup. This set up consisting of placing the junctions that are made to the multimeters into a water bath filled with crushed ice. This ensures that the junction temperature is roughly 0°C which allow for the use of NIST tables which are based on junction temperatures of 0°C. A more comprehensive explanation of thermistor calibration is provided in the next section.

Once thermistor and thermocouple signals have been brought outside of the vacuum chamber, they are connected to two digital multimeters (DMM), the Agilent HP 33401A and the Fluke 83. The Agilent is capable of taking measurements of voltages signals in the μV range, suitable for thermocouples, and a Fluke allows for a simple readout of the resistance of the thermistor. Therefore the readout from the

thermocouple circuit will consist of the voltage produced by the thermocouple on the chuck and this will be offset by the voltage produced by the thermocouple on the QCM cooling line. Since the temperature of the thermocouple is known through the thermistor which has been calibrated, the offset induced can be accounted for and the actual temperature of the chuck can be determined either by using the NIST polynomials, or by the look up tables.

4.2.4 Thermistor Calibration

It was required to have a reliable method of measuring the temperature of the chuck. Ensure confidence in our setup, we calibrated the thermistor against the T-type thermocouples. Since the T-type thermocouples are NIST certified we could use them as our calibration standard.

The apparatus used to calibrate the thermistor required that the junctions that the thermocouples made with the test leads to be at a known and fixed temperature. A 1 L glass beaker was used, filled partly with cold water and topped up with crushed ice. This ensured that the temperature inside the beaker would be at or very near the melting point of water $0°C$. To obtain data of the performance of the thermistor, a second beaker was used where the thermocouple junction and the thermistor were immersed in water as well. This bath was filled with water that had been brought up to boil. With the use of a syringe, hot water was removed and cooler tap water was added to the second beaker to lower the overall temperature of the bath. The water was stirred until a stable temperature was obtained in the beaker upon which a measurement would be taken. Using the NIST tables, which are referenced using an ice bath setup, a series of measurements were made of the water temperature of a variable temperature bath.

The Agilent 33401A and the Fluke 83 were used to acquire data from the exper-

64
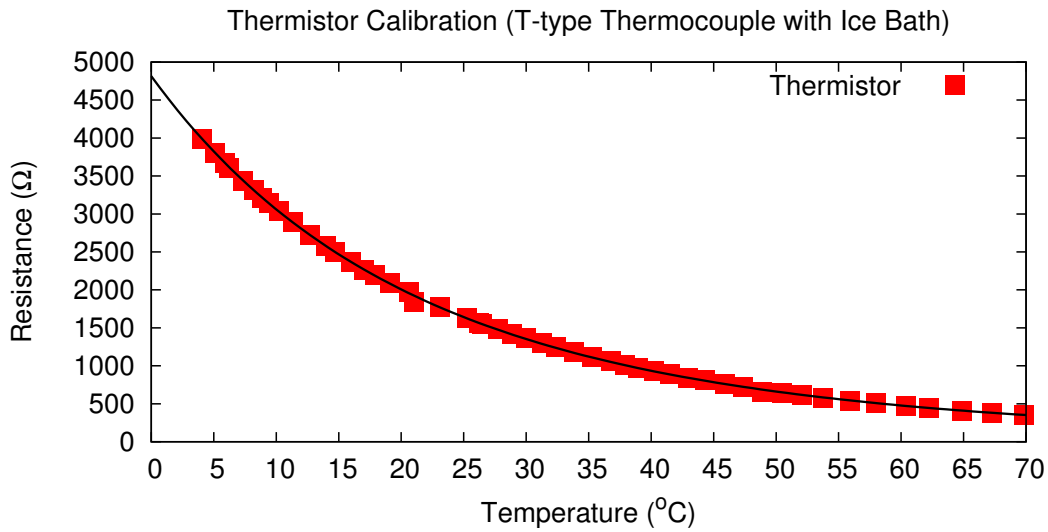
Figure 4.4: Calibration of thermistor against T-Type thermocouple using CJC. Sensing temperature was varied by exchanging boiled water from beaker and replacing with cold water using a syringe.

imental setup for thermistor calibration, as presented in Figure 4.4. An empirical exponential equation of the form

$$y = a \cdot e^{\frac{b}{x+273.15}}$$

was used to fit the collected data.

With the calibration of the thermistor completed, it was then possible to obtain an accurate performance of the heating system in vacuum. A test with the dual bulb setup was performed as well as a test with only one bulb. The results from these two runs are presented in Figure 4.5. An empirical decaying exponential equation of the form,

$$y = a \cdot \left(1 - e^{\frac{x}{b}}\right) + c,$$

was used to quantify the system. An interesting note to make from the data obtained
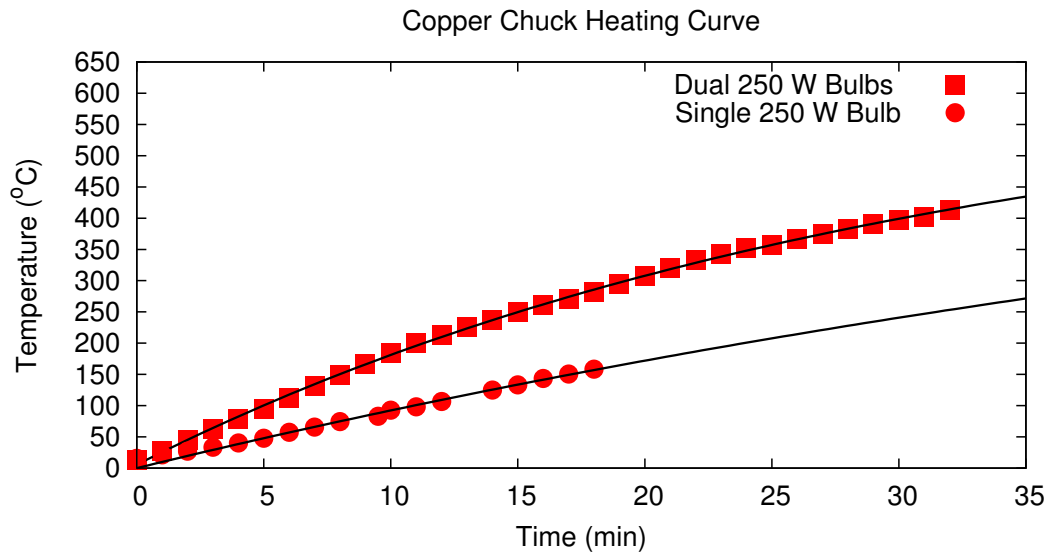
Figure 4.5: Heating of painted copper chuck using single and dual 250 W bulbs set at 120 VAC.

from the heating curve is that setup should reach a temperature of approximately 600°C with sufficient time.

4.2.5 Precautions and Usage

Since extreme temperatures and high currents are inherent to the high power heating system, a few extra steps and precautions need to be taken when attempting to use the heating system effectively and safely.

When replacing the headpiece with the Macor headpiece it is important to fasten the pin that goes through the headpiece and through the stainless steel shaft so it doesn't fall out during rotation. Tightening of the set screw on the that is 90° of the through hole will minimize error introduced by the loose fitting headpiece as mentioned in Section 4.2.2 and depicted in Figure 4.3. When mounting the chuck onto the Macor headpiece it is important not to over tighten the screws as Macor is a glass/ceramic and does not handle shearing forces very well, much like glass.

Before the pump down procedure, it is important to check the electrical connection of the lamps to the variable AC transformer. Before turning on the transformer it is important to check for any short circuits in the wiring. Ensure the DMMs are functional and that the thermocouple and thermistor are connected to their respective meters. Since proper foiling is a necessary step under normal conditions (to minimize system contamination and speed up cleaning) special attention should given to avoid introducing extra paths of thermal conduction to the rest of the system from the chuck. Special care should also be given in protecting the cryo pump from unintentional heating by placing foil in between the deposition arm and the cryo baffles yet still allowing for proper pumping of the system. During normal operation of the heating system, the deposition arm and the substrate substrate will warm up and emit more than a normal amount of radiative energy which has the potential to compromise the operation of the pump.

Energy that is radiated from the chuck as the temperature increases is then absorbed by the chamber walls. This increases the effect of degassing from the chamber walls and effectively acts as a bakeout. Therefore it is recommended that when the high vacuum gate valve is opened, to turn on the heat lamps and to bake out the system as this will assist in obtaining a lower ultimate base pressure.

Since the Macor headpiece and vacuum act as an excellent insulator, venting the system with dry nitrogen to 400 Torr will assist in cooling the chuck faster to a manageable temperature as this allows for convective cooling. Cycles of evacuating and venting can be done to speed up the cooling processes even more.

The reflectors require periodic cleaning and polishing, as depositions at elevated temperatures causes oxidation and unwanted source material deposition.

4.2.6 Heated Deposition

Although it is possible to create a capping layer by just depositing a material at a lower deposition angle α, the quality of it will be quite poor. Although areas of completely capped areas will exist, examination of a larger film area will reveal cracking due to stress in the capped film, as seen in Figure 4.7b. Therefore, there exists a need to increase the quality of the capping layer by minimizing film stress and/or by increasing adatom mobility.

All films were grown using TiO_2 obtain from with a 99.9% purity. The base layer had an intended thickness of 3 μm and was grown at 81° on three 3 in. Si<100> wafers obtained through University Wafer. Base films were grown at a rate of 10 Å/s as seen at the QCM with a pitch of 2nm/revolution. Films were then cleaved into quarters and stored for use in subsequent depositions. The algorithm used to grow the capping layers consisted of 400 nm grown at $\alpha = 45°$ with a pitch of 2 nm/revolution but a QCM rate of 4 Å/s. A pictorial representation of the film structures is shown in Figure 4.6. Heat was applied via the heating system and controlled using the variable transformer to maintain temperatures during deposition. Input power to maintain 200°C was ≈50 W, 300°C required ≈160 W, and 400°C required ≈310 W.

4.3 Experimental Results

This section presents data from calibration, testing of system performance, and a study involving capping layer deposition at elevated temperatures.

4.3.1 Capped GLAD Films

Heating capping layer films were imaged looking top down at the sample, at low magnifications, while capturing a large area as to obtain a representative crack

68
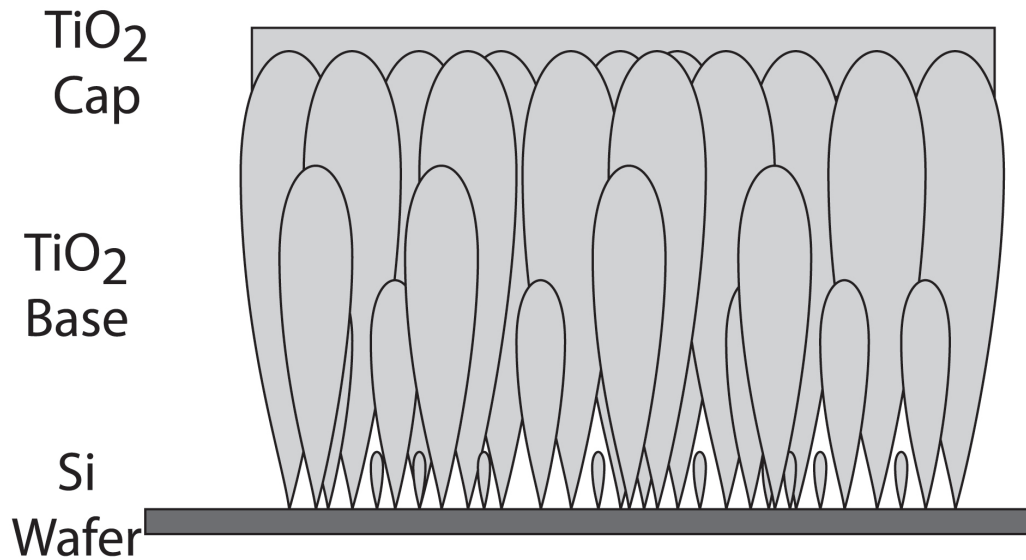
Figure 4.6: Schematic of the film structure used to explore capping layers that were deposited at at various temperatures.

density for the whole film. Since we were only concerned with what is occurring on the surface of the TiO_2 capping layer, the following imaging techniques were used: a low beam accelerating voltage (1 kV) as to minimize beam penetration into the film, and a conductive layer of chromium coating ($\approx$10 nm) to reduce charging effects. A top-down picture of the base film is shown in Figure 4.7a and is clearly a porous film. Subsequent images in Figure 4.7 showcase the uncapped base film and the 400 nm capping layer grown at varying temperature from an uncontrolled/unheated temperature of 50°C to a controlled and heated 200°C. Higher capping temperatures are shown in Figure 4.8 with a visually noticeable improvement in crack size, area and distribution.

To numerically quantify the improvements made to the heated capping layers an image analysis program was used, ImageJ [73], along with a plug-in that allows for the skeleton analysis of cracks. Scanning electron microscope (SEM) images
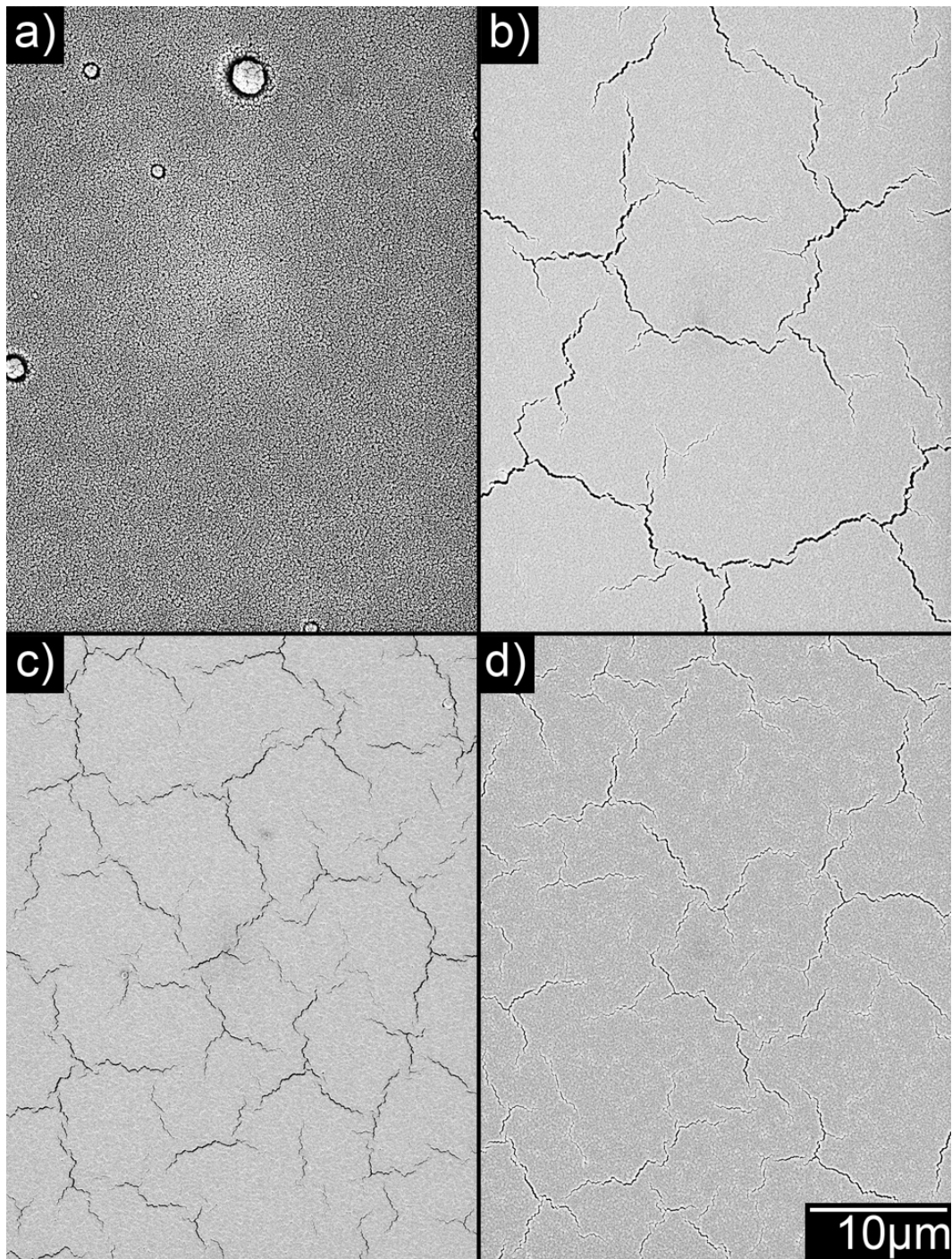
Figure 4.7: Top down images of film used produced in cracking experiment a) base film uncapped with nodules caused by source spitting, b) capping layer grown an insulated substrate, unheated (50°C), c) 150°C, and d) 200°C.
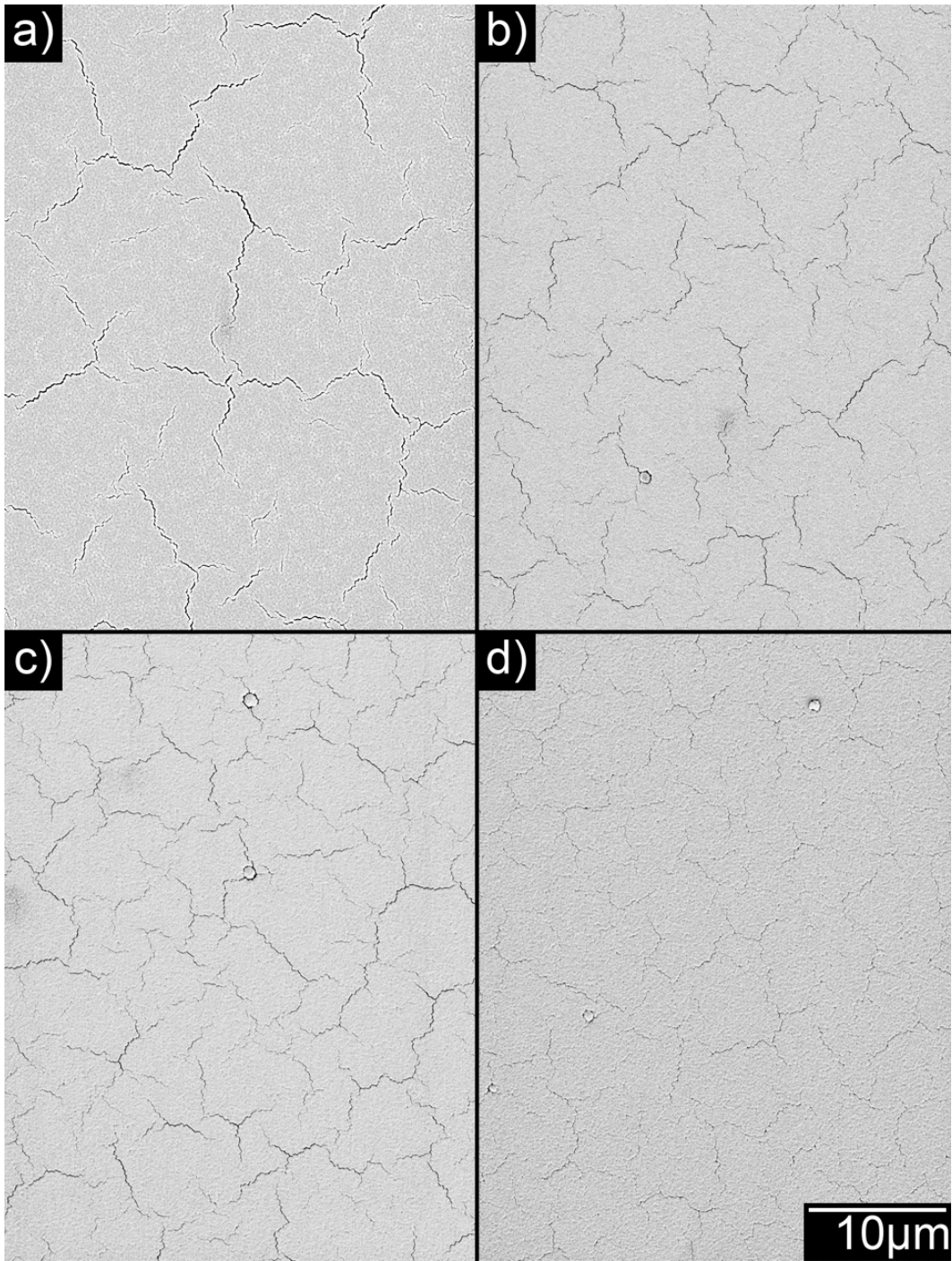
Figure 4.8: Top down images of capping layers grown at the following temperatures: a) 250°C, b) 300°C, c) 350°C, and d) 400°C.

obtained are gray scale images with cracks being represented as dark areas (low intensity), with the bulk of the capped film being represented by grey/white areas (high intensity). To properly and consistently distinguish cracks from bulk film, a method of correctly choosing a threshold value was needed. In some cases, the histograms from the images represent the two regions distinctly, as seen in Figure 4.9a and b. In all cases, the bulk of the film was fitted to a histogram to characterize the film (Figure 4.9g and h). Anything below a threshold represents the cracks (Figure 4.9c and d) or their boundaries (Figure 4.9e and f). With this selection we were able to have a quantitative analysis without a subjective bias.

By selecting a threshold value (between 3σ and 5σ based on the gaussian distribution) we were able to obtain a set of data corresponding to the variation of crack length due to selection of threshold values. From Figure 4.10a it is clear that the temperature effect is greater than the threshold effects, signaling that our analysis is reasonable to quantify our experimental data. Some temperatures were not included for reasons of clarity.

The data presented in Figure 4.10b is a cumulative distribution function (CDF) of crack size. In this case, the CDF represents the fraction of cracks above a length given on the x-axis. Therefore, at 20 nm, all cracks are longer thus giving a CDF of 1, or 100% representation. As we increase crack length on the horizontal axis, less and less of the crack population is above the x value. To give a direct example, for a crack length of 1 µm at 50°C ≈20% of the film has yet to be accounted for, whereas at 350°C only ≈2% of the film has yet to be accounted for. Therefore, we can conclude that larger cracks are being preferentially reduced with increasing temperature.

If the above statements are true, then we should be noticing a decrease in crack area with increasing temperature as well. A summary of the total crack length and
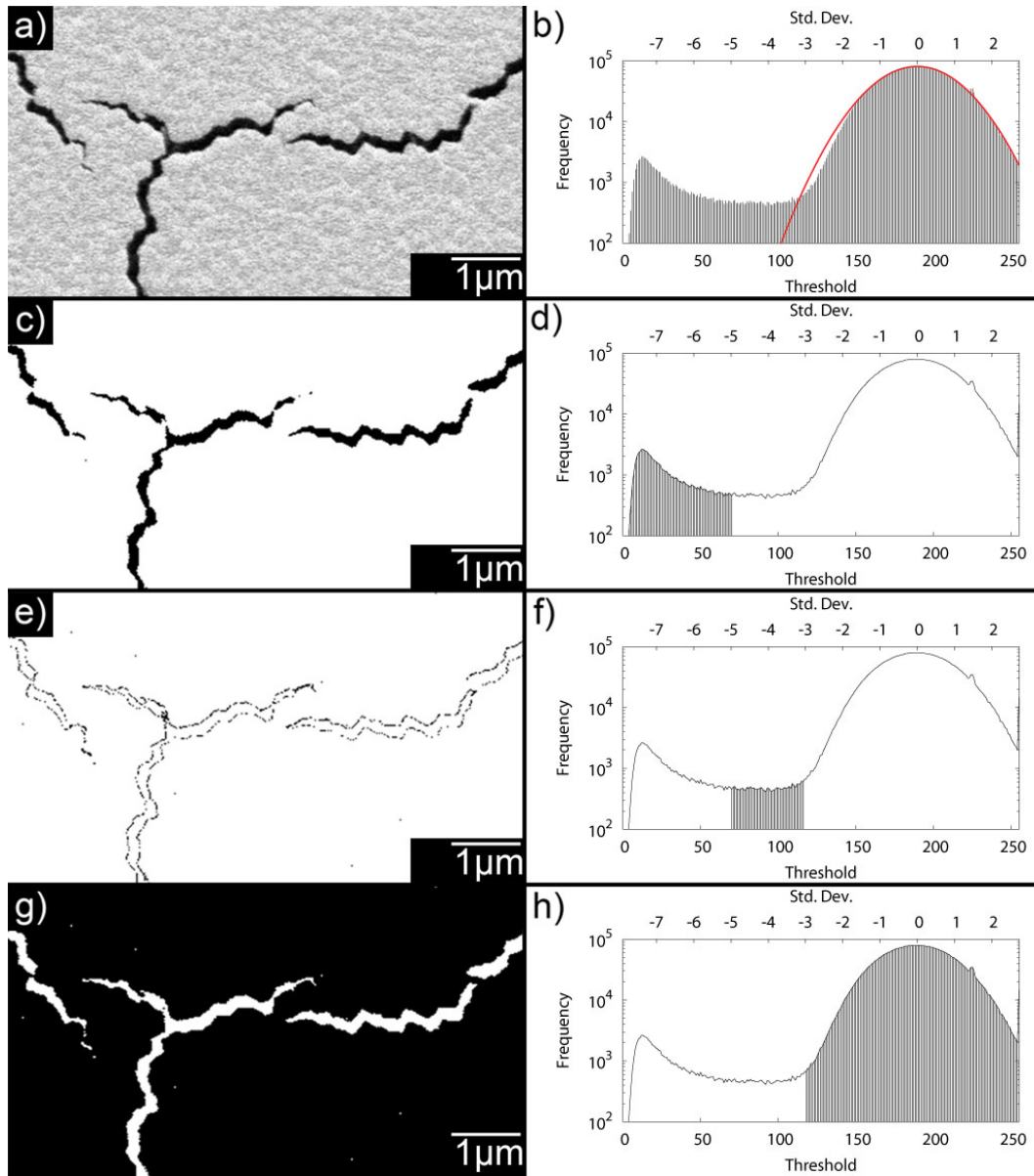
Figure 4.9: A section of an SEM image from a capped film is show in a) along with its representative histogram and a gaussian fit of the bulk film in b). Minimum crack size is represented in figure c) which corresponds to a histogram threshold values below ≈60, 5σ, seen in d). Crack outline is represented in e) which corresponds to histogram threshold values ≈60 and ≈110, between 3σ–5σ, seen in f). The remainder of the film is shown g) with it's corresponding histogram in h).
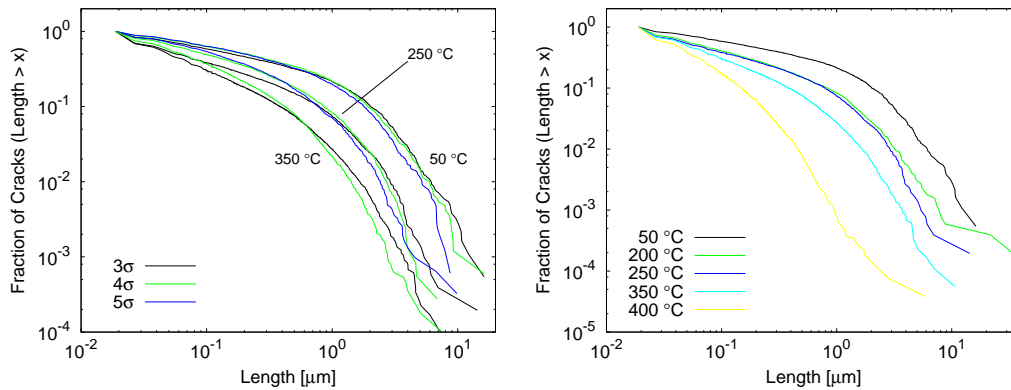
Figure 4.10: Left: Threshold values for select temperatures demonstrating repeatability regardless of threshold value. Right: Cumulative distribution function of crack length with different temperatures.

total crack area are represented in Table 4.2. Although there is fluctuation in the data, if the two extremes are compared once again the, crack area is $\approx 32.7\ \mu m^2$ at $50°C$ and $\approx 15.5\ \mu m^2$ at $400°C$, over a factor of two difference. An interesting outcome from further analysis shows that total crack length remains relatively constant which is indicating that heating transforms cracks into smaller ones. This conclusion could could also signify a redistribution of stress in the film producing more cracks but smaller in size.

Crack branching analysis is also readily obtained from the image analysis program. Visually, it is clear that the cracks are becoming smaller and individual, which coincides with the analysis done in Figure 4.11. Therefore, as substrate temperature is increased, branching decreases and ultimately leads to a majority of singular cracks.

Although complete capping was not achieved, it is possible that higher temperatures yet would be required to achieve this. It is hypothesized that once the film's crack distribution is full of singular cracks, then the filling of the cracks may begin.

74

Table 4.2: Crack Lengths and Areas for Different Temperatures, 3 sigma, Total Area is 1750 μm^2

Temperature (°C)	Crack Area (μm^2)	Crack Length μm
50	33	324
150	31	290
200	25	395
250	21	354
300	31	351
350	28	404
400	16	223
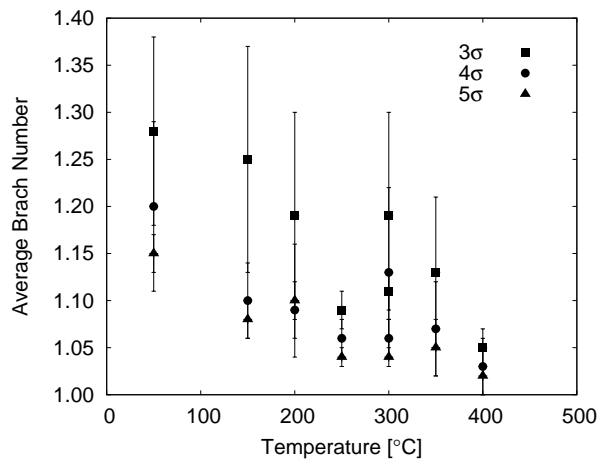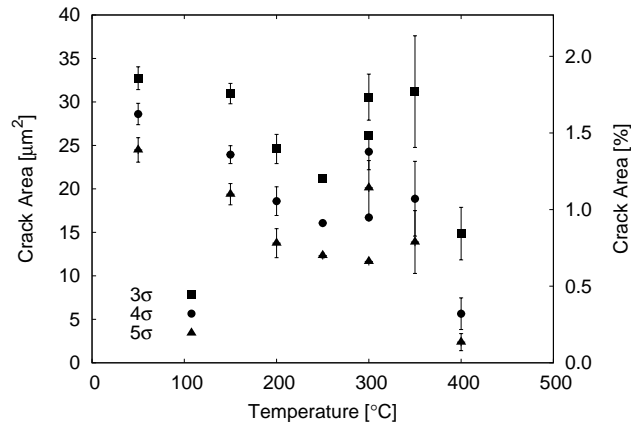
Figure 4.11: Average branching per crack with varying temperature.

4.3.2 Pattern Transfer and Capped Films

The lithographic pattern transfer process involves the use of liquids such as photoresists, developers and solvents (acetone, isopropyl alcohol and water) which is generally incompatible with GLAD films due to clumping and stiction, as was demonstrated in Chapter 3. Therefore there is a need to create a barrier between the GLAD thin film and the pattern transfer processes. With the ability to create sufficient capping layers out of TiO_2, another set of experiments was carried out involving pattern transfer.

The film consisted of a base layer, capping layer and sacrificial layer. The base layer, a 1 µm TiO_2 GLAD thin film, was grown on a 4 in. wafer Si<100> with capping layer of 400 nm of alpha 45°, with a substrate temperature of 400°C. Deposition rate was 4 Å/s at the QCM with a pitch of 2 nm/revolution. A 200 nm sacrificial layer of aluminum was deposited onto the TiO_2 capped film through sputter. The lithographic processes consisted of a layer of HPR504 photoresist, later cured and then developed, using a UV source, through a mask obtained from the Nanofab. This mask contains designs for electrostatic comb drives and other MEMS designs which have minimum feature sizes of 1 to 2 µm. Although the photoresist could have been spun directly onto the TiO_2, no experiments have been done to determine the selectivity between HPR504 and TiO_2 in CF_4:O_2 etch recipe. Previous experiments in Chapter 3 showed that aluminum is a sufficient mask with this recipe. After developing the exposed photoresist, along with a thorough cleaning with acetone and IPA, the wafer was cleaved into smaller pieces and etched using the CF_4:O_2 recipe developed in the etching chapter. Etches consisted of 100 sccm flow of a 3:1 mixture of CF_4:O_2 at a pressure of 0.120 Torr with RF power of 200 W. A pictorial representation of the intended film structure after processing is shown in Figure 4.12. Actual results are shown with varied etch durations in Figure 4.13.

76
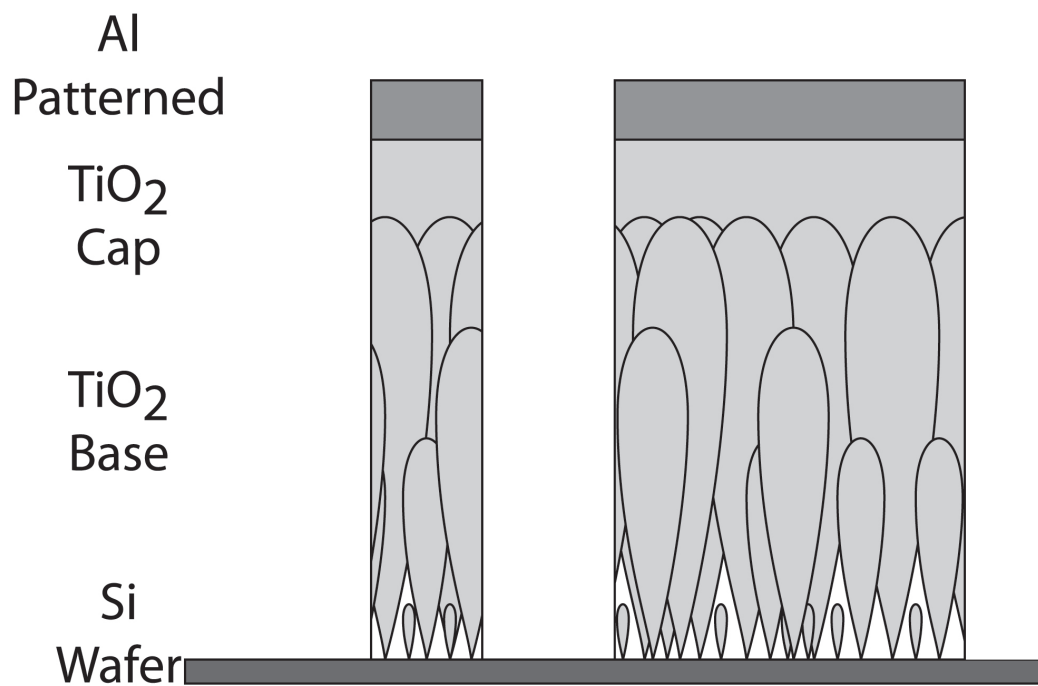
Figure 4.12: Schematic of the film structure, post lithography and etching, used to achieve a high resolution pattern transfer using a capping layer deposited at elevated temperatures.
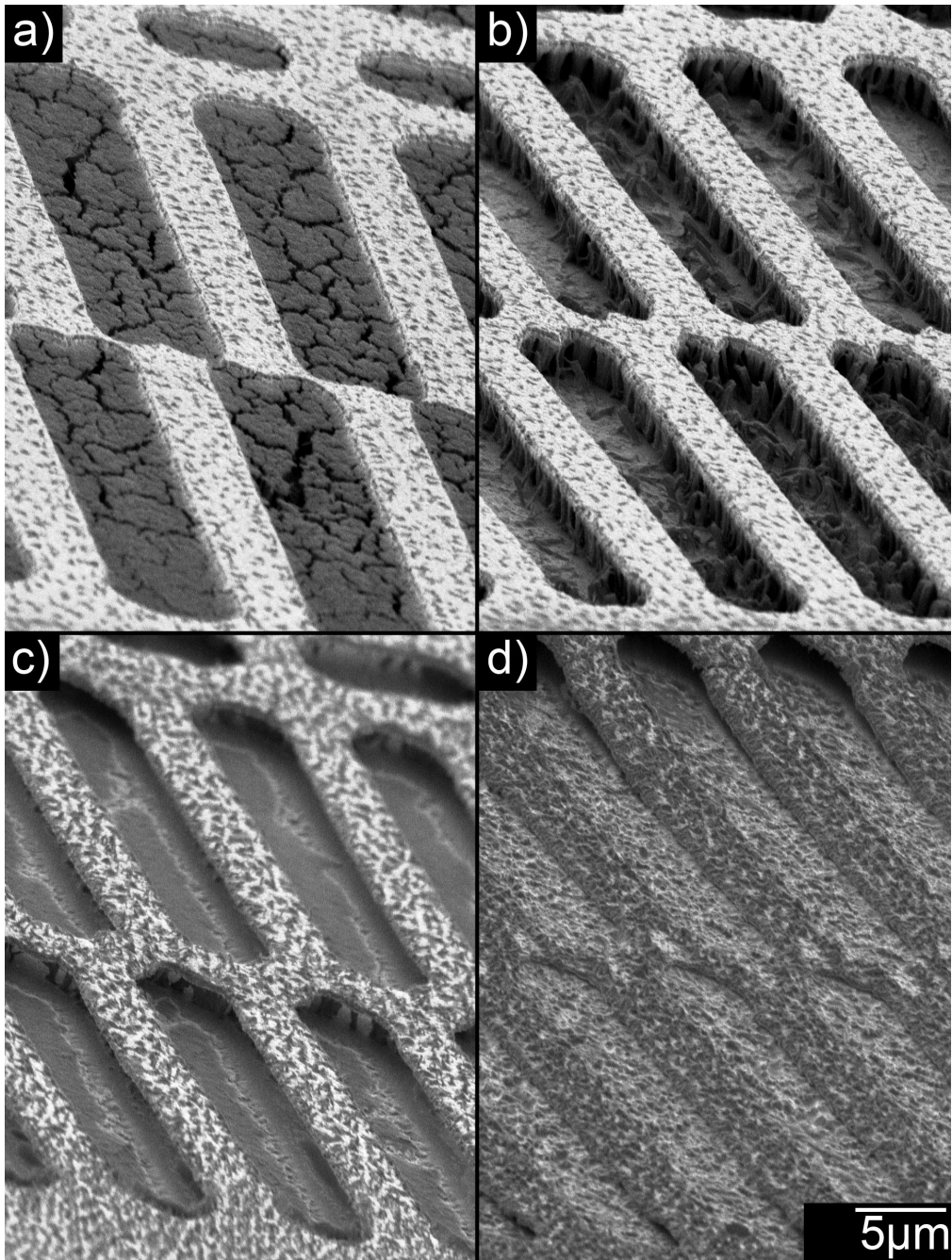
Figure 4.13: High resolution pattern transfer was achieved depositing aluminum onto a heated capping layer which is on top of a GLAD TiO_2 thin film. Using an etching technique explored Chapter 3 pattern transfer into a GLAD thin film was achieved. Figures show different etch times a) 1 minute b) 5 minutes c) 6 minutes d) 10 minutes.

Pattern transfer with high resolution through lithographic methods into GLAD thin films is possible with the refinement of capping layer deposition process. Although this process has not been optimally refined, the resolution possible with this method is lower and results in cleaner, sharper edges as opposed to the jagged and tapered edges seen in the shadow masked patterns. To determine the quality of the masked GLAD film, the aluminum layer would need to be removed through etching and then critical point drying. Although there is sufficient cracking seen in the film, as per Figure 4.13a, this effect is possibly due to the destruction of the film during etching. This effect was also seen in Chapter 3, Figure 3.7, where an increase in etch time from 0–60 sec creates these large diffusion channels. It is clear that there is a optimal end point between 5 and 6 minutes due to the images in Figure 4.13b and c. Further interesting observations to make from Figure 4.13c is the undercutting of the film and the etch recipe attacking the Si wafer. Individual posts can also be seen underneath the aluminum layer supporting structure above. Over etching, as seen in Figure 4.13d, causes the collapse of the aluminum layer onto the Si wafer along with significant roughing of all surfaces. These effects could be minimized with improvements made to the etch recipe by using methods detailed in Chapter 2.

4.4 Conclusions and Improvements

A custom, vacuum compatible, 500 W radiative heating system was designed and implemented in an AXXIS system for *in situ* substrate heating. By controlling the output power of the two 78 mm quartz halogen bulbs through a variable AC transformer, temperatures of 400°C can be achieved and maintained, with a ramp up time of ≈30 min. Real time temperature feedback was accomplished by using T-type thermocouples in a cold junction compensated setup. By using a calibrated thermistor, using a NIST standard method, accurate knowledge of the cold junction

can be obtained. Electrical connections between atmosphere and vacuum were made using a 6–pin electrical feedthrough. Thermal isolation between the deposition system and the chuck was accomplished by using Macor, a machineable ceramic, and replacing the existing aluminum shaft. Heating system performance was demonstrated by evaporating TiO_2 to produce capping layers, grown atop a TiO_2 GLAD thin film, at elevated temperatures. Image analysis was performed, using ImageJ, to produce data with regards to crack area, crack length and branching. With the use of a capped GLAD thin film, standard lithographic processes, and an etch recipe consisting of CF_4 and O_2, a high resolution pattern transfer, compared to that of shadowing masking done in Chapter 3, of 2 µm features was possible.

Higher temperatures are possible with the base design with improvements in equipment used. To output higher power, a variable transformer would be need that provides 1 kW output at voltages of 240 VAC. The wiring of the bulbs would need to be change from being in parallel to being in series in order to keep wire gauge small. Existing bulbs, 78 mm and 250 W, would need to be increased in size and power handling capabilities to 118 mm and 500 W. A thermocouple with a wider elevated range, also being vacuum compatible, would need be selected or to implement an alternate method of measuring elevated temperatures in vacuum through infrared measurements.

Improvements in the temperature measurement system would allow for a more reliable system with less downtime due loss of contact with surface being probed. Attaching the thermocouple to a spring based platform would allow the thermocouple to apply a more consistent pressure to the chuck and therefore overcoming loss of contact due to deformations/softening in the thermocouple caused by elevated temperatures. Increasing thermal equilibrium between the CJC thermocouple along and the thermistor could be accomplished by encapsulating both in a metallic tube

80

filled with thermally conductive grease. This modification would allow for better heat transfer between the cooled water line and the temperature measurement devices along with easing installation and service.

With elevated substrates temperatures comes an increase in radiative energy being dispersed and absorbed throughout the system. This is of significant concern and dealing with a cryo pump. To protect the cryo pump from absorbing large amounts of radiated energy, a baffle or shield should be installed in the 10 inch port used to connect the cryo pump to the deposition chamber. Since radiative losses become the main source of energy loss in vacuum at elevated temperatures, another possible modification could be to design a shroud around the deposition arm to reflect back the energy loss as well as minimize chamber wall heating.

By replacing the two multimeters with a microcontroller based logging and display system would allow for easier data acquisition and post-processing. This system would allow for programming of parameters pertaining to thermocouple voltage to temperature relationship along with the thermistor resistance to temperature conversion. This system would allow for real time temperature monitoring and allow for data logging through a serial based connection to a computer.

Please take time to digest the previous material and prepare for what lies ahead.

Chapter 5

Depositing onto Cooled
Substrates

5.1   Introduction

The last chapter dealt with chuck heating through radiative means and increasing
substrate surface energy, thus allowing for condensed atoms to have longer diffusion
lengths. This chapter focuses on design and implementation of a system that will
cool the chuck through thermal contact and allow for reduced substrate temperatures
in a glancing angle deposition (GLAD) system. The design will preserve substrate
tilt and rotation needed for GLAD thin films. Experiments with copper films are
carried out, demonstrating the ability to deposit low melting point materials with the
modified system. The motivation for developing such a system is to allow exploration
of thin film surface properties with in GLAD thin film form.

5.2 Experimental Setup

5.2.1 Design and Installation

This design has simplicity in mind, and is based on using LN_2 as a medium that extracts heat from the system. It relies on physical contact between the cooling loop and the rotating chuck. The tilt α of the substrate creates a dilemma in maintaining contact between the two surfaces and ensuring enough surface area interactions between the two surfaces to properly maintain a large heat transfer. If a stationary substrate was used, this would only allow the growth of slanted posts which limits the nanostructure possibilities by using a rotating substrate as explained in Chapter 2.

Many ideas were considered before settling on the use of LN_2 as the medium to transport the heat from the system. First, the use of cooled water would have only been adequate with maintaining chuck temperature around room temperature. The use of Peltier cells was also considered and would allow lower temperatures to be reached but would require high currents which could not be supported by our existing electrical feedthroughs. Therefore to achieve cryogenic temperatures, a more extreme cooling liquid needed to be used. Since LN_2 is relatively cheap, easy to transport and to handle, it was a more natural choice.

Material choice was relatively straight forward. Thermal isolation from the rest of the system was achieved using Macor, the same material used in Chapter 4 when a simple and cost effective heating system was implemented. For the storage of energy (or lack of large thermal energy), oxygen-free copper (OFC) was used. OFC's increased purity compared to "regular" copper give it superior thermal conductivity. Its cost is reasonable and it is easy to machine.

The copper cooling block was designed to fit into a rotating deposition arm.

84

The design for the copper block is show in Figure 5.1 along with the important dimensions. As obtained, the original OFC block measured 6 inches by 6 inches by 1 inch, with the design only needing a 6 inch by 3 inch by 1 inch piece. The narrow design retains the ability to accommodate the radiative heat lamps from Chapter 4. The LN_2 flows through a bored, 3/8-inch diameter, U-shaped channel within the block. The design demands a minimum 1/8 inch wall thickness. Because of the way in which the LN_2 channel was bored out, some of the bore holes needed to be plugged; plugs were made from OFC copper, machined to fit the holes, and affixed by silver brazing for a vacuum-compatible seal. The center of the OFC block is bored out to accommodate the rotating shaft with the interchangeable head piece described in Chapter 4. The head piece has a diameter 3/2 inches which leaves 1/8 inches on clearance between the OFC block and head piece on each side. Threaded holes (#8-32) on either side of the block allow for the attachment of the copper leaves which make the thermal contact with the chuck (which is also OFC). Mounting of the OFC block into the deposition system was accomplished by using four standoffs made of Macor which are 1/2 inch diameter and 1 inch tall. The standoffs are narrowed at the top, by an 1/8 inch for easier alignment and tapped with 8-32 thread on the top and bottom. The OFC block was designed to mate with these pieces. When installed, the gap between the OFC chuck and the OFC block is 1/10 inch. The completed OFC block is shown in Figure 5.2

Substrates are mounted on an OFC chuck, depicted in Figure 5.2b. The circular chuck was cut to have a diameter of 7 1/4 inches with a thickness of 1/4 inch. Aluminum chucks normally used have a typical thickness of 1/8 inch. The extra thickness of the new chuck along with the higher density resulting in a chuck with a larger thermal mass. This was a deliberate choice as an attempt to dampen radiative heating effects from the source and poor thermal contact between the chuck and thin
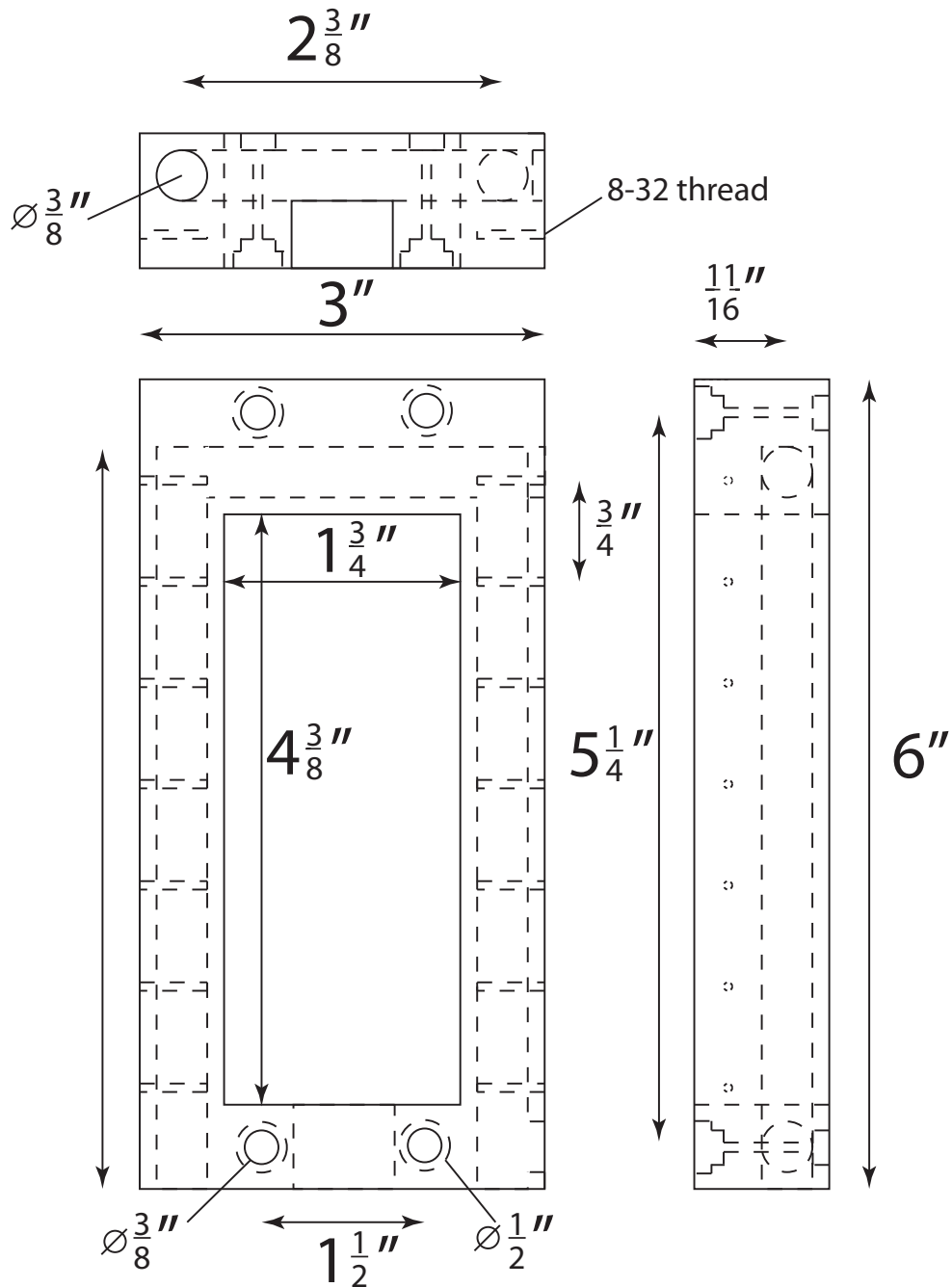
Figure 5.1: Schematic of OFC block placed in deposition arm. LN_2 flows through the bored holes which cools the block to near LN_2 temperatures. Copper leaves are screwed into the block which make contact with the OFC chuck.
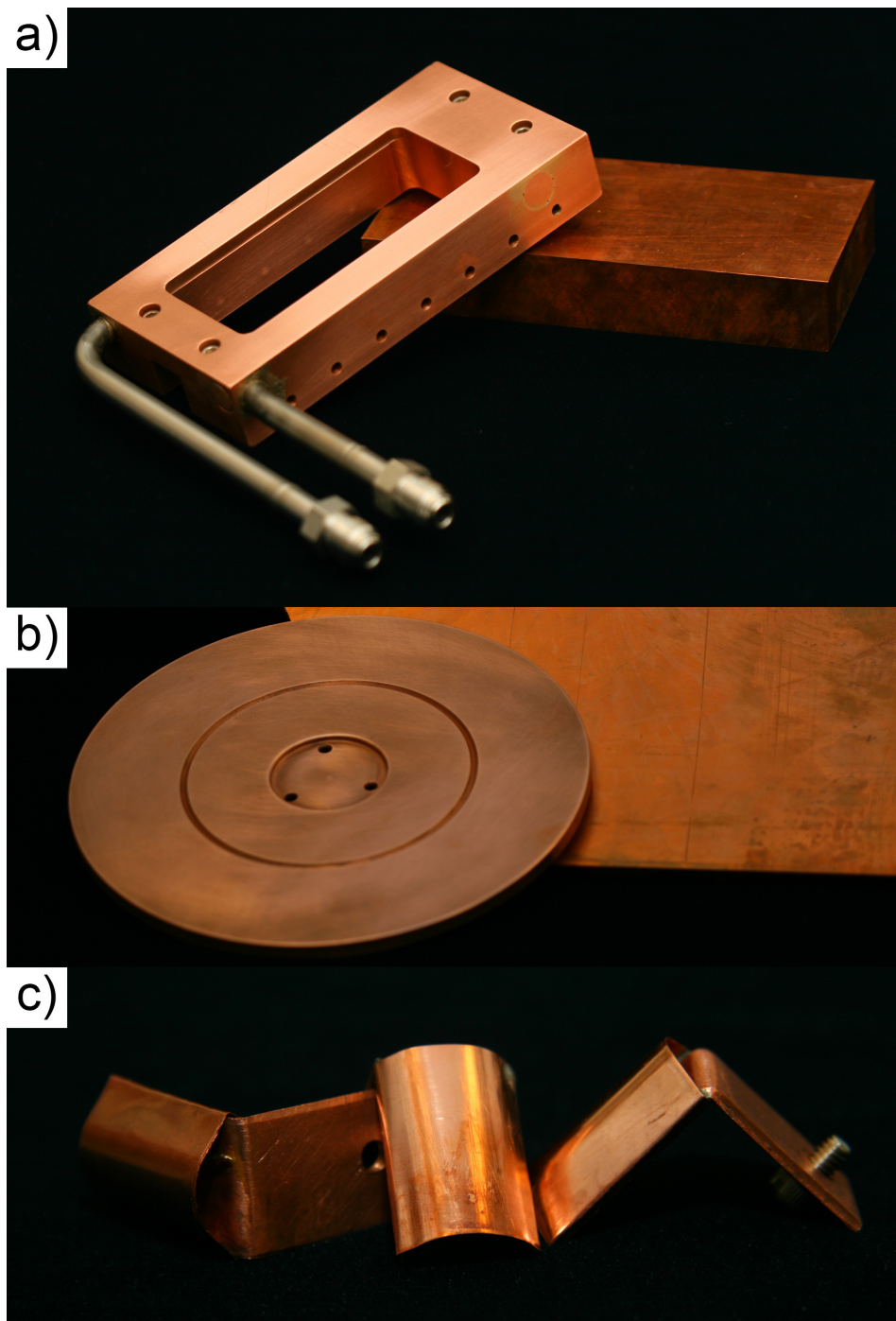
Figure 5.2: Experimental setup of LN_2 cooling of substrates: a) OFC cold block, b) OFC chuck with a track for the thermocouple, c) copper leaves that are in contact with the chuck from underneath with #8-32 screw.

leaves, which are depicted in Figure 5.2c. A groove was made on the backside in the chuck which serves as a guide for the thermocouple. Although not shown, the bottom of the chuck was also polished using Brasso, a metal polish, to achieve a smoother surface.

To flow LN_2 through the system, a liquid feedthrough was installed. Feedthrough tube sizes, offered by Kurt J. Lesker, were either 1/8 inch or 1/4 inch. Therefore, to have maximal flow, the larger diameter was chosen. Vacuum compatible fittings, known as VCR fittings, were used on the vacuum side and on the atmospheric side even though VCR fittings were not needed on the atmospheric side. This choice was made as to keep everything similar, which proved to be an inconvenience in the end, as explained later. A flexible connection, supplied by Swagelok, was needed between the feedthrough and the OFC block. The flexible tubes are rated for ultrahigh vacuum (UHV) environments and are capable of operating at LN_2 temperatures. A 3 foot length of tube was chosen to anticipate pitfalls and lapses in design. The connection to the cooling block was made by ordering a stainless steel pipe with two high flow 1/4 inch VCR fittings welded onto the ends of the 3/8 inch, outside diameter, pipe. The pipe was later cut to the proper lengths, bent, and installed into the copper block using silver solder.

Installation consideration outside of vacuum were less stringent but equally important. Correct fittings and creative plumping were needed to connect the 240 L LN_2 dewar to the liquid feedthrough. LN_2 is placed in a pressurized dewar, from which the liquid could be easily extracted through the pressure developed in the tank from the evaporating LN_2. Standard fittings for LN_2 connecting to higher capacity dewar are of 1/2 inch flare type; adapters were needed to interface with the VCR feedthrough fittings. The original design of the LN_2 circuit did not have a design for throttling the cryogenic fluid and allowed the venting of the LN_2 to atmosphere after

88

passing through the system. The only throttling that was done was by the valve on the dewar which didn't allow for controllable liquid flow through the system. By installing a valve on the exhaust port and throttling the flow of LN_2 the tubing could be pressurized. By pressurizing the tubing, liquid could be accumulated in system. The valve also helped regulate LN_2 usage and minimize excessive spillage. National pipe threaded (NPT) pipe was used for the exhaust piping, which required teflon tape on the threading to ensure a tighter seal and to prevent leaking.

Excess flexible tubing, inside the vacuum system, was to be positioned inside the 10 inch port use for the cryo pump. This proved to be a poor design choice and exposed an overlooked aspect. As the arm was rotated from the the 180° position to the GLAD angle, the tubing was forced to make a 90° turn. This 90° turn created a small bend radius, which put the flexible tubing outside of its design specification. Furthermore, the tubing would catch and rub on the nuts that were on the inner chamber walls. This was overcome with using elbows (Swagelok) which fit the installation but also lead to ideas for further improvements to the system which should be implemented in the next revision. Subsequent revisions should focus on minimizing the amount of bends and turns that the flexible tubing needs to perform: the permanent bends should be done using rigid pipe as not to excessively stress the flexible tubing.

When rotating the arm from 180° to GLAD angles, the tubing will flex and therefore will need to be anchored in one location to make the tube pivot about that point and prevent it from rubbing on the chamber walls. This was done by using two wires attached to a ceramic standoff. One copper wire was tied down to the copper tubing and looped through the ceramic standoff and the other copper wire was looped through the standoff and attached using a screw to one of the nuts on the inner chamber wall.
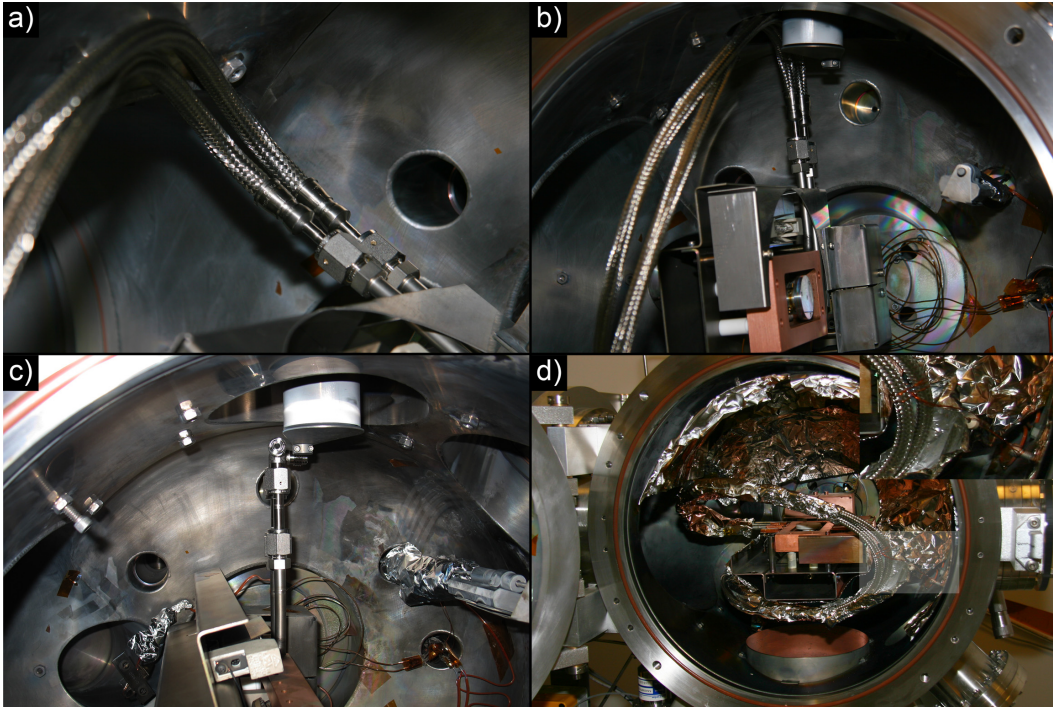
Figure 5.3: System implementation of cooling apparatus. Preliminary design without elbows is showed in a) and b), with unacceptable stress and bending of flexible tubing. A resolution was found by using 90° elbows seen in c). The final installation, after a deposition is show in d) with the inset depicted the anchoring of the tubes.

Finally, to make contact between the chuck and the cooled copper block, an elbow/copper foil assembly was made which is seen in Figure 5.2c. Unfortunately in the time of the construction of this last and crucial part, OFC copper of the required thickness was not available and therefore standard copper was used for the elbow and the leaf.

5.2.2 Source Material & Film Structure

As was explained earlier in Chapter 2, GLAD thin film growing process relies on oblique incident vapour flux angles well as low adatom mobility. Many GLAD experiments that are performed use relatively high melting point materials, which

yield beautifully sculpted thin films. Using lower melting point materials yields film structure that poorly defined and/or does not yield the intended structures that the deposition algorithm called for. Therefore in order to fill this void and showcase the ability of the new installation, a proper material needed to be selected.

Several materials were considered in order to demonstrate the effects of a cooled substrate. A list of materials and their melting points are showing in Table 5.1 [69]. Also included in this table are the T/T_m ratios at different temperatures. This spread of ratios is to determine which material would offer the best spread in ratio over the achievable substrate temperatures. Silicon, a low melting point metal, has already been grown with great success without extra substrate temperature modification therefore wouldn't offer great opportunities. Based on this knowledge, a material with a lower melting point then Silicon was needed. Typical substrate temperatures when growing films under these typical conditions are 20°C to 50°C, while growing higher melting point materials (TiO_2), chuck temperatures could potentially reach 70°C as the evaporation source radiates heat to its surroundings. Since defined GLAD structures are possible with a substrate to melting point ratio of ≈0.18 and lower, copper was chosen as the material to demonstrate the system. Without putting extra demand on the system, it would be possible to achieve a reasonable example that adatom mobility plays a significant factor in growing GLAD thin films. By growing a heated film using the setup explain in Chapter 4 it should be possible to showcase the complete degeneration of the film structure.

A favorable consequence of using lower melting point materials, is that when a melt is achieved the radiative energy emitted from the source is substantially lower as per Stefan-Boltzmann Law

$$W = \sigma A T^4$$

which states that the temperature/power related through a quartic function.

Table 5.1: Various Substrate Temperature to Material Melting Point Temperature Ratios

Material	Melting Point °C / (K)	150°C 423K/T_m	30°C 303K/T_m	−50°C 223K/T_m	−100°C 173K/T_m
Tin	232 (737)	0.574	0.411	0.303	0.235
Aluminum	658 (931)	0.434	0.325	0.240	0.186
Copper	1080 (1353)	0.313	0.224	0.165	0.128
Silicon	1414 (1687)	0.251	0.180	0.132	0.103
Silica	1650 (1923)	0.220	0.158	0.116	0.090
Titania	1843 (2116)	0.200	0.143	0.105	0.082

The cooling system was designed to preserve substrate motion. To show this a deposition algorithm was made to create helical structures with a pitch of 200 nm/turn. The rate at which copper was evaporated was 5 Å/s at the quartz crystal microbalance (QCM), for a desired thickness of 1.5 μm at an α of 81°. A choice of 0.7 as the tooling factor was made as typical material tooling factors in the deposition system range from 0.6 to 0.8 at an α of 81°. From this algorithm, it was expected to achieve a film with a helical structure with 7.5 turns. Chamber pressures during the deposition was consistent for all depositions and was maintained between 1-2×10^{-6} Torr.

Source material used was 99.99% pure Copper, from Cerac. Substrates used were 3 inch Si<100> quarters obtained from University wafer.

5.2.3 Temperature Measurement

To measure the temperature at the substrate, a similar method was employed as in Chapter 4. A T-Type thermocouple was used, as it has the ability to sense temperature down to −250°C (−185°C long term) as per NIST standards. The cold junction compensation (CJC) method was used where there was another thermocouple placed

onto the QCM cold water cooling line. A calibrated thermistor was placed alongside the second thermocouple and its leads being connected to a Fluke 83 multimeter. The thermistor circuit was probed using an Agilent 33401A DMM.

5.3 Experimental Results

5.3.1 LN$_2$ System Performance

Initial testing of the system was performed before any films were grown. The first run was done without a throttling valve placed on the exhaust. The temperature of the chuck after 30 minutes of cooling was −8°C. This prompted the rethinking of the design and eventually to add a valve to the exhaust port. The next test was done with the thermocouple in contact with the cooling block. In high vacuum, LN$_2$ was fed through the system and throttled. Within approximately 10 minutes, the copper cold block reached a temperature of −144°C. This verified that LN$_2$ indeed was flowing through the system and that the thermocouple was able to read low temperatures. The next test involve testing heat transfer from the chuck to the cold block through the leaves. While spinning, the chuck was cooled to a temperature of −50°C within 30 minutes. Since it is difficult to throttle and record the temperature at the same time only two calibration curves were obtained, featured in Figure 5.4. An empirical decaying exponential equation of the form,

$$y = a \cdot \left(1 - e^{\frac{x}{b}}\right) + c,$$

was used to quantify the system. At this point, the system performance was sufficient to attempt a deposition. It was determined that 30 minutes was needed to cool down the chuck to an adequate temperature, during which a graphite crucible filled with copper was conditioned and stable melt achieved.
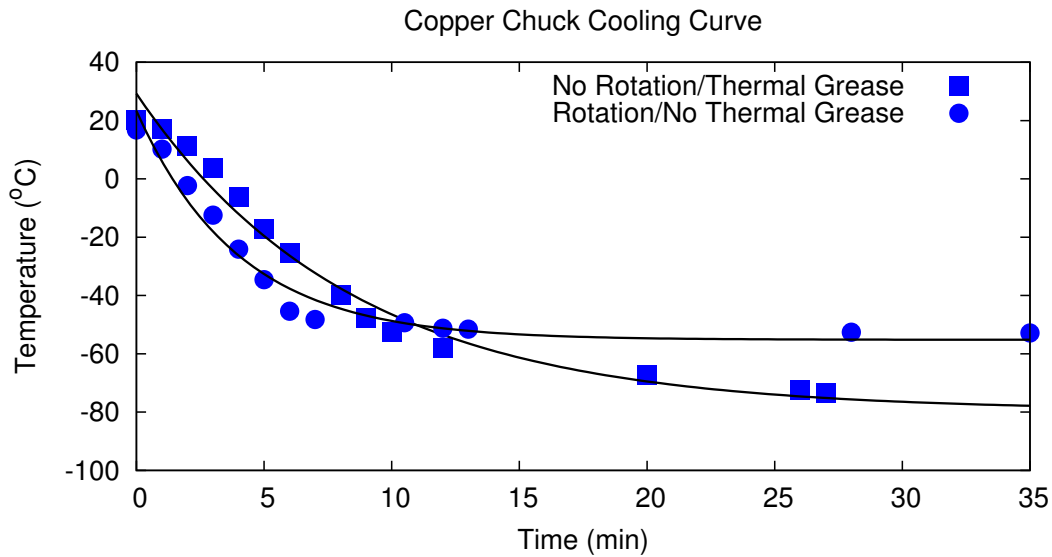
Figure 5.4: Cooling curve with chuck on foil contacts. Run 1 was with rotation but no Apiezon's cryogenic grease, and run 2 was without rotation but with the cryogenic grease.

After a successful deposition with the cooled substrate, Apizeon's N type grease was used in an attempt to increase thermal conductivity and contact. The grease was applied to the surface of between OFC chuck and the copper leaf. Grease was also applied between the OFC cold block and the copper leaves. Although substrate motion was not possible, the chuck temperature after reached –95°C after approximately 1 hour. Although a significant improvement in temperature, it was considered a failure because substrate motion was impeded.

5.3.2 Copper GLAD Films

A film of copper was grown at room temperature in order to determine the quality of the GLAD film at this temperature. The chuck was thermally isolated from the system by using the Macor head piece. Radiative energy from the source caused a temperature rise of 23°C was noticed from 20°C. The deposition lasted 67 min-

utes, which was common to all copper depositions as similar deposition parameters, excluding temperature, were used. The results are featured in Figure 5.5b and Figure 5.6b. Although the desired thickness was not reached, a is visible but poorly defined structured film is shown. Both side images and oblique images show a densely packed film, where as films grown at 81° show lower film density.

The heated copper deposition was done by increasing the temperature of the chuck to 150°C. Temperatures ranged from 150°C to 158°C with while using 37 V @ 1 A on the variable transformer. The results are seen in Figures 5.5a and 5.6a. The expected result was to produce a planar film, without voids or any visible structure. An interesting note to make that at the interface between the Si wafer and the copper a planar film is present with an approximate thickness of 50 nm.

The SEM images of the heated copper GLAD film showed there was a preferred film orientation that dominated and is irrelevant to substrate orientation. To quantify film orientation an XRD analysis was performed, with the assistance of Dr. M. Fleischauer (Research Officer, NRC-NINT), on the samples to determine their crystallinity. Data was collected by using $Cu_{k\alpha}$ x-rays. Results are shown in Figure 5.7. An immediate observation is that grain size is related to the substrate temperature and higher temperatures are expected to promote increased diffusion and crystallization, owing to the increased kinetic energy of the adatoms and preferential arranged.

5.4   Conclusions and Improvements

A custom, vacuum compatible, LN_2 based cooling system was designed and implemented in an AXXIS system for *in situ* substrate cooling. An OFC chuck was brought into thermal contact with an OFC block, rigidly mounted inside a deposition but capable of rotation, which is cooled by LN_2 flowing through it. Flexible tubing,
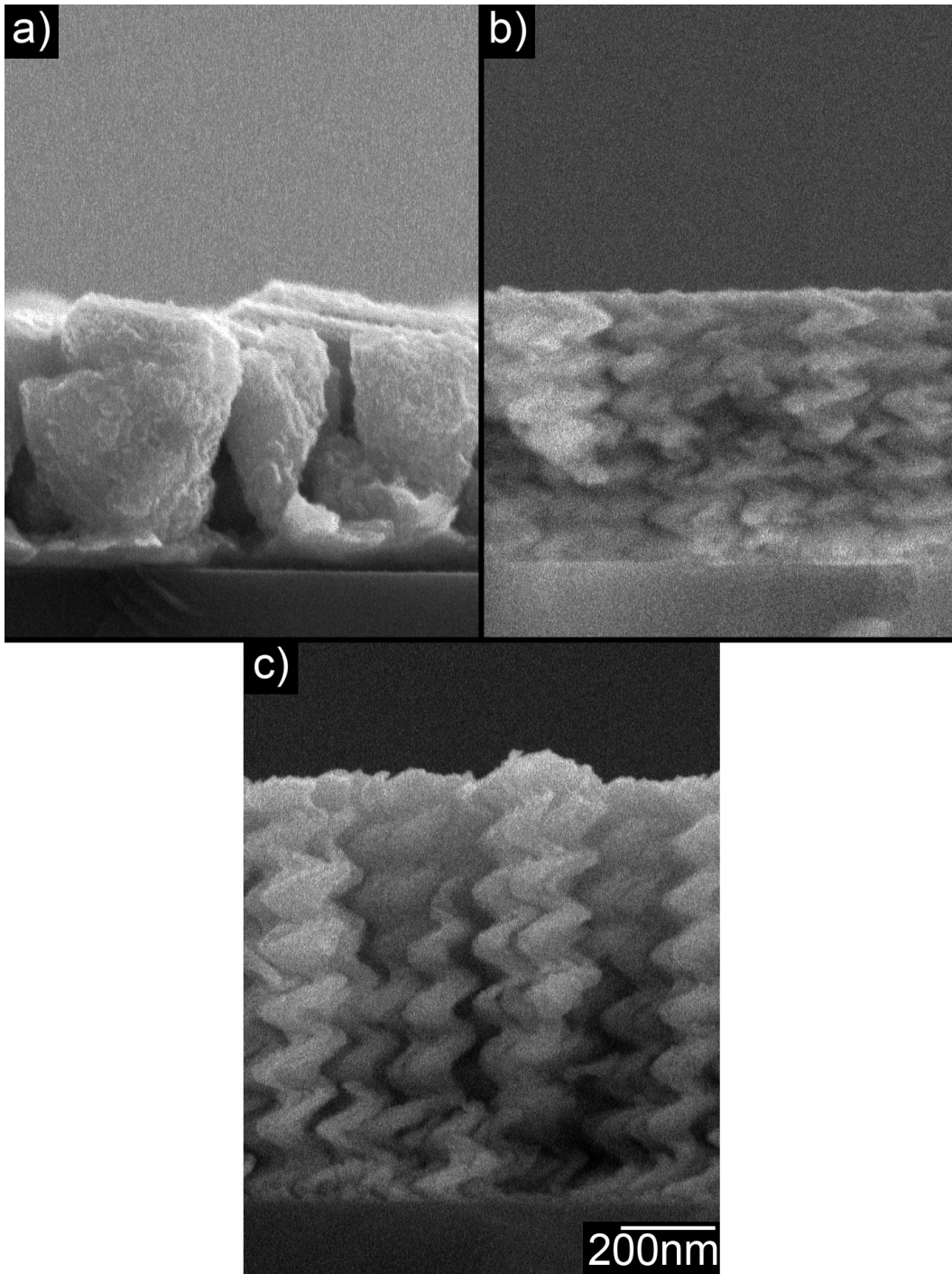
Figure 5.5: Side images of copper grown at various temperatures: a) 150°C, b) Room Temperature (Average of 30°C), c) −50°C.

96
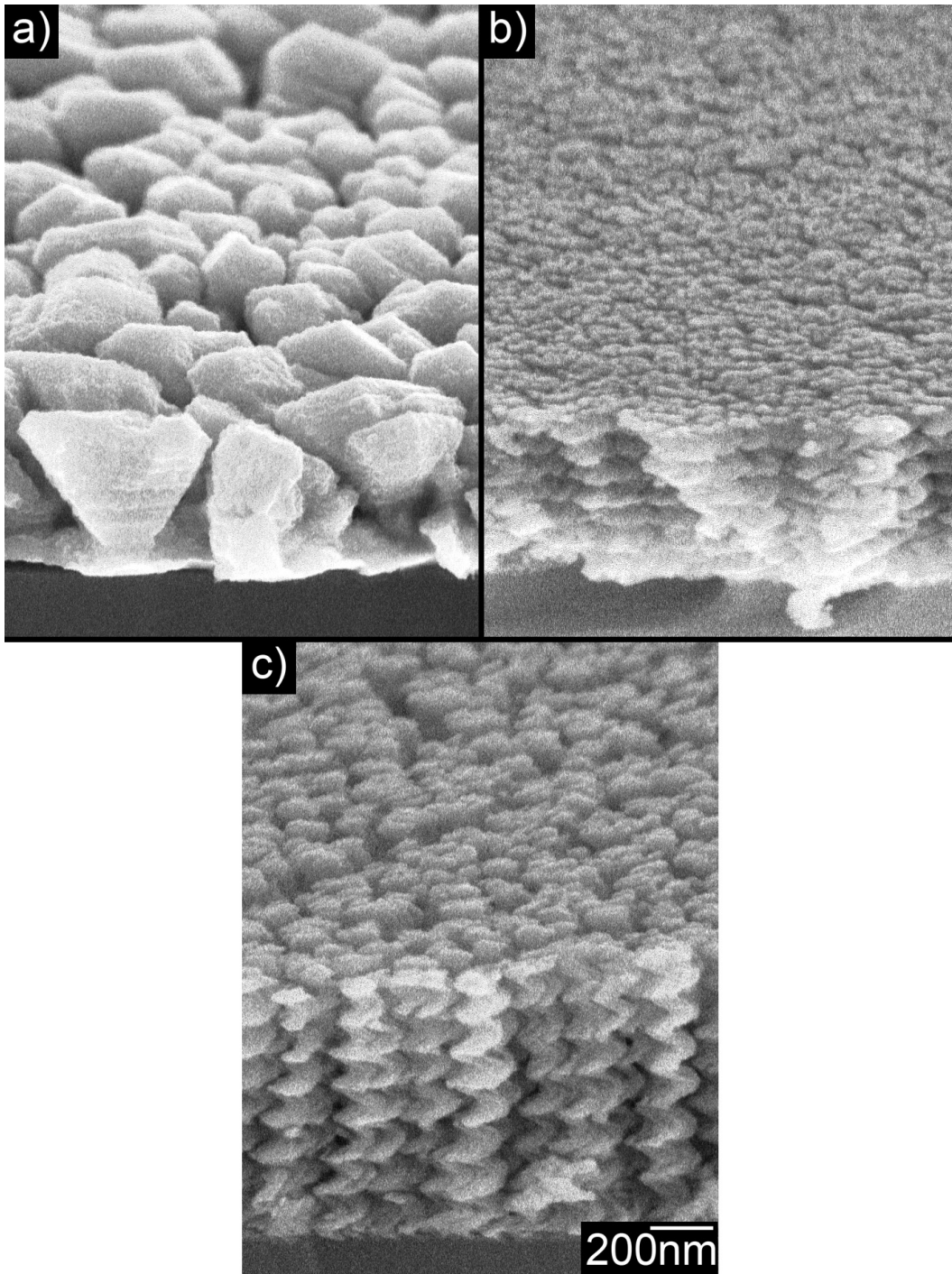
Figure 5.6: Oblique images of copper grown at various temperatures: a) 150°C, b) Room Temperature (Average of 30°C), c) −50°C.
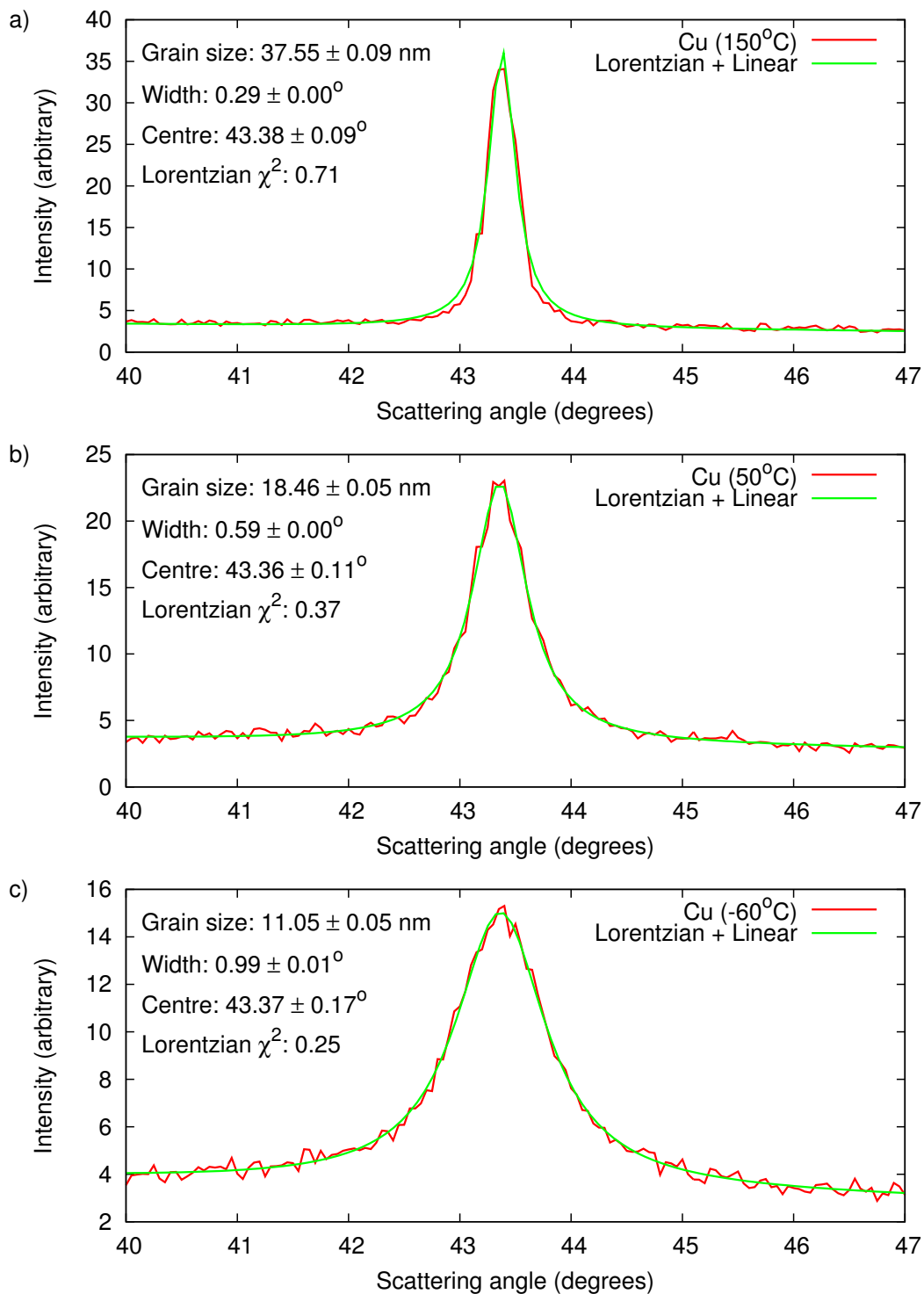
Figure 5.7: XRD analysis of copper grown at various temperatures: a) 150°C, b) Room Temperature (Avg 30°C), c) -50°C.

capable of dynamic operation under UHV conditions and cryogenic temperatures, was used to route LN_2 inside the deposition system from the liquid feedthrough. Cryogenic liquid flow through the lines was ensured by using a pressured 250 L LN_2 dewar by implementing a valve throttling system at the outlet of the liquid feedthrough. Temperatures of −95°C, without substrate rotation, and −60°C, with substrate rotation, could be measured using the T-type thermocouple temperature measurement system. Thermal isolation between the system and the chuck was accomplished by using custom built Macor headpiece. Cooling system performance was demonstrated by evaporating copper, a low melting point material, to produce defined structured thin films. Along with the SEM images, an XRD analysis was done to determine grain size and crystallinity of the films grown.

Lower temperatures are possible with improvements in heat transfer between the OFC chuck/copper leaf interface and the copper leaf/OFC block interface. Although Apiezon's N-type grease was used on both interfaces, its effectiveness on the rotating interface was poor and should not be used in that application. If the copper leaves are to be used then the standard copper parts should be replaced with OFC to ensure optimal heat transfer. Since each interface produces a non-ideal contact and provides poor thermal contact, an attempt should be made to bring the OFC chuck into direct contact with the OFC block. This could be accomplished by raising the standoffs, but also placing them on springs to accommodate any imperfections in alignment between the two surfaces.

Although flexible tubing was used in order to easy design consideration and installation, some very important lessons were learned for future design consider-ations. Flexible tubing could be shaped to follow specific paths but preform very poorly when required to make abrupt and sharp turns. Space is a premium in the deposition chamber therefore 90° turns should be made with rigid pipe to achieve

99

a compact design. There should only be one bend in the flexible tubing, which is the bend that follows the deposition arm, all other bends in the flexible tubing are permanent and should be replaced. Although this adds extra points for potential leaks, it will however allow for an efficient design. The ultimate goal of this change is to make the flexible tubing have the bending motions and the VCR fittings to be in the same plane and to minimize stress on the flexible tubing.

The screws that fasten the chuck to the head piece are currently flat head screws, which have a taper to the threaded part. Since the chuck holes for the screws are also tapered the two parts mate well. This is not the ideal setup. It is desired to control the amount of pressure that is applied between the copper leaves and the chuck. Having tapered edge in the chuck and a tapered screw will force the two surface to creep up on one another during rotation which increases downward force onto the copper leaves, thus increasing mechanical resistance which ultimately leads to motor seizing. This change would require the use the low head style screws, which do not have a taper, and drilling the chuck to remove the taper. Some mechanical resistance is still desired to provide good thermal contact. This still puts an extra demand on the φ motors, there some consideration should be placed into altering/modifiying or upgrading the φ rotation system. This could be done with a higher torque motor, different gearing or placement of the spline, which allows head rotation through the shaft, in contact with the other edges of chuck.

The groove on the bottom side of the chuck is located 2 inches from the center. By moving the groove to the very edge (groove radius of 3.5 inches) of the chuck would allow for more thermal contact between two surfaces.

Improvements to temperature measurement stated in Chapter 4, Section 4.4 would also benefit the LN$_2$ based *in situ* substrate cooling system.

Chapter 6

Conclusions and Future Directions

6.1 Introduction

This thesis explores areas pertaining to thin films and surface science. The experiments pursued in this thesis were not meant to provide definite answers or solutions attempted problems, but rather to offer insight and allow further and potentially more fruitful work to be done. I will provide a list of my accomplishments, but I will also critique what I have done and what I believe should be improved upon. I will also provide, potential experiments that can be done stemming from the work that I have done.

6.2 Etching

In Chapter 3, I demonstrated the ability to enhance the response time of existing glancing angle deposition (GLAD) relative humidity sensors. This modification was accomplished using a reactive ion etch recipe that was made for etching TiO_2, the

devices' sensing material, but tailored for GLAD thin film etching. The etch recipe was further developed to accomplish the complete removal of the TiO_2 film which was demonstrated through pattern transfer by using a shadow mask.

Short etch times allowed for creation of diffusion channels which improved the infiltration of analyte into the most sensitive region of the sensor. Although the channels were created, it would be more beneficial to see if the posts can be individually thinned to distribute/eliminate island formation. Experimenting with etch times, pressure, feed gasses, and RF power could yield better results. Using the current etch recipe the films seemed to clump but this might have been caused by the non-ideal conditions created by the defects posts which grew on the interface between the SiO_2 and Au interface. By using a truly planar sensor this effect would be eliminated.

Instead of using IDE, which created an added complexity in the design process, a parallel plate design could be used. With the ability to create high quality capping layers, detailed in Chapter 4, a lithographic mask design that creates a perforated top layer electrode, which would be engineered to give the best ratio between sensitivity and response time. The fabrication of this sensor would consist oxide layer growth on the silicon wafer, patterning an aluminum bottom electrode, growth of a GLAD film with a cap and then depositing and patterning an aluminum top electrode. By designing the top electrode correctly and applying the etch, the contact pad would rest on the SiO_2 thus having top and bottom electrode on the same plane.

Methodology for sensor characterization would be identical, but a refinement to the equipment would easy testing and optimize conditions for sensor characterization. By replacing the simple 555 timer circuit, which depends on swapping resistors to achieve the desired desired period and duty cycle for humidity step response chamber's solenoid vales, with a microcontroller-based switching circuit it

102

would be possible to adjust timing of the switching circuit to user defined parameters. Also, the chamber used to test the device should be redesigned to minimize its size and minimize error introduced by variation in placement of the sensor in the chamber. The use of the new sample holder designed would assist in new chamber design and sample alignment. Since the step response of the sensors could not be fully characterized due to a limit set by the sampling frequency of the LCR meter used, a custom probing circuit would benefit in a more complete characterization of the sensors response.

A UV based RH sensor regeneration was used. If these devices are to be seriously considered for commercial deployment then a step in incorporating an light emitting diode into the sample holder as to allow for *in situ* regeneration of the sensor. This experiment would determine the optimal wavelength to be used for sensor regeneration, as well duration and frequency of exposure for optimal sensor performance.

6.3   Heating

In Chapter 4 I designed and implemented a low cost, compact, and adjustable radiative heating system with capabilities to reaching 400°C while retaining substrate rotation and tilt needed for GLAD thin film growth. Temperature measurement was accomplished using T-type thermocouples, which are suitable for vacuum use, and a thermistor, which was calibrated using NIST and ATSM standards. The temperature measurement system allowed for real time feedback and control of temperature through the adjustment of bulb power output using a variable AC transfer. By increasing substrate temperature through the heating system, capping layers were grown on top of a GLAD thin film. Increasing substrate temperatures increased capping film quality. By creating capping layer and using standard lithographic

methods pattern transfer with μm resolution was possible.

Since TiO_2 was the only material used, elevated temperature deposition on a larger variety of materials can be done. SiO_2 is a lower melting point temperature therefore should require lower temperatures with regards to creating a continuous capping layer. By creating a continuous capping layer, underlying structures can be encapsulated therefore allowing for the creation of higher quality microfluidic devices through e-beam evaporation methods.

Experiments determining column broadening as a function of temperature could be done which would lead to column diameter control. Currently, GLAD column diameters are on the order of tens of nanometers, therefore by seeding substrates, column diameter can be preserved and allow for the creation of μm column diameters suitable for electrodes in photovoltaic applications.

Further refinements can be made to the pattern transfer techniques to potentially enable microelectrical mechanical systems (MEMS) and GLAD. By using a silicon on insulator wafer, where the insulator is Si_3N_4, MEMS mass-based sensors using TiO_2 GLAD thin films can be produce. The etchant used for releasing Si_3N_4 will not attack the TiO_2 nanostructured thin film or native oxide and therefore allowing the releasing of the structure while keeping the GLAD film intact. Since the releasing is going to be done using a wet etchant, the capping layer would assist in minimizing the nanocarpet effect.

6.4   Cooling

In Chapter 5, I designed and implemented a LN_2 based thermal conductive cooling system capable of obtaining and maintains chuck temperatures of −60°C while ensuring substrate rotation and tilt, not previously demonstrated in literature. I used the same temperature measurement techniques used Chapter 4 as the thermocouple

was suitable for cryogenic use. The heating lamps also remained in the system, to allow for heating of the substrate from its low temperatures. Copper helical films were grown at cooled temperatures to demonstrate the enabling effect of producing structured thin films from low melting point materials. A comparison is also made between heated copper GLAD film, which produces films with higher crystallinity, and room temperature copper GLAD film.

First, the ability to control substrate temperature is an obvious application. Although extremely cold temperatures are possible, but this design also enables the maintaining chuck temperature through the throttling of the cooling liquid. Experiments minimizing column broadening can be executed to demonstrate column diameter control, a problem which plagues many GLAD thin films. Initial nucleation experiments as a function of temperature could be done to characterize the effects of different oblique angles, while decoupling effects from diffusivity.

By creating spring like structures out of metals, have favourable material properties such as ductility and conductivity. Devices created could be made to achieve larger displacement with a lower requirement on energy spent on deforming the material. This automatically lends itself to application in microfluidics by creating a diaphragm style pump which is actuated through top and bottom electrodes.

The ability to create porous metallic vertical post film could be used to enhance solar cell performance. These vertical posts would behave like electrodes, with a high conductivity, and could be coated with a photovoltaic material via low pressure CVD, a method of depositing atomic layers thus coating the electrodes. This would allow for more excitonic reactions, the process in which an electron-hole pair dissociation thus giving the ability to produce current, per area footprint.

The ability to cool the substrate opens the opportunity to explore a new set of materials in previous applications where higher melting point materials may not

have been the optimal choice.

Appendix A

LN$_2$ Cooling: Precautions and Usage

Dealing with extreme variation between normal operation and experimental conditions requires the user must pay attention to many aspects: proper thermal contact between cooling elements, no spurious contact with chamber, gas leaks in vacuum, and the inherent danger associated with LN$_2$.

Chuck and leaf preparation are important when good thermal contact is required. The bottom of the chuck should be polished to achieve a mirror like finish, which can be achieved by using 400 grit alumina sand paper and then using a finer grit (1200) paper. After the particulate has been washed off, a treatment of metal polish, Brasso, should be used. The copper leaves on the copper cooling block should be rounded out to ensure for the chuck to deform the leaf in order to mate with the chuck. The rounding of the leaves can be achieved by using a cylindrical pipe that is 1/4 in. in diameter.

Loading of the substrates onto the copper chuck doesn't require excessive attention. For added thermal conductivity and adherence to the substrate, Apiezon's N

grease, suitable for cryogenic temperatures, can be used on the interface between the chuck and the substrate.

The installation of the chuck into the system is a delicate process as it will ensure proper contact between the two surfaces. When placing the chuck into the system, gently let it rest on the leaves. Rotate the chuck to align with the mounting holes on Macor head piece underneath. When screwing down the chuck, take great caution when tightening the screws. Introducing too much mechanical force can lead to seizing and unnecessary stress on the stepper motors when attempting to rotating the chuck. Try to make 1/2 or 1/4 turns to each screw and rotate through each screw until the resistance in the screws becomes noticeably higher. Loosen the screws by 1/4 turn increments if the motor is unable to rotate the chuck. Since the chuck is at the 180° position, the system should be rotated to the intended deposition angle and this test should be done again. Before leaving the chuck setup, a check should be made on whether the thermocouple is properly aligned in the groove on the chuck.

A check on the tubing and foiling should be made. The main purpose of this check is ensure that no unwanted thermal contact occurs. Check if the foil, used to minimize vapour flux contamination, comes into during the α rotation. Since the tubing flexes outward when angles are decreased from 180° special notice should be taken when the arm is at the desired deposition angle and adjustment should be made, as required. Normal precautions and checks, typically associated with a system pumpdown, should be made as well.

During system pumpdown external LN_2 plumping connections can be made. Connect the dewar's liquid feed line to the port on the system and tighten the fitting until there is a significant rise in resistance. When high vacuum has been reached in the deposition chamber, a check needs to be made on leaks from the LN_2 connections inside the chamber. This test is done by closing the exhaust port

108

valve, and opening the dewar valve and allows the lines pressurize without allowing flowing LN_2 through the system. If there is a leak, then pressurizing the lines will be accompanied by a rise in pressure in the vacuum chamber. If a leak is present, close the dewar valve open the exhaust port (to release the pressure), and vent the deposition system. Tighten the VCR fittings by an extra 1/8 of a turn.

If adequate vacuum has been achieved, and all checks have been made it will be time to start the substrate cooling process. The arm should be placed at an α of 100° as to avoid unwanted deposition during source conditioning and to minimize stresses on the tubing when flowing LN_2. Assuming that the LN_2 dewar valve is wide open, slowly open the exhaust valve. This is an extremely violent and loud process - hearing protection, eye protection and gloves are recommended. At first the exhaust port will be discharging the air and warmed nitrogen gas from the lines. The second stage is signaled when the exhaust of cooled nitrogen begins, apparent by a white/cloudy exhaust. The third stage is apparent by the spitting of LN_2 from the exhaust. Until this point the dominant sound is the gas rushing through the pipe. During the third stage, pressure in the chamber should begin to decrease faster as the LN_2-cooled lines and block act as a pseudo-cryopump. The fourth stage is when LN_2 begins to approach the exhaust port valve. This is indicated by an intermittent gargling of the LN_2 through the valve. At this point the user should throttle the valve. The fifth stage will be reached when the tubing is completely filled with LN_2. This is accomplished by determining correct valve positioning. Correct position is determined by ensuring enough flow to keep liquid in the lines, but to minimize LN_2 spitting/spilling. If LN_2 is present at the exhaust port then a positive indicator is a substantial dampening of exhaust sound. Adjustments will need to be made until a steady state is reached. If the valve opening is too narrow then sound of rushing air will become noticeable. If the valve is excessively open then large amounts of LN_2

spitting will occur.

One iteration that was attempted, that is not recommended, was to improve thermal contact by using cryogenic grease. Apiezon's N type grease was used on the surface between the leaves and the OFC chuck. Although it improved the thermal contact and ultimate temperature, this iteration produced so much mechanical resistance, indicated by motor current, that it eventually lead to motor seizing.

Bibliography

[1] K. Robbie and M.J. Brett. Method of depositing shadow sculpted thin films. U.S. Patent 5 866 204, February 2, 1999.

[2] C. Ratsch and J.A. Venables. Nucleation theory and the early stages of thin flm growth. *Journal of Vacuum Science Technology A*, 21(5):S96–S108, 2003.

[3] A. Powell, P. Minson, G. Trapaga, and U. Pal. Mathematical modeling of vapor-plume focusing in electron-beam evaporation. *Metallurgical and Materials Transactions A*, 32(8):1959–1966, 2001.

[4] M.O. Jensen and M.J. Brett. Porosity engineering in glancing angle deposition thin films. *Applied Physics A: Materials Science and Processing*, 80(4), 2005.

[5] M.M. Hawkeye and M.J. Brett. Glancing angle deposition: Fabrication, properties, and applications of micro- and nanostructured thin films. *Journal of Vacuum Science and Technology A*, pages 1317 – 1335, 2007.

[6] K. Robbie, J.C. Sit, and M.J. Brett. Advanced techniques for glancing angle deposition. *Journal of Vacuum Science and Technology B*, 16:1115–1122, 1998.

[7] K.D. Harris,A.C. Van Popta, J.C. Sit, D.J. Broer and M.J. Brett. A birefringent and transparent electrical conductor. *Advanced Functional Materials*, 18(15):2147–2153, 2008.

[8] S.R. Kennedy and M.J. Brett. Porous broadband antireflection coating by glancing angle deposition. *Applied Optics*, 42(22):4573–4579, 2003.

[9] M. Summers and M.J. Brett. Optimization of periodic column growth in glancing angle deposition for photonic crystal fabrication. *Nanotechnology*, 19(41):415203, 2008.

[10] J.J. Steele, J.P. Gospodyn, J.C. Sit, and M.J. Brett. Impact of morphology on high-speed humidity sensor performance. *IEEE Sensors Journal*, Vol. 6:24 – 27, 2006.

[11] J.J. Steele, A.C. Van Popta, M.M. Hawkeye, J.C. Sit and M.J. Brett. Nanostructured gradient index optical filter for high-speed humidity sensing. *Sensors and Actuators B*, 120(1):213–219, December 2006.

[12] G.D. Dice, M.J. Brett, D. Wang and J.M. Buriak. Fabrication and characterization of an electrically variable, nanospring based interferometer. *Applied Physics Letters*, 90(25):253101, 2007.

[13] M.D. Fleischauer, Jing Li, and M.J. Brett. Columnar thin films for three-dimensional microbatteries. *Journal of the Electrochemical Society*, 156(1):A33–A36, 2009.

[14] L.W. Bezuidenhout and M.J. Brett. Ultrathin layer chromatography on nanostructured thin films. *Journal of Chromatography A*, 1183(1-2):179–185, 2008.

[15] J.J. Steele and M.J. Brett. Nanostructure engineering in porous columnar thin films: recent advances. *Journal of Materials Science: Materials in Electronics*, 18:367–379, 2007.

112

[16] J.J. Steele, G.A. Fitzpatrick, and M.J. Brett. Capacitive humidity sensors with high sensitivity and subsecond response times. *IEEE Sensors Journal*, 7:955 – 956, 2007.

[17] J.J. Steele, M.T. Taschuk, and M.J. Brett. Nanostructured metal oxide thin films for humidity sensors. *IEEE Sensors Journal*, 8:1422 – 1429, 2008.

[18] H.B. Valman, B.M. Wright and C. Lawrence. Measurement of respiratory rate in the newborn. *British Medical Journal*, 286:1783–1784, June 1983.

[19] T. Tatara and K. Tsuzaki. An apnea monitor using a rapid-response hygrometer. *Journal of Clinical Monitoring*, 13:5–9, 1997.

[20] P.L. Kebabian and C.E. Kolb and A. Freedman. Spectroscopic water vapor sensor for rapid response measurements of humidity in the troposphere. *Journal of Geophysical Research*, 107:4670, 2002.

[21] R. Fenner and E. Zdankiewicz. Micromachined water vapor sensors: a review of sensing technologies. *IEEE Sensors Journal*, 1(4):309–317, December 2001.

[22] K. Robbie and L. J. Friedrich and S. K. Dew and T. Smy and M. J. Brett. Fabrication of thin films with highly porous microstructures. *Journal of Vacuum Science and Technology A*, 13:1032–1035, 1995.

[23] K. Robbie, M.J. Brett and A. Lakhtakia. Chiral sculptured thin films. *Nature*, 384:616, 1996.

[24] B. Dick and M.J. Brett. *Nanofabrication by glancing angle deposition*, volume 6 of *Encyclopedia of Nanoscience and Nanotechnology*, page 703. American Scientific Publishers, Stevenson Ranch, CA, 2004.

[25] M. Ohring. *Materials Science of Thin Films*, chapter 2.2, pages 58–65. Academic Press, San Diego, CA, 2nd edition, 2002.

[26] W.F. Smith. *Foundations of Materials Science and Engineering*, chapter 5.2, pages 177–184. McGraw-Hill Higher Education, Boston, MA, 4th edition, 2006.

[27] R. Igreja, C.J. Dias. Analytical evaluation of the interdigital electrodes capacitance for a multi-layered structure. *Sensors and Actuators A*, Vol. 112:291 – 301, 2004.

[28] J.G. Fan, D. Dyer, G. Zhang, and Y.P. Zhao. Nanocarpet effect: Pattern formation during the wetting of vertically aligned nanorod arrays. *Nano Letters*, 4(11):2133–2138, 2004.

[29] Y.P. Zhao and J.G. Fan. Clusters of bundled nanorods in nanocarpet effect. *Applied physics letters*, 88(10):103123, 2006.

[30] J.G. Fan, J.X. Fu, A. Collins, and Y.P. Zhao. The effect of the shape of nanorod arrays on the nanocarpet effect. *Nanotechnology*, 19(4):045713, 2008.

[31] A. Hariri, J. Zu and R.B. Mrad. Modeling of wet stiction in microelectromechanical systems. *Journal of microelectromechanical systems*, 16(5):1276–1285, 2007.

[32] H.F. Winters, J.W. Coburn, and T.J Chuang. Surface processes in plasma-assisted etching enviroments. *Journal of Vacuum Science & Technology. B*, 1(2):469–480, 1983.

[33] P.H. Yih, V. Saxena, and A.J. Steckl. A review of sic reactive ion etching in fluorinated plasmas. *Physica Status Solidi*, 202:605–642, 1997.

[34] Z. Huang, K.D. Harris, and M.J. Brett. Morphology control of nanotube arrays. *Advanced Materials*, 21(29):29832987, 2009.

[35] A. Hagfeldt and M. Gratze. Molecular photovoltaics. *Accounts of Chemical Research*, 33(5):269277, 2000.

[36] O.K. Varghese, D. Gong, M. Paulose, K.G. Ong, E.C. Dickey, and C.A. Grimes. Extreme changes in the electrical resistance of titania nanotubes with hydrogen exposure. *Advanced Materials*, 15(7-8):624–627, 2003.

[37] M.A. Henderson, W.S. Epling, C.H.F. Peden, and C.L. Perkins. Insights into photoexcited electron scavenging processes on TiO_2 obtained from studies of the reaction of O_2 with OH groups adsorbed at electronic defects on $TiO_2(110)$. *Journal of Physical Chemistry B*, 107:534–545, 2003.

[38] U. Diebold. Structure and properties of TiO_2 surfaces: a brief review. *Applied Physics A*, 76:681687, 2003.

[39] R. Wang, N. Sakai, A. Fujishima, T. Watanabe, and K. Hashimoto. Studies of surface wettability conversion on TiO_2 single-crystal surfaces. *Journal of Physical Chemistry B*, 103:2188–2194, 1999.

[40] O. Powell and D. Sweatman and B.H. Harrison. The use of titanium and titanium dioxide as masks for deep silicon etching. *Smart Meter. Stuc.*, Vol. 15:S81 – 86, 2006.

[41] S. Matsuo. Selective etching of SiO_2 relative to Si by plasma reactive sputter etching. *J. Vac. Sci. Technol.*, Vol. 17:587 – 594, 1980.

[42] M. Ohring. *Materials Science of Thin Films*, chapter 2.2, pages 238–239. Academic Press, San Diego, CA, 2nd edition, 2002.

[43] A. Matsutani and F. Koyama and K. Iga. Microfabrication of dielectric multilayer reflector by reactive ion etching and characterization of induced wafer damage. *Japanese J. Appl. Phys.*, Vol. 30:428 – 429, 1991.

[44] D. Szmigiel, K. Domanski, P. Prokaryn, P. Grabiec, and J.W. Sobczak. The effect of flourine-based plasma treatment on morphology and chemical surface composition of biocompatible silicone elastomer. *Applied Surface Science*, pages 1506 – 1511, 2006.

[45] S. Norasetthekul, P.Y. Park, K.H. Baik, K.P. Lee, J.H. Shin, B.S. Jeong, V. Shishodia, E.S. Lambers, D.P. Norton, and S.J. Pearton. Dry etch chemistries for TiO_2 thin films. *Applied Surface Science*, 185:27–33, 2001.

[46] R. Messier. The nano-world of thin films. *Journal of Nanophotonics*, 2:021995, 2008.

[47] R. Knepper and R. Messier. Thin film morphology at low adatom mobility. *Proceedings of SPIE*, 4467:87–101, 2001.

[48] S.A. Campbell. *The Science and Engineering of Microelectronics*, chapter 3, pages 39–67. Oxford University Press, New York, NY, 2nd edition, 2001.

[49] B.A. Movchan and A.V. Demchish. Study of structure and properties of thick vacuum condensates. *Physics of Metals and Metallography*, 28(4):83, 1969.

[50] D.W. Flaherty, Z. Dohnalek, A. Dohnalkova, B.W. Arey, D.E. McCready, N. Ponnusamy, C.B. Mullins, and B.D. Kay. Reactive ballistic deposition of porous TiO_2 films: Growth and characterization. *Journal of Physical Chemistry C*, 111(12):4765–4773, 2007.

116

[51] C. Patzig and B. Rauschenbach. Temperature effect on the glancing angle deposition of si sculptured thin films. *Journal of Vacuum Science and Technology A*, 46(4):881–886, 2008.

[52] E. Schubert, J. Fahlteich, T. Hoche, G. Wagner, B. Rauschenbach. Chiral silicon nanostructures. *Nuclear Instruments and Methods in Physics Research B*, 244(1):40–44, 2006.

[53] M. Malac and R.F. Egerton. Observations of the microscopic growth mechanism of pillar and helices formed by glancing angle thin-film deposition. *Journal of Vacuum Science and Technology*, 19(1):158–166, 2001.

[54] J. Kim, Z. Dohnalek, B.D. Kay. Structural characterization of nanoporous Pd films grown via ballistic deposition. *Surface Science*, 586(1-3):137–145, 2005.

[55] K. Itoh, F. Ichikawa, Y. Takahashi, K. Tsutsumi, Y. Noguchi, K. Okamoto, T. Uchiyama and I. Iguchi. Columnar grain structure in cobalt films evaporated obliquely at low substrate temperatures. *Japan Society of Applied Physics*, 45(4):2534–2538, 2006.

[56] E. Gmelin, M. Asen-Palmer, M. Reuther, and R Villar. Thermal boundary resistance of mechanical contacts between solids at sub-ambient temperatures. *Journal of Physics D*, 32(6):R19–R43, 1999.

[57] *Manual on the use of thermocouples in temperature measurement*, chapter 3. American Society for Testing and Materials, Philadelphia, Pa., 3rd edition, 1981.

[58] M.J. Viens. *NIST ITS-90 Thermocouple Database.* Viewed at http://srdata.nist.gov/its90/main/.

[59] *Manual on the use of thermocouples in temperature measurement*, chapter 2. American Society for Testing and Materials, Philadelphia, Pa., 3rd edition.

[60] W. Boyes. *Instrumentation reference book*, chapter 14, pages 268–269. Oxford University Press, Boston, MA, 3rd edition, 2003.

[61] H. Prestonthomas. The international tempearture scale of 1990(ITS-90). *Metrologia*, 27(1):3–10, 1990.

[62] M. Seto, K. Westra, M. Brett. Arrays of self-sealed microchamers and channels. *Journal of Materials Chemistry*, 12:2348 – 2351, 2002.

[63] K.R. Williams, K. Gupta, and M. Wasilik. Etch rates for micromachining processing - part II. *Journal of Micrpelectromechanical Systems*, 12(6):761–778, 2003.

[64] M.T. Taschuk, J.J. Steele, A. van Popta and M.J. Brett. Photocatalytic regeneration of interdigitated capacitor relative humidity sensors fabricated by glancing angle deposition. *Sensor and Actuators B*, 134:666 – 671, 2008.

[65] Christian Vargel. *Corrosion of aluminium*, chapter 2, pages 398–399. Elsevier, Boston, MA, 1st edition, 2004.

[66] R.N. Tait, T. Smy, S.K. Dew, and M.J. Brett. Nodular defect growth and structure in vapor deposited films. *J. of Electronic Materials*, 24:935–940, 1995.

[67] M.W. Seto, B. Dick and M.J. Brett. Microsprings and microcantilevers: studies of mechanical response. *J. of Micromechanics and Microengeering*, (11):582–588, 2001.

118

[68] T. Morimoto, T.Iwakiy. Dielectric behaviour of adsorbed water. part i: Measurement at room temperature on TiO$_2$. *Journal of the Chemical Society, Faraday Transactions*, Vol. 83:943 – 956, 1987.

[69] J.F Shackelford, W. Alexander, and J.S. Park, editor. *CRC Materials Science and Engineering Handbook.* CRC Press, Boca Raton, FL, 2nd edition, 1994.

[70] S.J. Schneider, editor. *Ceramics and Glasses Engineered Materials Handbook*, volume 4. ASM International, Metals Park, OH, 1st edition.

[71] S.M. Pompea, R.P. Breault. *Handbook of optics, Volume 2*, chapter 37. McGraw-Hill,, New York, 2nd edition, 1995.

[72] M.J. Viens. *Outgassing Data for Selecting Spacecraft Materials Online.* Available at http://outgassing.nasa.gov/.

[73] W.S. Rasband. *ImageJ.* Available at http://rsb.info.nih.gov/ij/.